AN INVESTIGATION INTO THE FREE VIBRATION ANALYSIS OF INTACT AND DEFECTIVE LAMINATED COPOSITE BEAMS SUBJECTED TO COMBINED AXIAL FORCE AND END MOMENT

by

Mir Tahmaseb T. Kashani
Master of Science, University of Semnan (2011)
Bachelor of Science, Ferdowsi University of Mashad (2009)

A dissertation

presented to Ryerson University

in partial fulfillment of the

requirements for the degree of

Doctor of Philosophy

in the program of

Aerospace Engineering

Toronto, Ontario, Canada, 2017

AUTHOR'S DECLARATION

I hereby declare that I am the sole author of this dissertation. This is a true copy of the dissertation, including any required final revisions, as accepted by my examiners. I authorize Ryerson University to lend this dissertation to other institutions or individuals for the purpose of scholarly research. I further authorize Ryerson University to reproduce this dissertation by photocopying or by other means, in total or in part, at the request of other institutions or individuals for the purpose of scholarly research. I understand that my dissertation may be made electronically available to the public.

Acknowledgements

This thesis would not have been possible without the support and encouragement of my advisor and my mentor, Prof. Seyed M. Hashemi: for his extensive knowledge and innovative ideas. I would like to thank him for unconditional support, unending patience, wisdom, and guidance throughout my research.

I would also like to thank my friend and colleague, Supun Jayasinghe for countless discussions that opened my mind to new possibilities, my friend and colleague, Ishan Ali Khan for his support and friendship and my dear friend, Ghassem Tofighi for always being there for me when I needed him.

Finally, I would like to thank my family for their unconditional love, endless support and constant encouragement during my time in academia. Without them not only this thesis but any other accomplishments, in this interestingly mysterious journey called life, would not have been possible. To my mother Farideh Zandvakili, my father Hossein T. Kashani, my sister Tahmineh T. Kashani and my brother Tahmoures T. Kashani.

AN INVESTIGATION INTO THE FREE VIBRATION ANALYSIS OF INTACT AND DEFECTIVE LAMINATED COPOSITE BEAMS SUBJECTED TO COMBINED AXIAL FORCE AND END MOMENT

Mir Tahmaseb T. Kashani
Doctor of Philosophy, Aerospace Engineering, Ryerson University, Toronto 2017

Abstract

This research is focusing on the bending-torsion coupled free vibration modeling as well as the analysis of intact and defective pre-stressed beams subjected to combined axial force and end moment. In the recent years, many studies have been conducted in an attempt to investigate the free vibration of pre-stressed beams using numerical and analytical techniques. However, despite their numerous applications, there is limited research done on pre-stressed beams subjected to both axial force and end moment in addition to the coupled behavior caused by the latter one. In the present study, current trends in the literature are critically examined, new models are proposed, and numerical and semi-analytical formulations are developed to find the natural frequencies and mode shapes of different pre-stressed slender beam configurations. The proposed methods are compared in terms of accuracy and convergence. Furthermore, the effects of axial force, end moment and delamination defect on the vibrational behavior of each model are also investigated.

Four different general types of thin beams, including isotropic, layered, composite and delaminated beams, are modeled using traditional Finite Element Method (FEM) and frequency-dependent Dynamic Finite Element (DFE) technique. The DFE formulation is distinct from the conventional FEM by the fact that the former exploits frequency-dependent basis and shape functions of approximation space, whereas the polynomial ones are used in the latter method. With regard to layered beams, a novel layer-wise method is introduced for both DFE and FEM. Delaminated beam is also modeled using both ‘free mode’ and ‘constrained mode’ models showing that the continuity (both kinematic and force) conditions at delamination tips, in particular, play a large role in formulation of ‘free mode’ model. In this case, the defect is assumed to be a single-symmetric through the thickness delamination. However, the presented models and formulations could be readily extended to more general cases. Where available, the results were validated against existing limited experimental, analytical, and numerical data in literature. In addition, the investigated cases

are modeled in the commercial finite element suite ANSYS® for further validation. Finally, general concluding remarks are made on the performance of the presented models and solution techniques, where the advantages and disadvantages of the proposed formulations as well as possible future research works are highlighted.

Table of Contents

Author's declaration ii
Acknowledgements iii
Abstract iv

1 Introduction 1

1.1 Overview 1
1.2 Free vibration of layered beams 5
1.3 Free vibration of fiber-reinforced laminated composite beams 6
1.4 Delaminated and defective layered composite beams 7
1.5 Motivation 12
1.6 Objectives 13
1.7 Thesis organization 14

2 Free vibration of pre-stressed isotropic beams 17

2.1 Development of governing differential equations 17
2.2 Classical finite element method (FEM) 21
2.3 Finite element numerical results 26
2.4 The dynamic finite element (DFE) 36
2.5 DFE Numerical Results; Simple Beam 43
2.6 Discussions and concluding remarks 53

3 Free Vibration of Pre-stressed Layered Beams 55

3.1 Introduction 55
3.2 Method of Homogenization 56
3.3 Layer-wise Formulation of Pre-stressed Layered Beams 58
3.4 The Layer-wise Beam Finite Element (LBFEM) formulation 61
3.5 The Layer-wise Beam Dynamic Finite Element (LBDFE) 63
3.6 Method of Homogenization Numerical Results 69
3.7 Layer-wise formulation numerical tests; two-layer aluminium-steel beam 75
3.8 Numerical tests; two-layer Glass/Epoxy composite beam 79
3.9 Numerical tests; steel-rubber-steel layered beam 81
3.10 Numerical tests; fibre-metal laminated (FML) beam 82
3.11 Numerical tests; three-layered laminated composite beam 85
3.12 Discussions and concluding remarks 88

4 Modal analysis of laminated composite beams subjected to axial force and end moment 90

4.1 Finite element formulation (FEM) 90

4.2 Dynamic finite element (DFE) formulation 95
4.3 Numerical tests 99
4.4 Conclusion 109

5 Free vibration of pre-stressed delaminated beam 111
5.1 Introduction 111
5.2 Mathematical model 111
5.3 Free mode delamination model 113
5.4 Classical finite element method (FEM) 116
5.5 Constrained mode model 121
5.6 Dynamic finite element 122
5.7 Numerical Results 124
5.7.1 Validation of presented formulation 124
5.7.2 Vibration analysis of delaminated pre-stressed beams 127
5.8 Discussion and concluding remarks 133

6 Discussion on the presented methods 135

7 Conclusion 138
7.1 Contributions 138
7.2 Future work 141

Appendices 142

References 157

List of Tables

TABLE 1: COMPARISON BETWEEN THE ANALYTICAL [97] AND FEM RESULTS FOR THE FIRST THREE NATURAL FREQUENCIES WITH P=0 AND M_{ZZ}= 0. 28
TABLE 2: COMPARISON BETWEEN ANSYS AND FEM RESULTS OF FIRST NATURAL FREQUENCY WITH CANTILEVER BOUNDARY CONDITION, FOR THREE DIFFERENT LOADING CONDITIONS. 29
TABLE 3: FUNDAMENTAL FREQUENCY FOR CLAMPED-CLAMPED BOUNDARY CONDITION WHEN FORCE AND END MOMENT ARE APPLIED. 29
TABLE 4: FUNDAMENTAL FREQUENCY FOR PINNED-PINNED BOUNDARY CONDITION WHEN FORCE AND MOMENT ARE APPLIED. 30
TABLE 5: FUNDAMENTAL FREQUENCY FOR PINNED-CLAMPED BOUNDARY CONDITION WHEN FORCE AND MOMENT ARE APPLIED. 30
TABLE 6: CRITICAL BUCKLING MOMENT FOR CANTILEVERED BOUNDARY CONDITION WITH VARYING AXIAL FORCE. 31
TABLE 7: CRITICAL BUCKLING COMPRESSIVE FORCE FOR CANTILEVERED BOUNDARY CONDITION WITH VARYING END MOMENT. 31
TABLE 8: FIRST NATURAL FREQUENCIES OF DFE FOR CANTILEVER BOUNDARY CONDITION. 45
TABLE 9: FIRST NATURAL FREQUENCIES OF DFE FOR CLAMPED-CLAMPED BOUNDARY CONDITION. 45
TABLE 10: FIRST NATURAL FREQUENCIES OF DFE FOR PINNED-PINNED BOUNDARY CONDITION. 46
TABLE 11: FIRST NATURAL FREQUENCIES OF DFE FOR PINNED-CLAMPED BOUNDARY CONDITION. 46
TABLE 12: CRITICAL BUCKLING MOMENT FOR CANTILEVERED BOUNDARY CONDITION WITH VARYING COMPRESSIVE FORCE. 47
TABLE 13: CRITICAL BUCKLING COMPRESSIVE FORCE FOR CANTILEVERED BOUNDARY CONDITION WITH VARYING END MOMENT. 47
TABLE 14: COMPARISON OF BUCKLING RESULTS FOR DIFFERENT METHODS. 48
TABLE 15: COMPARISON OF DIFFERENT METHODS (DFE, FEM AND ANSYS MODELS USING 5 ELEMENTS). 52
TABLE 16: FIRST SIX NATURAL FREQUENCIES FOR END MOMENT M_{ZZ}=0 AND DIFFERENT VALUES OF COMPRESSIVE AXIAL FORCE P. 70
TABLE 17: FIRST SIX NATURAL FREQUENCIES FOR END MOMENT M_{ZZ}=0 AND THREE DIFFERENT VALUES OF TENSILE AXIAL FORCE. 71
TABLE 18: FIRST SIX NATURAL FREQUENCIES FOR END AXIAL FORCE P=0 AND THREE DIFFERENT VALUES OF END MOMENT. 71
TABLE 19: BUCKLING END MOMENTS FOR DIFFERENT VALUES OF AXIAL FORCE HOMOGENIZATION METHOD. 73
TABLE 20: BUCKLING AXIAL FORCE FOR DIFFERENT VALUES OF END MOMENT HOMOGENIZATION METHOD. 74
TABLE 21: FUNDAMENTAL FREQUENCIES FOR CLAMPED-FREE BOUNDARY CONDITION. 76
TABLE 22: VARIATION OF BUCKLING MOMENT WITH AXIAL FORCE FOR TWO LAYERED ALUMINIUM-STEEL BEAM. 77
TABLE 23: FUNDAMENTAL FREQUENCIES FOR CLAMPED-FREE BOUNDARY CONDITION (DFE AND FEM USING 5 ELEMENTS AND ANSYS USING 20 ELEMENTS) FOR TWO-LAYER COMPOSITE BEAM (M_{ZZ}=6.14MN.M, P=1.23MN). 80

TABLE 24: COMPARISON BETWEEN EXPERIMENTAL RESULTS [101], DSM [101], LBDFE, LBFEM AND HOMOGENIZATION METHODS WITH P=0 AND M_{ZZ}=0 WITH CANTILEVERED BOUNDARY CONDITION. 82
TABLE 25: FUNDAMENTAL FREQUENCY OF PRE-STRESSED CANTILEVERED FML BEAM, SUBJECTED TO VARIOUS AXIAL LOADS AND END MOMENT OF 52.5KN.M. 83
TABLE 26: FIRST THREE NATURAL FREQUENCIES OF CANTILEVERED, PRELOADED, THREE-LAYER, UNIDIRECTIONAL COMPOSITE BEAMS (LAYUPS 1 AND 2) OBTAINED FROM 5-ELEMENT LBDFE AND LBFEM, AND 20-ELEMENT ANSYS® MODELS, SUBJECTED TO AN AXIAL LOAD OF 1.85MN AND END MOMENT OF 6.14MN.M. 85
TABLE 27: COMPARISON OF FEM AND DFE NATURAL FREQUENCY RESULTS FOR M_{ZZ}=0 AND P=0 WITH THE ANALYTICAL DSM VALUES [64]. 102
TABLE 28: NON-DIMENSIONAL FIRST NATURAL FREQUENCY (Λ_1^2) OF A CLAMPED–CLAMPED ISOTROPIC BEAM WITH A MID-PLANE DELAMINATION. 126
TABLE 29: NON-DIMENSIONAL SECOND NATURAL FREQUENCY (Λ_2^2) OF A CLAMPED–CLAMPED ISOTROPIC BEAM WITH A MID-PLANE DELAMINATION. 126
TABLE 30: NON-DIMENSIONAL FIRST NATURAL FREQUENCY (Λ_1^2) OF A CLAMPED–CLAMPED ISOTROPIC BEAM WITH A MID-PLANE DELAMINATION USING DFE FORMULATION. 132

List of Figures

FIGURE 1: SCHEMATIC AND COORDINATE SYSTEM OF THE PROBLEM. 17
FIGURE 2: INFINITESIMAL ELEMENT OF A BEAM SUBJECTED TO AXIAL FORCE AND END MOMENT. 18
FIGURE 3: DISCRETIZED DOMAIN ALONG THE BEAM SPAN 23
FIGURE 4: PERCENTAGE OF ERROR VERSUS NUMBER OF ELEMENTS REPRESENTING THE CONVERGENCE RATE OF FEM METHOD FOR FUNDAMENTAL FREQUENCY. 27
FIGURE 5: VARIATION OF FUNDAMENTAL FREQUENCY WITH APPLIED TENSILE FORCE AND END MOMENT, FOR CANTILEVERED BOUNDARY CONDITION. 32
FIGURE 6: VARIATION OF FUNDAMENTAL FREQUENCY WITH APPLIED TENSILE FORCE AND END MOMENT, FOR CLAMPED-CLAMPED BOUNDARY CONDITION. 32
FIGURE 7: VARIATION OF FUNDAMENTAL FREQUENCY WHEN TENSILE FORCE AND END MOMENT ARE APPLIED FOR PINNED-PINNED BOUNDARY CONDITION. 33
FIGURE 8: VARIATION OF FUNDAMENTAL FREQUENCY WHEN TENSILE FORCE AND END MOMENT ARE APPLIED FOR CLAMPED-PINNED BOUNDARY CONDITION. 33
FIGURE 9: VARIATION OF CRITICAL BUCKLING COMPRESSIVE FORCE WITH END MOMENT. 34
FIGURE 10: VARIATION OF CRITICAL BUCKLING END MOMENT WITH AXIAL FORCE. 34
FIGURE 11: FIRST FIVE FEM BENDING COMPONENTS OF MODE SHAPES. 35
FIGURE 12: FIRST FIVE FEM TORSION COMPONENTS OF MODE SHAPES. 35
FIGURE 13: CONVERGENCE ANALYSIS FOR THE FIFTH NATURAL FREQUENCY RESULTS, OBTAINED FROM DFE METHOD FOR CANTILEVERED BEAM 44
FIGURE 14: COMPARISON OF CONVERGENCE EFFICIENCY BETWEEN DFE METHOD AND CONVENTIONAL FEM FOR CANTILEVERED BEAM, THE FIFTH NATURAL FREQUENCY. 44
FIGURE 15: VARIATION OF NATURAL FREQUENCIES WHEN TENSILE FORCE AND END MOMENT IS APPLIED FOR CANTILEVERED BOUNDARY CONDITION. 48
FIGURE 16: VARIATION OF NATURAL FREQUENCIES WHEN TENSILE FORCE AND END MOMENT IS APPLIED FOR CLAMPED-CLAMPED BOUNDARY CONDITION. 49
FIGURE 17: VARIATION OF NATURAL FREQUENCIES WHEN TENSILE FORCE AND END MOMENT IS APPLIED FOR PINNED-PINNED BOUNDARY CONDITION. 49
FIGURE 18: VARIATION OF NATURAL FREQUENCIES WHEN TENSILE FORCE AND END MOMENT IS APPLIED FOR PINNED-CLAMPED BOUNDARY CONDITION. 50
FIGURE 19: VARIATION OF CRITICAL BUCKLING END MOMENT WITH AXIAL FORCE FOR CANTILEVERED BOUNDARY CONDITION 50
FIGURE 20: VARIATION OF CRITICAL BUCKLING COMPRESSIVE FORCE WITH END MOMENT FOR CANTILEVERED BOUNDARY CONDITION. 51
FIGURE 21: BENDING COMPONENT OF MODE SHAPES USING DFE. 52
FIGURE 22: TORSIONAL COMPONENT OF MODE SHAPES USING DFE. 53
FIGURE 23: SCHEMATIC AND COORDINATE SYSTEM OF THE PROBLEM, WITH AXIAL LOAD AND END-MOMENT APPLIED AT X=0, AND X=L. 57
FIGURE 24: N-LAYERED BEAM, WITH AXIAL LOAD AND END-MOMENT APPLIED AT $X=0$ AND $X=L$. 59
FIGURE 25: BENDING COMPONENTS OF THE NATURAL MODES FOR M_{ZZ}=3MN AND P=0.6MN HOMOGENIZATION METHOD. 72
FIGURE 26: TORSION COMPONENTS OF THE NATURAL MODES FOR M_{ZZ}=3 MN AND P=0.6 MN HOMOGENIZATION METHOD. 73
FIGURE 27: BUCKLING AXIAL FORCE VS. END MOMENT HOMOGENIZATION METHOD. 74

FIGURE 28: BUCKLING END MOMENT VS. AXIAL LOAD USING HOMOGENIZATION METHOD. 75
FIGURE 29: VARIATION OF NATURAL FREQUENCIES WITH TENSILE FORCE AND END MOMENT FOR CANTILEVERED BOUNDARY CONDITION. 77
FIGURE 30: BENDING COMPONENTS OF MODE SHAPES (DFE) M=52.5 KN.M, P=17.5KN 78
FIGURE 31: TORSION COMPONENTS OF MODE SHAPES (DFE) MOMENT=52.5KN.M, FORCE=17.5KN 78
FIGURE 32: THE SCHEMATIC OF TWO-LAYER COMPOSITE BEAM. 79
FIGURE 33: FUNDAMENTAL FREQUENCY VARYING BY DIFFERENT APPLIED AXIAL FORCE AND END MOMENT FOR TWO-LAYER COMPOSITE BEAM. 80
FIGURE 34: THE SCHEMATIC OF STEEL-RUBBER-STEEL SANDWICH BEAM 81
FIGURE 35: THE CONVERGENCE STUDY FOR THE TWO PROPOSED LAYER-WISE LBFEM AND LBDFE FORMULATIONS; FUNDAMENTAL FREQUENCY OF CANTILEVERED FML THREE-LAYER BEAM SUBJECTED TO AN AXIAL LOAD OF 17.5MN AND END MOMENT OF 52.5KN.M. 84
FIGURE 36: FUNDAMENTAL FREQUENCY VS. TENSILE FORCE AND END MOMENT FOR THE CANTILEVERED THREE-LAYER FML BEAM. 84
FIGURE 37: FUNDAMENTAL FREQUENCY OF CANTILEVERED, PRELOADED, THREE-LAYER, UNIDIRECTIONAL COMPOSITE BEAM (LAYUP 1) OBTAINED FROM A 5-ELEMENT LBDFE MODEL, SUBJECTED TO VARIOUS AXIAL LOADS AND END MOMENTS 86
FIGURE 38: BENDING COMPONENT OF THE FIRST FIVE MODE SHAPES OF THE CANTILEVERED, PRELOADED, THREE-LAYER, UNIDIRECTIONAL COMPOSITE BEAM (LAYUP1) OBTAINED USING A 20-ELEMENT LBDFE MODEL, SUBJECTED TO AN AXIAL LOAD OF 1.85MN AND END MOMENT OF 6.14MN.M. 87
FIGURE 39: TORSION COMPONENT OF THE FIRST FIVE MODE SHAPES OF THE CANTILEVERED, PRELOADED, THREE-LAYER, UNIDIRECTIONAL COMPOSITE BEAM (LAYUP1) OBTAINED USING A 20-ELEMENT LBDFE MODEL, SUBJECTED TO AN AXIAL LOAD OF 1.85MN AND END MOMENT OF 6.14MN.M. 88
FIGURE 40: GEOMETRY AND COORDINATE SYSTEM OF THE MODEL 91
FIGURE 41: POSITIVE DIRECTION OF FIBER ANGLE 100
FIGURE 42: ERROR VERSUS THE NUMBER OF ELEMENTS FOR FIRST FIVE NATURAL FREQUENCIES (PERCENT ERROR IS RELATIVE TO THE EXACT VALUES OBTAINED FROM THE DSM [26]. 102
FIGURE 43: VARIATION OF FIRST NATURAL FREQUENCY VS. AXIAL COMPRESSIVE FORCE FOR FEM AND DFE WITH M_{ZZ}=18.5MN.M AND K=0.1143 NM^2. 103
FIGURE 44: VARIATION OF NATURAL FREQUENCIES WITH GLASS-EPOXY COMPOSITE PLY ANGLE, USING A 5-ELEMENT DFE MODEL WITH M_{ZZ}=6.14 MN.M, P=1.23 MN AND K=0.1143 NM^2. 104
FIGURE 45: BUCKLING ANALYSIS FOR SINGLE LAYER GLASS-EPOXY COMPOSITE CANTILEVERED BEAM WITH FIBER ANGLE OF +15˚, USING A 5-ELEMENTS DFE MODEL. 105
FIGURE 46: FIRST FIVE BENDING COMPONENTS OF MODE SHAPES USING DFE METHOD WITH M_{ZZ}=6.14 MN.M, P=1.23 MN AND K=0.1143 NM^2. 106
FIGURE 47: FIRST FIVE TORSIONAL COMPONENTS OF MODE SHAPES USING DFE METHOD WITH M_{ZZ}=6.14 MN.M, P=1.23 MN AND K=0.1143 NM^2. 106
FIGURE 48: THREE-LAYER FIBER-METAL LAMINATED (FML) BEAM SCHEMATIC 107
FIGURE 49: VARIATION OF FIRST NATURAL FREQUENCY VS. AXIAL COMPRESSIVE FORCE FOR THREE LAYER GLASS-EPOXY AND ALUMINIUM SANDWICH BEAM USING 5-ELEMENT DFE AND FEM MODELS WITH M_{ZZ}=18.5 MN.M. 108
FIGURE 50: BUCKLING ANALYSIS FOR THREE LAYER GLASS-EPOXY AND ALUMINIUM SANDWICH CANTILEVERED BEAM USING 5-ELEMENT DFE. 109
FIGURE 51: SCHEMATIC OF A BEAM WITH SINGLE DELAMINATION UNDER AXIAL LOAD AND END MOMENT 112

FIGURE 52: CONVERGENCE ANALYSIS FOR CLAMPED–CLAMPED ISOTROPIC BEAM, WITH P=0, M_{ZZ} =0, H_2/H=0.3, AND L_2/L=0.4. 125
FIGURE 53: FUNDAMENTAL NATURAL FREQUENCY Λ^2 OF AN ISOTROPIC HOMOGENEOUS BEAM WITH CLAMPED-CLAMPED BOUNDARY CONDITION, M_{ZZ}/M_B=0.4 AND CENTRAL DELAMINATION LOCATED IN MID-PLANE H_2/H=0.5, VERSUS NORMALIZED AXIAL FORCE IN 'FREE MODE' MODEL FOR DIFFERENT VALUES OF L_2/L. 128
FIGURE 54: VARIATION OF THE FIRST AND SECOND NATURAL FREQUENCIES (Λ^2) WITH RESPECT TO NORMALIZED BUCKLING LOAD P/P_{CR} FOR H_2/H=0.3, M_{ZZ}/M_B=0.4 AND DIFFERENT VALUES OF L_2/L. ..129
FIGURE 55: TREND OF CHANGE IN FUNDAMENTAL NATURAL FREQUENCIES (Λ^2) WITH RESPECT TO NORMALIZED BUCKLING LOAD P/P_{CR} FOR BOTH CONSTRAINED AND FREE MODES WITH H_2/H=0.5, M_{ZZ}/M_B=0.4 AND DIFFERENT VALUES OF L_2/L. 130
FIGURE 56: FUNDAMENTAL NATURAL FREQUENCIES (Λ^2) WITH RESPECT TO NORMALIZED APPLIED END MOMENT M_{ZZ}/M_B FOR BOTH CONSTRAINED AND FREE MODES WITH H_2/H=0.5, P/P_{CR}=0.4 AND DIFFERENT VALUES OF L_2/L. 131
FIGURE 57: THE FIRST OPENING MODE SHAPE FOR A DELAMINATED BEAM WITH A CENTRAL DELAMINATION ON THE MID-PLANE USING 'FREE MODE' MODEL. 131
FIGURE 58: FIRST AND SECOND NATURAL FREQUENCIES (Λ^2) VERSUS NORMALIZED BUCKLING LOAD P/P_{CR} FOR H_2/H=0.3, M_{ZZ}/M_B=0.4 AND DIFFERENT VALUES OF L_2/L USING DFE METHOD. 133
FIGURE 59: PERCENTAGE OF FUNDAMENTAL NATURAL FREQUENCY ERROR FOR DFE AND FEM WITH M_{ZZ}=6.14MN.M AND P=1.23MN USING 5 ELEMENTS INCLUDING THE FOUR DIFFERENT CASES WITH CANTILEVER BOUNDARY CONDITION. 137
FIGURE 60: PERCENTAGE OF ERROR FOR CANTILEVER STEEL BEAM WITH P=1.23MN AND M_{ZZ}=0 USING 5 ELEMENTS. 137
FIGURE 61: DIFFERENCE OF LBDFE AND LBFEM METHODS, USING 5 ELEMENTS, WITH EXPERIMENTAL RESULTS FOR FUNDAMENTAL NATURAL FREQUENCY OF STEEL-RUBBER-STEEL SANDWICH BEAM [101]. 138

Nomenclature

$[K]$	Stiffness Matrix
$[M]$	Mass Matrix
A	Beam cross-sectional area (m^2)
b	Beam width (m)
E	Young's modulus (N/m^2)
F	Horizontal component of shear force (N)
G	Shear modulus (Pa)
H	Height of the beam (m)
I	Second area moment of inertia (m^4)
I_α	Mass moment of Inertia per unit length
I_P	Polar moment of inertia per unit length
J	Torsional constant (m^4)
K	Material coupled bending-torsion stiffness (N/m)
L	Length of the beam (m)
l	Element length (m)
$M(x)$	Moment function
M_b	Critical buckling moment ($N.m$)
M_{zz}	Applied end moment ($N.m$)
m	Mass per unit length ($\rho.A$)
N_f	Flexural shape function
N_t	Torsional shape function

P	Static axial force (N)
P^t	Perturbed axial force (N)
P_{cr}	Critical buckling load (N)
S	Vertical component of shear force (N)
$S(x)$	Shear force function
S_f	Transverse shear force (N)
t	Time (s)
W	Amplitude of bending displacement *(m)*
W_{INT}	Internal virtual work
W_{EXT}	External virtual work
W_f^k	Elemental work component corresponding to bending
W_t^k	Elemental work component corresponding to torsion
w	Bending displacement (m)
x	Distance variable along the axis of beam
α	Root of characteristic Equation
β	Root of the characteristic equation
Γ_r	Reference variable
γ	Coefficient to the governing differential equation of motion for torsion
Δ_f	Denominator of flexural shape functions
θ	Angle of twist amplitude
Λ	Coefficient of bending continuity equation
Λ^*	Coefficient of perturbation equation

λ	Eigenvalue
ξ	Local mapping coordinate (x/l)
ρ	Mass density (kg/m^3)
τ	Root of the characteristic equation
ϕ	Angle of twist
ω	Frequency of vibration (Hz)

1 Introduction

1.1 Overview

Vibrational analysis of beam-like structures is of great importance in aerospace engineering since vibration is one of the major causes of structural failure in this field and many important structures can be modeled as a simple beam or assemblies of beams. Based on the application of structures being studied, different geometries, loading and boundary conditions arise in modeling, which lead to a variety of different problems. A key example of these conditions is presence of pre-stress in structures subjected to axial force, end moment or both, which depend on its magnitude, can affect the dynamic behavior of structure significantly. There are many practical situations where pre-stress appears in the system. Helicopter and turbine blades, wing structures and rockets or missiles subjected to axial acceleration are some examples of these situations. End moments are commonly exerted on beams by the connections, which are expected to transmit various loads such as axial force, shear and moment between connecting members [1]. For example, welded connection behavior in structures is often semi-rigid with a resultant end moment upon the supporting members, beams, columns and plates, etc. [2], representing an example of a structure subjected to combined loading. Another good example of a structure subjected to combined end moment and axial force is a helicopter blade connected to a rotor by an inclined hinge. Other examples include, but not limited to, imperfect joints in beam-columns mainly used for framing or truss.

The governing differential equations of motion for any system can be found using Euler-Lagrange or Hamilton's equations [3]. For the cases that beam is subjected to end moment acting about the vertical axis (i.e., causing the in-plane or lead-lag bending), there will be a coupling between the differential equations of motion governing Flexural (Bending) and Torsional (Twist) vibrations. This

physically means that applying a vertical force to beam, in addition to bending displacement would also results in some angular displacement. Similarly a torsion torque causes both angular and bending displacements. Some other examples of bending-torsion couplings are composite beams with non-zero ply angle (i.e., material coupling), beams with a cross-section that its shear and geometric (mass) centers are non-coincident (i.e., geometric coupling), or composite beams exhibiting both couplings.

The vibrational analysis of a pre-stressed beam has been the focus of study over four decades, as columns and beams are continuously being used in a variety of engineering applications. Neogy and Murthy [4] carried out one of the earliest studies in this area and found first natural frequency of an axially loaded column for two different boundary conditions of pinned-pinned and clamped-clamped. Prasad *et al.* [5] introduced an approximate solution using Rayleigh-Ritz principles in an iterative form. Gallert and Gluck [6] investigated the effect of applied axial force on the lateral natural frequencies of a clamped-free beam with transverse restraint. Pilkington and Carr [7] also introduced an approximation for non-iterative solution form of rotating bars subjected to end moment and axial force. Wang et *al.* [8] used Galerkin's formulation in their study while Tarnai [9] investigated lateral buckling of beams hung at both ends with the more generalized variational technique. However, most of these works that study either uncoupled lateral vibration or coupled vibration of rotating beams. Later, Jensen and Crawley [10] studied the application of frequency determination techniques for cases that coupling is caused by warping of composite laminate. They also compared the results of Rayleigh-Ritz and partial Ritz methods with their experimental results. Joshi and Suryanarayan [11] developed a closed-form analytical solution for vibrational analysis of a beam subjected to both end moment and axial load. Later, they unified their solution for different boundary conditions [12] and next they developed an iterative method for coupled flexural-torsional vibration of initially stressed beams in general [13]. Mohsin and Sadek [14] and Banerjee and Fisher

[15] implemented Dynamic Stiffness Matrix (DSM) method for finding natural frequencies of an axially loaded beam. DSM was first developed by Kolousek [16] and [17] for an Euler-Bernoulli beam who later published it in a text book [18]. Since then this method has been taken further by many researchers [19-27].

In the recent years, with development of computers, there is an increasing interest among researchers in using computational methods in structural vibration analysis mainly because experimental methods are expensive and analytical solutions are only applicable for simple cases. Finite Element Method (FEM), as the most popular computational method in structural mechanics, has been extensively implemented by researchers [28-34]. In FEM element matrices are developed by assuming fixed shape functions. Usually, because of their ease of manipulation, Hermite cubic shape functions are used to predict beam elements lateral deformations, and result in an approximate solution including mass and static stiffness matrices. In 1998, Hashemi [35] introduced a new Dynamic Finite Element (DFE) formulation, that bridged gap between DSM and classic FEM. DFE formulation is based on the same procedure as conventional FEM but instead of fixed shape functions it implements frequency-dependent trigonometric shape functions, which results in a frequency dependent stiffness matrix. Unlike DSM, DFE is applicable for all the cases that FEM is applicable and has much higher rate of convergence in comparison with FEM. Since its introduction, DFE has been used for solving various problems of beam-like structures [36-43] including a work by Hashemi and Richard [36], in which they found coupled bending-torsion natural frequencies of an axially loaded beam with DFE and compared them with those found by classic finite element, DSM [15], and Vlasov's theory [37].

In the present study, the free vibration of pre-stressed slender beams, subjected to a constant axial load and end moment and various boundary conditions, is examined. Based on the Euler-Bernoulli bending and St. Venant torsion beam theories, the differential equations governing coupled flexural-

torsional vibrations and stability of a uniform, slender, isotropic, homogeneous, and linearly elastic beam, undergoing linear harmonic vibration, are first reviewed. The existing formulations are then briefly discussed and a conventional finite element method (FEM) is developed. Exploiting the MATLAB-based code, the resulting linear Eigenvalue problem is then solved to determine the Eigensolutions (i.e., natural frequencies and modes) of illustrative examples, exhibiting geometric bending-torsion coupling. Various classical boundary conditions are considered and the FEM frequency results are validated against those obtained from a commercial software (ANSYS) and the data available in the literature. A buckling analysis of the beam is also carried out to determine the critical buckling end moment and axial compressive force. Furthermore, the dynamic analysis of pre-stressed, bending-torsion coupled beams is revisited. The axially loaded beam is assumed to be slender, isotropic, homogeneous, and linearly elastic, exhibiting coupled flexural-torsional displacement caused by the end moment. Based on the Euler-Bernoulli bending and St. Venant torsion beam theories, the vibration and stability of such beams are explored. Using the closed-form solutions of the uncoupled portions of the governing equations as the basis functions of approximation space, the dynamic, frequency-dependent, interpolation functions are developed, which are then used in conjunction with the weighted residual method to develop the Dynamic Finite Element of the system. Having implemented the DFE in a MATLAB-based code, the resulting nonlinear eigenvalue problem is then solved to determine the coupled natural frequencies of illustrative beam examples, subjected to various boundary and load conditions. The proposed method is validated against limited available experimental and analytical data, those obtained from an in-house conventional Finite Element Method (FEM) code and FEM-based commercial software (ANSYS). In comparison with FEM, the DFE exhibits higher convergence rates and in the absence of end moment it produces exact results. Buckling analysis is also carried out to determine the critical end moment and compressive force for various load combinations.

1.2 Free vibration of layered beams

Applications of sandwich structures continue to expand and diversify mainly because of their attractive characteristics, namely high strength, buckling resistance, excellent thermal and acoustical insulation, ease of mass production, and easy repairability [44]. Due to the many advantages sandwich construction offers over traditional aerospace materials, the analysis of sandwich beams has been investigated by a large number of authors for more than four decades. Sandwich beam construction can also offer energy and vibration damping when a visco-elastic core layer is used. A typical setup could be two aluminium, steel, or composite face layers bonded to a honeycomb, corrugated, foam, or viscoelastic polymer core. However, such systems are not the focus of the current work.

The sandwich structure performance depends mainly on the properties of the core, adhesive, faces, and the geometrical shape of the core [45]. In the late 1960s, Di Taranto [45] and Mead and Marcus [46] performed investigation on the characteristics of viscously damped sandwich beams using classical methods to solve the governing differential equations of motion. In 1971, Ahmed [47] used FEM for a twisted sandwich beam with an elastic material as core. He compared performances of different formulations in determining the natural frequencies and mode shapes of different layer configurations. Later, more complex finite element models were developed by Baber *et al.* [48], Fasana and Marchesiello [49] and Sainsbury and Zhang [50]. Improvement on computational and analytical methods continued by Banerjee [51] and Howson and Zare [52], who used symbolic calculations to merge the coupled governing differential equations of sandwich beams and formed a single higher order equation, then solved it using DSM. Hashemi and his co-workers have also investigated the vibrations of sandwich configurations using DFE method. They used dynamic, frequency-dependent, trigonometric shape functions, derived from the solution of the uncoupled

equations to find element matrices for a three layered sandwich beam [53] and their results showed good agreement with those obtained from DSM [51]. They also investigated the free vibration of carved beams in other studies (see, e.g., [54], [55]). However, to the best of author's knowledge, the dynamics analysis of flexible pre-stressed sandwich beams has not been presented in the open literature.

1.3 Free vibration of fiber-reinforced laminated composite beams

There are many situations arising in various manufacturing sectors ranging from shipbuilding to aerospace, where materials or components built up in layers of composite material are used. The ever increasing application of such layered structural elements is primarily due to their many attractive features such as high specific stiffness, high specific strength, formability into complex shapes, longer fatigue life, designable stiffness, lighter density, good buckling resistance, corrosion resistance and higher strength, to name a few (see, Jones [56] and Berthelot [57], etc.). Changing the ply orientation and stacking sequence can lead to alteration of the composite material stiffness characteristics. For ply angles other than 0 and 90˚ bending and torsion deformations are coupled and this coupling will predominantly influencing the natural frequencies and modes shapes of free vibration (Hashemi and Borneman [58] and [59]). Abramovich and Livshits [60], Jaehong and Kim [61], Chen *et al.* [62] and Jung *et al.* [63] simplified a composite wing as a beam in their models and investigated the coupling between bending and torsion in free vibration using various numerical technics. They used numerical models based on Rayleigh-Ritz, Galerkin and Finite FEM as well as fixed interpolation functions to evaluate element matrices. In order to find element mass and stiffness matrices, FEM is commonly used as it provides a general systematic approach to formulate them.

Next, the natural frequencies and modes of free vibration can be found by solving the resulting linear eigenvalue problem from matrix form of the equations of motion.

Modeling an isotropic metallic beam by finite element method is fairly simple but the composite material characteristics bring complexity to system. This complexity in addition to the time consuming nature of FEM models for meshing and solving the equations, have led many researchers into trying analytical and semi-analytical approaches for early stages of design and optimization. Dynamic Stiffness Matrix method can be employed to determine the free vibration response of a structure. The DSM was first developed by Kolousek [18] for isotropic Euler-Bernoulli beams and since been refined continuously. Banerjee and his partners extended this method to the vibration analysis of different isotropic and composite beam models. The DSM for a uniform Euler-Bernoulli beam was developed by Banerjee and Williams [64] and was later extended to the Timoshenko beam theory [26]. Banerjee [65] further extended the model to include axial force for many different composite beams. In all of these works, the DSM models for composite beams are based on the exact member theory [66], limited to simple geometries and special cases. Hashemi and his co-workers have also investigated the vibrations of layered composite beam configurations using DFE method (see, e.g., [67], [68], [58] and [59]). However, to the best of author's knowledge, the dynamics analysis of flexible pre-stressed composite beams has not been reported in the open literature.

1.4 Delaminated and defective layered composite beams

Despite all the advantages composite material have over their metallic/isotropic counterparts, they are vulnerable to a wide range of defects and damage. The most common amongst different types of defects that might happen during service is delamination which usually develops as a result of manufacturing imperfections or impact [69]. A reduction in the system's stiffness, resulting from

delamination, will affect certain design parameters, such as natural frequencies and modes. Natural frequencies decrease as a direct result of the stiffness reduction, which may cause resonance if the reduced frequency is close to the working frequency. It is therefore important to understand the influence of the delamination on the vibration characteristics of the structures. The delaminated sub-laminate generally exhibits new vibration modes and frequencies that depend on the number, size and location of the delamination.

Among several experimental methods developed to predict the onset, size and growth of delamination (as a failure mode in layered constructions) is the use of acoustic emission (AE) sensors, where different levels of amplitude signals emitted by the materials can be monitored [70]. Using this technique, continuous experimental monitoring of damage is possible. The acoustic emission has also been proven a viable and effective tool for identifying damage and distinguishing damage types in self-reinforced polyethylene composites [71]. More recently, further research has also been carried out to apply neural networks and unsupervised learning techniques to the data set of acoustic emission signals [72], leading to successful classification of AE patterns caused by different damage mechanisms in carbon-reinforced composites (delamination and matrix cracking). The time-domain stability of vibrating delaminated systems has also been studied and it has shown that time-dependent normal forces in the delaminated segments do not influence the global free vibration frequencies but may contribute to localized buckling [73 and 74]. Instability and critical dynamic forces can then be predicted, allowing for study of the onset of delamination opening.

The vibration modelling and analysis of delaminated layered structural elements has been a topic of interest for many researchers. One of the earliest models for vibration analysis of composite beams with delamination was proposed by Kulkarni and Fredericks [75]. They investigated a one-dimensional (1D) problem with a single delamination and considered a circular cylindrical shell with a circumferentially symmetric delamination crack of a small length at the middle surface. In their

analysis, flexural rigidity of the delamination region has been taken as the sum of the flexural rigidities of the delaminated layers. The frequencies computed through the presented analysis were found to be considerably lower than the experimental results. Ramkumar et al. [76] analyzed the vibration characteristics of through the width delaminated composite beams. They modeled a defective beam with one through-the-width delamination by simply using four Timoshenko beams connected at delamination edges. Natural frequencies and mode shapes were then evaluated by solving the system's boundary eigenvalue problem and, once again, the predicted natural frequencies were consistently lower than those measured experimentally. Authors attributed this discrepancy to the contact between the delaminated free surfaces during vibrations, suggesting that the inclusion of the contact effect might improve the analytical prediction. It was later discovered that the free mode under-predicted natural frequencies for off mid-plane delamination due to unrestricted penetration of the beams into each other. Wang *et al.* [77] developed a theoretical model to investigate the effect of through width split on free vibration characteristics of isotropic beams. They used the Euler beam theory to calculate natural frequencies by assuming that each beam segment vibrates freely without touching each other. However, they improved the analytical solution, found to be closer to experimental results, by including the coupling between flexural and axial vibrations of the delaminated sub-laminates. Mujumdar and Suryanarayan [78] proposed a solution for constrained mode to prevent opening modes predicted by Wang et al. [77]. Their solution was based on the assumption that the delaminated beam segments have identical transverse displacements. They developed a delamination model, known as the ‘constrained mode’ model to predict vibration behavior more accurately for off mid-plane delamination configurations. On the other hand, the constrained mode implementation results in additional system constraints, which increase system stiffness and sometimes causes over-prediction of natural frequencies. Furthermore, capturing opening delamination modes seen in experimental analysis [79] and [80], is not possible using the

constrained model. Tracy and Pardoen [81] also used the constrained model to assess the effect of delamination on natural frequency of symmetric laminated Euler beams containing mid-plane delamination. Their frequency results were compared with those obtained from experiments and the finite element method. Based on both the classical and high-order shear deformation beam theories, Nagesh and Hanagud [82] used the finite element method to study the effects of delamination on the system's natural frequencies. Shen and Grady [83] performed experiments and observed the presence of opening modes, undetected by the constrained model. They also investigated the effects of delamination on the natural frequency and mode shape of composite laminated beams by using the Galerkin method. Stamos *et al.* [84] presented a delaminated composite beam model exhibiting coupling between longitudinal and bending motion. They also suggested an inverse method to determine position and size of delamination based on the degradation of the first two natural frequencies. Chen [85] investigated free vibrations relative to the static pre-buckled and post-buckled states for delaminated isotropic plates using a constrained model and showed that the vibrational characteristics in these two states were quite different. Chen *et al.* [86] developed an analytical model for free vibration of a delaminated composite laminate in the pre-buckled state and presented a new constrained model, including both effects of compressive force and bending-extension coupling. To validate their analytical model they have also performed experiments. Della and Shu ([87] and [88]) reported an analytical solution method and Erdelyi and Hashemi [89] used Dynamic Stiffness Matrix (DSM) and presented a FEM-based novel assembly technique [90] to investigate the behavior of a delaminated beam and compared their results with Wang et al. [77] and Lee [91]. Liu and Shu [92] implemented semi-analytical method of Joshi and Suryanarayan [12] to investigate the coupled vibration of a single delaminated beam subjected to static end moment and axial force and showed that the effects of delamination on reducing natural frequencies, critical buckling load and critical moment for lateral instability are aggravated by the presence of static end

moment. In a recent work, Szekrényes [93] performed stability analysis on axially loaded delaminated composite beams undergoing coupled flexural–longitudinal vibration. Timoshenko beam theory was first applied to solve the problem, then by reducing the model, the corresponding Euler–Bernoulli solution was presented, considering both free and constrained models. In addition, the equality of axial forces in the top and bottom beams was derived and shown in an exact way. Also, the continuity of the effective bending moments was related to the equilibrium equations and it was also concluded that delamination buckling can take place if the normal force is compressive in one of the half-periods of the vibration and reaches a critical value [93].

The conventional Finite Element Method (FEM) has a long, well-established history and with the advent of digital computers is commonly used for structural analysis. The FEM is a general and systematic approach to formulate the element matrices for a given system and is easily adaptable to complex systems, such as non-uniform geometry, often modeled as a stepped, piecewise-uniform configuration. Exploiting polynomial interpolation (shape) functions, the FEM leads to constant element mass and stiffness matrices, and ultimately a linear eigenvalue problem from which the natural frequencies and modes of the system can be readily extracted. The FEM method for a single beam can be modified to accurately model delaminated multi-layer beams. Among others, Lee [91] used theory to investigate the free vibration of delaminated beams. In the recent years, layered, sandwich and composite elements have been integrated in certain commercial software and are used to analyze the vibration of composite structures. However, modelling a delaminated configuration in commercial software packages such as ANSYS in not straight forward and can involve cumbersome, complex, time-consuming and error-prone processes. It requires manual model creation, involving the use of, for example, Multipoint Constraint Rigid Link (ANSYS element type MPC-184) to enforce the displacement and slope continuity at the edges of delamination region [94]. Recently, Erdelyi and Hashemi used FEM, DSM and DFE to investigate the free vibration of single

and multiple delaminated beams (see, e.g., [89], [90] and [95]). However, to the best of author's knowledge, the dynamics analysis of flexible pre-stressed delaminated beams has not been reported in the open literature.

1.5 Motivation

The study of layered pre-stressed beams composed of advanced engineered materials, such as composites, is imperative for aerospace applications. As new materials are invented and new applications are introduced, analysis of these materials and new imposed conditions must follow, before they can be comfortably used in industry. To prevent or minimize damage to composite structures, investigation into behaviour of both intact and defective configurations is necessary. This research is focused towards the vibrational behaviour of pre-stressed defective beams subjected to end moment and axial force, exhibiting coupled bending-torsion behaviour. Conventional Galerkin-type Finite Element Method (FEM) as well as frequency-dependent Dynamic Finite Element (DFE) formulations are developed and used to evaluate the free vibration modes and natural frequencies of various pre-stressed beam configurations, including isotropic, layered, and composite beams. The investigation is also extended to the free vibration analysis of delaminated layered beam configurations.

This research is firstly motivated by the fact that the thorough information on the vibrational behaviour of various pre-stressed beam configurations are scarce, if not non-existing. The motivation for development and use of the DFE methodology in this research is that the technique has shown generally to have higher accuracy and convergence rates in the calculated natural frequencies and modes of beam structures when compared to other existing methods, and more specifically for cases with a higher degree of complexity (e.g., combined material and geometric coupling). The

development and implementation of conventional and layer-wise FEM formulations in the present study are to establish benchmark for comparison and validation of other methods, as well as to pave the road for the development of DFE formulations. The DFE has proven to be an excellent tool in the preliminary free vibration analysis of pre-stressed and composite beams.

1.6 Objectives

The general objective of this thesis is to develop and test a number of new highly convergent dynamic composite (frequency dependent) elements to more accurately capture the free vibrational response in defective layered sandwich and composite beams. The list of specific objectives includes:

1) To develop the coupled differential equations of bending and torsion for pre-stressed, uniform, sandwich and layered composite beams from Hamilton principles.
2) To provide FEM and DFE model for the free vibration of pre-stressed beams.
3) To develop a novel numerical method for modeling the free vibration of pre-stressed sandwich and composite beams using both FEM and DFE.
4) To introduce numerical solution for defective (delaminated) pre-stressed beams.
5) To validate the numerical models with limited existing experimental results and those obtained from commercial software.
6) To investigate the convergence rates of numerical models and introduce the most efficient method for predicting natural frequencies and mod shapes of free vibration.

1.7 Thesis organization

In Chapter 2, the mathematical model is initiated by developing the equations of motion for a simple isotropic beam subjected to axial force and end moment undergoing coupled bending-torsion vibration. Next, Galerkin-type weighted residual formulation is applied to develop the integral form of these equations and to obtain FEM solution of the problem. Later, the frequency dependent shape functions as well as solutions of uncoupled equations are used to find DFE formulation. Further, the numerical results for simple uniform beams without any pre-stress effect as well as beams with only applied axial force are obtained after finding the optimum number of elements using the grid convergence study by both FEM and DFE and they are validated by comparison with existing results from literature. Next, the natural frequencies for beams subjected to both axial force and end moment are found and compared with ANSYS results or with existing literature results where available. The effect of increase or decrease in axial tensile or compressive force as well as end moment on the vibrational behavior and fundamental natural frequencies of uniform isotropic beams are also investigated. Finally, the results are discussed and in conclusion section and the rate of convergence of the two DFE and FEM methods are comparted.

In Chapter 3, the natural frequencies of two-layered and three-layered sandwich beams subjected to end moment and axial force are first found using homogenization method and by finding properties of an equivalent single-layer beam. Next, in order to further improve the accuracy of the solution, a new method is implemented which considers each layer as a separated beam and then applies constraints for their motion. The solution has also been extended for different material and layups including: metal sandwich, glass-epoxy, metal-rubber-metal and GLARE. For all the cases numerical results are obtained using both FEM and DFE and each problem is modeled in ANSYS for validation purposes. Where available, the results are also compared with exact analytical solution

or experimental results. At the end of this Chapter, the numerical results are discussed and concluding remarks are made.

Chapter 4 is dedicated to development of numerical models for free vibration analysis of pre-stressed composite beams with ply angle between 0º and 90º with applied axial force and end moment. The ply angles other than 0º and 90º create another coupling term between bending and torsion equations of motion in addition to the coupling term caused by end moment. This double coupling effect is modeled using both FEM and DFE method and the results are validated and discussed in the numerical test section. At the end of this chapter, a comparison between the suggested models is done and a discussion on the usefulness of these methods is presented.

In Chapter 5, a mathematical model for free vibration analysis of single delaminated beams undergoing bending-torsion coupling is made, using traditional finite element technique as well as dynamic finite element method. The Galerkin weighted residual method is applied to convert the coupled differential equations of motion into to a discrete problem. The linear Eigenvalue problem resulting from the discretization along the length of the beam is solved to determine the natural frequencies and mode shapes of free vibration. Both 'free mode' and 'constrained mode' models are considered in formulation and it is shown that the continuity (both kinematic and force) conditions at delamination tips, in particular, play a large role in formulation of 'free mode' model. Current trends in the literature are critically examined, and insight into different types of modeling techniques and constraint types are introduced. In addition, the data previously available from a commercial finite element suite are also utilized to validate the natural frequencies of the systems analyzed here. Followed by, general concluding remarks on the usefulness of the presented theories.

Finally, main contributions of this study are listed and a general conclusion is made in Chapter 6, considering all the presented formulations including a comparison between accuracy and

convergence rate of different formulations for each model. Possible future works, as natural extension of present study, are then introduced at the end of this chapter, followed by list of author's publications.

2 Free vibration of pre-stressed isotropic beams

2.1 Development of governing differential equations

Consider a linearly elastic, homogeneous, isotropic beam subjected to an end moment, M_{zz}, about z-axis and an axial load, P, undergoing linear vibrations. Figure 1 depicts the schematic of the problem. Equations of motion for a beam subjected to axial force and end moment, and undergoing coupled Bending (about Y axis) and Torsion (about X axis) vibrations can be developed by defining an infinitesimal element (Figure 2), and by using the following assumptions:

1. The beam is made of a linearly elastic material;

2. The displacements are small;

3. The stresses induced are within the limit of proportionality;

4. The cross section of the beam has at least one axis of symmetry;

5. The transverse cross sections of the beam remain plane during bending;

6. The cross sectional dimensions of the beam are small compared to the span;

7. The beam's torsional rigidity (GJ) is assumed to be very large compared with its warping rigidity ($E\Gamma$), and ends are free to warp; i.e., state of uniform torsion.

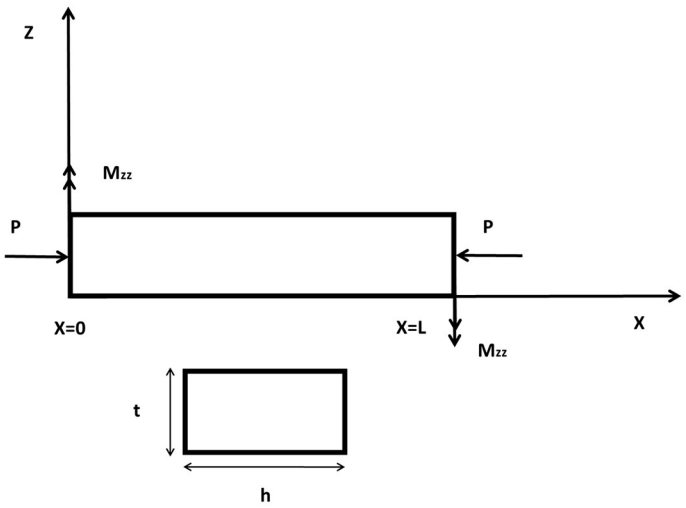

Figure 1: Schematic and coordinate system of the problem.

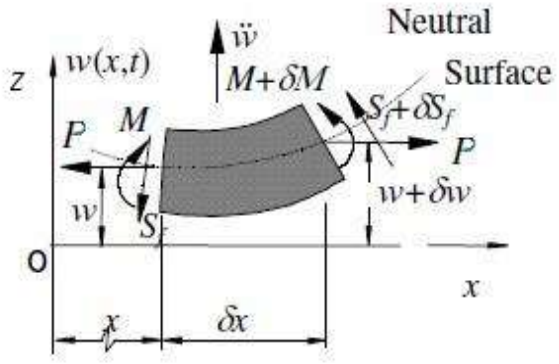

Figure 2: Infinitesimal element of a beam subjected to axial force and end moment.

Let us replace the transverse shearing force S_f with its components, S in the lateral direction and F in the longitudinal direction. Here w represents lateral displacement along z-axis, E is young modulus, I is the minimum second area moment of inertia of the beam's cross-sectional area (with respect to y-axis, in this case), M_{zz} is applied end moment and P is applied axial force. The density is represented by, ρ, and the cross-sectional area of the beam is denoted by, A. Summing the moments on the infinitesimal element and equating to zero gives:

$$(M + \delta M) - M + S(\delta x) + F(\delta w) + P(\delta w) + M_{zz}\sin(\delta\phi) = 0, \tag{1}$$

But F(dw) being a product of two small dynamic terms is negligible. Also, $\delta\phi$ is infinitesimal so $\sin(\delta\phi)=\delta\phi$ and as δx is also infinitesimal, this gives:

$$S = -\frac{\partial M}{\partial x} - P\frac{\partial w}{\partial x} - M_{zz}\frac{\partial \phi}{\partial x}. \tag{2}$$

The net elastic action in the positive lateral direction is:

$$-S + (S + \delta S) = \delta S, \tag{3}$$

By using Equation 2:

$$\delta S = \delta\left(-\frac{\partial M}{\partial x} - P\frac{\partial w}{\partial x} - M_{zz}\frac{\partial \phi}{\partial x} \right)$$
$$= -\frac{\partial^2 M}{\partial x^2}\delta x - P\frac{\partial^2 w}{\partial x^2}\delta x - M_{zz}\frac{\partial^2 \phi}{\partial x^2}\delta x. \quad (4)$$

From mechanics of material one can write:

$$M = EI\frac{\partial^2 w}{\partial x^2}. \quad (5)$$

Using Equation 4, Expression 5 can be re-written as:

$$\delta S = -\frac{\partial^2}{\partial x^2}\left(EI\frac{\partial^2 w}{\partial x^2} \right)\delta x - P\frac{\partial^2 w}{\partial x^2}\delta x - M_{zz}\frac{\partial^2 \phi}{\partial x^2}\delta x. \quad (6)$$

Since there are no external dynamic forces, this is the net lateral force. Applying Newton's second law in the lateral direction we get:

$$\delta S = (\rho A \delta x)\frac{\partial^2 w}{\partial t^2}. \quad (7)$$

By substitution of Equation 7 in 6:

$$\frac{\partial^2}{\partial x^2}\left(EI\frac{\partial^2 w}{\partial x^2} \right) + P\frac{\partial^2 w}{\partial x^2} + M_{zz}\frac{\partial^2 \phi}{\partial x^2} + (\rho A)\frac{\partial^2 w}{\partial t^2} = 0. \quad (8)$$

This is the partial differential equation governing the lateral vibration of an Euler-Bernoulli beam subjected to axial force and end moment. For an isotropic, uniform beam this reduces to the following form:

$$EI\frac{\partial^4 w}{\partial x^4} + P\frac{\partial^2 w}{\partial x^2} + M_{zz}\frac{\partial^2 \phi}{\partial x^2} + (\rho A)\frac{\partial^2 w}{\partial t^2} = 0. \quad (9)$$

Using Newton's second law for torsion one can write:

$$T = (\rho I_P)\frac{\partial^2 \theta}{\partial t^2}, \tag{10}$$

Governing differential equation of torsional vibration can be developed following a procedure similar to Expressions (1 through 8), which for uniform beam can be written in the following form:

$$GJ\frac{\partial^2 \theta}{\partial x^2} + \frac{PI_P}{A}\frac{\partial^2 \theta}{\partial x^2} + M_{zz}\frac{\partial^2 w}{\partial x^2} - \rho I_P \frac{\partial^2 \theta}{\partial t^2} = 0. \tag{11}$$

where θ is the torsional twist about x-axis, G is shear modulus, J is torsion constant of the cross-section, and I_p represents beam's polar moment of inertia.

So the coupled governing differential equations for the free vibration of a uniform Euler-Bernoulli beam subjected to axial force and end moment are:

$$EIw'''' + Pw'' + M_{zz}\theta'' + \rho A\ddot{w} = 0, \tag{12}$$

$$GJ\theta'' + \frac{PI_P}{A}\theta'' + M_{zz}w'' - \rho I_P\ddot{\theta} = 0, \tag{13}$$

where $()'$ is derivative with respect to x (displacement) and $(\dot{})$ denotes derivative with respect to t (time). In order to separate variables t and x, harmonic motion assumption is used by following definitions for displacements w and θ:

$$w(x,t) = W\sin(\omega t), \tag{14}$$

$$\theta(x,t) = \theta\sin(\omega t), \tag{15}$$

where ω denotes frequency. W and θ are flexural and torsion displacement amplitudes, respectively. Substituting equations 14 and 15, into equations 12 and 13 leads to:

$$EIW'''' + PW'' + M_{zz}\theta'' - \rho A\omega^2 W = 0, \tag{16}$$

$$GJ\theta'' + PI_P\theta'' + M_{zz}W'' + \rho I_P A\omega^2\theta = 0. \tag{17}$$

2.2 Classical finite element method (FEM)

Using Galerkin weighted residual formulation, the integral forms of the governing differential equations (16, 17) are written as:

$$\bar{W}_f = \int_0^L \delta W(EIW'''' + PW'' + M_{zz}\theta'' - \rho A\omega^2 W)dx = 0, \tag{18}$$

$$\bar{W}_t = \int_0^L \delta\theta(GJ\theta'' + \frac{PI_P}{A}\theta'' + M_{zz}W'' + \rho I_P\omega^2\theta)dx = 0, \tag{19}$$

where δW and $\delta\theta$ are weighting functions associated with flexure and torsion, respectively. Performing integrations by parts twice on Equation 18 and once on Equation 19 leads to the weak integral form of the governing equation, written as:

$$\begin{aligned}\bar{W}_f = &\int_0^L (EIW''\delta W'' - PW'\delta W' + M_{zz}\theta'\delta W' - \rho A\omega^2 W\delta W)dx \\ &+[(EIW''' + PW' + M\theta')\delta W]_0^L - [(EIW'')\delta W']_0^L = 0,\end{aligned} \tag{20}$$

$$\begin{aligned}\bar{W}_t = &\int_0^L (GJ\theta'\delta\theta' + \frac{PI_P}{A}\theta'\delta\theta' + M_{zz}W'\delta\theta' - \rho I_P\omega^2\theta\delta\theta)dx \\ &-[(GJ\theta' + \frac{PI_P}{A}\theta' + MW')\delta\theta]_0^L = 0.\end{aligned} \tag{21}$$

The above expressions (20, 21) also satisfy the principle of virtual work which is:

$$\bar{W} = \bar{W}_{INT} - \bar{W}_{EXT} = 0, \tag{22}$$

where for free vibrations,

$$\bar{W}_{EXT} = 0. \tag{23}$$

Therefore,

$$\bar{W}_{INT} = \bar{W}_f + \bar{W}_t, \tag{24}$$

where $\bar{W}$ is total virtual work, $\bar{W}_{INT}$ is internal virtual work and $\bar{W}_{EXT}$ is external virtual work, and $\bar{W}_f$ and $\bar{W}_t$ denote virtual work components associated with flexure and torsion, respectively. Considering expressions of shear force, *S(x)*, bending moment, *M(x)*, and torsional torque, *T(x)*:

$$M(x) = -EIW'', \tag{25}$$

$$S(x) = EIW''' + M_{zz}\theta' + PW', \tag{26}$$

$$T(x) = GJ\theta' + \frac{PI_P}{A}\theta' + M_{zz}W'. \tag{27}$$

It can be shown that for all the boundary conditions the boundary terms of equations 20 and 21 will be equal to zero. For example, zero displacements, $w=w'=\Psi=0$, and virtual displacements, $\delta w=\delta w'=\delta\Psi=0$, at the clamped end ($x=0$) (i.e., where the displacements are imposed), and null resultant shear force, $S(x)$, bending moment, $M(x)$, and torsional moment, $T(x)$, at the free end ($x=L$), etc. As a result, the boundary terms in expressions 20 and 21 vanish for all boundary conditions. Then, the system is discretized along the beam span by a certain number of 2-node elements (see Figure 3) such that:

$$\bar{W} = \bar{W}_{INT} = \sum_{k=1}^{No.ofElements} \bar{W}^k = \sum_{k=1}^{No.ofElements} \bar{W}_f^k + \bar{W}_t^k. \tag{28}$$

where $\bar{W}_f^k$ is element flexural virtual work, $\bar{W}_t^k$ is element torsional virtual work and they are with following expressions:

$$\bar{W}_f^k = \int_{x_j}^{x_{j+1}} (EIW''\delta W'' - PW'\delta W' + M_{zz}\theta'\delta W' - \rho A\omega^2 W\delta W)dx \tag{29}$$

$$\bar{W}_t^k = \int_{x_j}^{x_{j+1}} (GJ\theta'\delta\theta' + \frac{PI_P}{A}\theta'\delta\theta' + M_{zz}W'\delta\theta' - \rho I_P\omega^2\theta\delta\theta)dx \tag{30}$$

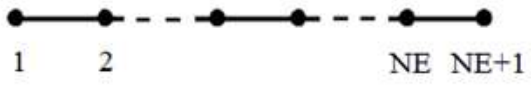

Figure 3: Discretized domain along the beam span.

Using classical finite element formulation and exploiting cubic basis functions of approximation space for bending displacement and linear approximation for torsion displacement, the resulting cubic Hermite interpolation (shape) functions for bending are written in the following form [96]:

$$N_1(x) = \frac{2x^3}{l^3} - \frac{3x^2}{l^2} + 1,$$

$$N_2(x) = \frac{x^3}{l^2} - \frac{2x^2}{l} + x, \tag{31}$$

$$N_3(x) = \frac{-2x^3}{l^3} + \frac{3x^2}{l^2},$$

$$N_4(x) = \frac{x^3}{l^2} - \frac{x^2}{l},$$

and the linear shape functions for torsional displacement are [96]:

$$L_1(x) = 1 - \frac{x}{l}, \tag{32}$$

$$L_2(x) = \frac{x}{l},$$

where l is the element length. Introducing the approximate flexural and torsional displacements expressed using interpolation functions 29 and 30 back into Expressions 20 and 21 results in the element matrices.

The approximate flexural and torsional displacements are expressed as:

$$W(x) = \begin{bmatrix} N_1 & N_2 & N_3 & N_4 \end{bmatrix} \begin{Bmatrix} W_1 & W_1' & W_2 & W_2' \end{Bmatrix},$$

and,

$$\theta(x) = \begin{bmatrix} L_1 & L_2 \end{bmatrix} \begin{Bmatrix} \theta_1 & \theta_2 \end{Bmatrix}$$

The resulting element mass matrix is developed as follows:

$$[m]^k = \begin{bmatrix} \frac{156ml}{420} & \frac{22ml^2}{420} & 0 & \frac{54ml}{420} & \frac{-13ml^2}{420} & 0 \\ & \frac{4ml^3}{420} & 0 & \frac{13ml^2}{420} & \frac{-3ml^3}{420} & 0 \\ & & \frac{\rho I_P l}{3} & 0 & 0 & \frac{\rho I_P l}{6} \\ & & & \frac{156ml}{420} & \frac{-22ml^2}{420} & 0 \\ & Sym. & & & \frac{4ml^3}{420} & 0 \\ & & & & & \frac{\rho I_P l}{3} \end{bmatrix}, \tag{33}$$

where m represents the mass per unit length (pA). First term of bending equation will result in an uncoupled four by four matrix, as follows:

$$[k]_{bending} = \begin{bmatrix} \frac{12EI}{l^3} & \frac{6EI}{l^2} & \frac{-12EI}{l^3} & \frac{6EI}{l^2} \\ & \frac{4EI}{l} & \frac{-6EI}{l^2} & \frac{2EI}{l} \\ & Sym. & \frac{12EI}{l^3} & \frac{-6EI}{l^2} \\ & & & \frac{4EI}{l} \end{bmatrix}. \tag{34}$$

Second term of bending equation will result in the following geometric stiffness matrix, associated with the axial force, written as:

$$[k]_g = P\begin{bmatrix} \frac{6}{5l} & \frac{1}{10} & \frac{-6}{5l} & \frac{1}{10} \\ & \frac{2l}{15} & \frac{-1}{10} & \frac{-l}{30} \\ & & \frac{6}{5l} & \frac{-1}{10} \\ & Sym. & & \frac{2l}{15} \end{bmatrix}, \tag{35}$$

and the first and second terms in the torsion equation (21) produce the following matrix:

$$[k]_{torsion} = \left(\frac{GJ}{l} + \frac{PI_P}{Al}\right)\begin{bmatrix} 1 & -1 \\ -1 & 1 \end{bmatrix}. \tag{36}$$

From third term of bending and third term of torsion equations, respectively, the bending–torsion and torsion–bending coupling stiffness matrices are generated (see Expressions 35 and 56 below). All the previous matrices are uncoupled matrices as they are generated from uncoupled terms in bending and torsion equations, but these latter two include coupling terms resulting from coupling terms in the equations. As can be seen, in the equations, coupled terms are the terms related to moment M_{zz}. This physically means that the coupling nature of vibration is a result of end moment and not axial force. The coupling matrices are as follows:

$$[k]_{BT} = \frac{M_{zz}}{l}\begin{bmatrix} 1 & 0 & -1 & 0 \\ -1 & 0 & 1 & 0 \end{bmatrix}, \tag{37}$$

$$[k]_{TB} = \frac{M_{zz}}{l}\begin{bmatrix} 1 & -1 \\ 0 & 0 \\ -1 & 1 \\ 0 & 0 \end{bmatrix}. \tag{38}$$

The final element stiffness matrix is sum of all the stiffness matrices:

$$[k]^k = \begin{bmatrix} \frac{12EI}{l^3} - \frac{6P}{5l} & \frac{6EI}{l^2} - \frac{P}{10} & \frac{M_z}{l} & \frac{-12EI}{l^3} + \frac{6P}{5l} & \frac{6EI}{l^2} - \frac{P}{10} & \frac{-M_z}{l} \\ & \frac{4EI}{l} - \frac{2Pl}{15} & 0 & \frac{-6EI}{l^2} + \frac{P}{10} & \frac{2EI}{l} + \frac{Pl}{30} & 0 \\ & & \frac{GJ}{l} + \frac{PI_P}{Al} & \frac{-M_z}{l} & 0 & \frac{-GJ}{l} - \frac{PI_P}{Al} \\ & Sym. & & \frac{12EI}{l^3} - \frac{6P}{5l} & \frac{-6EI}{l^2} + \frac{P}{10} & \frac{M_z}{l} \\ & & & & \frac{4EI}{l} - \frac{2Pl}{15} & 0 \\ & & & & & \frac{GJ}{l} + \frac{PI_P}{Al} \end{bmatrix} \tag{39}$$

As the next step, the above element stiffness and mass matrices are assembled to form the global stiffness and mass matrices. Finally, once the boundary conditions are applied, the equations 20 and 21 will form a linear Eigenvalue problem in the following form:

$$\langle \delta W_n \rangle \left(K - \omega^2 M \right) \{ W_n \} = 0, \tag{40}$$

where K stands for the global stiffness matrix, and M is global mass matrix. This Eigenvalue problem is solved using a code developed in MATLAB. The code gives the natural frequencies and also generates mode shapes by extracting data from corresponding Eigenvectors.

2.3 Finite element numerical results

The following properties are chosen for case study. Young modulus E=200GPa, density ρ=7800kg/m^3 (steel), beam length of 8m, width of 0.4m and depth of 0.2m. In order to optimize the number of elements, a convergence study (depicted in Figure 4) was first carried out. The error is found based on the exact values found from analytical closed form solution by Joshi and Suryanarayan [13]. The number of elements to have a reasonable accuracy is 40 with error less than 0.005%.

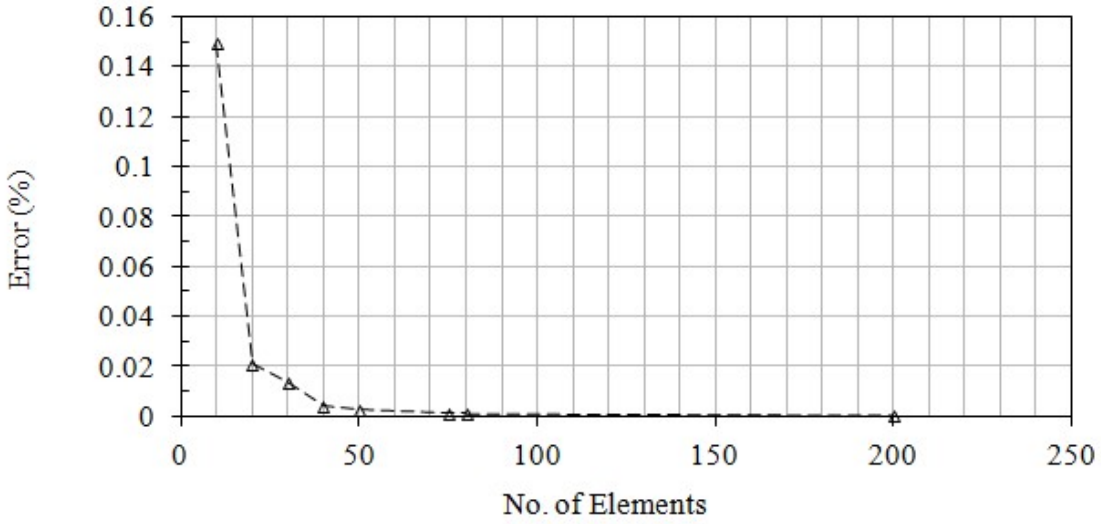

Figure 4: Percentage of error versus number of elements representing the convergence rate of FEM method for fundamental frequency.

Table 1 shows the results for the first three natural frequencies for various boundary conditions. Here c-f stands for clamped-free, p-p stands for pinned-pinned, c-c stands for clamped-clamped and p-c stands for pinned-clamped. In Table 1 there is no difference between the results as the accuracy of FEM using 40 elements is high for the first four natural frequencies. For the fifth natural frequency the error is 0.002 percent.

Table 1: Comparison between the analytical [97] and FEM results for the first three natural frequencies with P=0 and M_{zz}= 0.

Boundary Condition	Natural Frequencies (Hz)					
	Mode 1		Mode 2		Mode 3	
	Exact [97]	FEM	Exact [97]	FEM	Exact [97]	FEM
C - F	2.556	2.556	15.96	15.96	44.86	44.86
C - C	16.27	16.27	44.86	44.86	87.97	87.97
P - P	7.175	7.175	28.72	28.72	64.63	64.63
P - C	11.21	11.21	36.36	36.36	75.61	75.61

A pre-stressed model is also generated and analyzed using commercial software ANSYS to simulate the problem. SOLID-186 is used as element type, which is a 20-node element with six degree of freedom per node. Table 2 illustrates the comparison between 40 element-model created in ANSYS and FEM results for first natural frequency of cantilevered beam with three different loading conditions. Considering the buckling analysis that has been done, the values of these loadings are selected within the range of allowable axial force and end moment with reasonable intervals to almost cover the entire range. As can be seen from Table 1 and Table 2, FEM results are closer to the exact results, compared to the ANSYS simulation. This could be due to the shear and warping effect of the 3D element (SOLID-186) used in ANSYS that were not accounted for in the code developed in MATLAB based on present formulation. More details on the ANSYS model and geometry is presented in Appendix A.

Table 2: Comparison between ANSYS and FEM results of first natural frequency with cantilever boundary condition, for three different loading conditions.

C-F	End Moment					
	0 (MN.m)		6.14 (MN.m)		9.21 (MN.m)	
	Fundamental Frequency (Hz)					
Force (MN)	ANSYS	FEM Code (40 elements)	ANSYS	FEM Code (40 elements)	ANSYS	FEM Code (40 elements)
0	2.555	2.556	2.241	2.234	1.749	1.727
0.62	2.883	2.884	2.620	2.614	2.233	2.216
1.23	3.168	3.169	2.939	2.934	2.614	2.600
1.85	3.421	3.422	3.217	3.213	2.934	2.922

Table 3 through Table 5 show the results for the fundamental frequency for different combinations of tensile force and end moment for the c-c, p-p and p-c boundary conditions, respectively.

Table 3: Fundamental frequency for clamped-clamped boundary condition when force and end moment are applied.

C-C	End Moment (MN.m)		
	0	6.14	9.21
Force (MN)	FEM Fundamental Frequency (Hz)		
0	16.266	16.141	15.984
0.62	16.413	16.290	16.134
1.23	16.559	16.437	16.283
1.85	16.703	16.582	16.430

Table 4: Fundamental frequency for pinned-pinned boundary condition when force and moment are applied.

P-P	End Moment (MN.m)		
	0	6.14	9.21
Force (MN)	FEM Fundamental Frequency (Hz)		
0	7.175	6.947	6.651
0.62	7.440	7.220	6.935
1.23	7.695	7.483	7.208
1.85	7.942	7.736	7.471

Table 5: Fundamental frequency for pinned-clamped boundary condition when force and moment are applied.

P-C	End Moment (MN.m)		
	0	6.14	9.21
Force (MN)	FEM Fundamental Frequency (Hz)		
0	11.209	11.040	10.824
0.62	11.408	11.242	11.031
1.23	11.604	11.441	11.233
1.85	11.796	11.636	11.432

The critical buckling end moments and compressive forces are also determined for the cantilevered boundary condition and in Table 6 and Table 7 the results are shown.

Table 6: Critical buckling moment for cantilevered boundary condition with varying axial force.

Force (MN)	Buckling Moment (MN.m)
-1.85	3.900
-1.23	7.750
-0.62	10.60
0	12.28
0.62	13.76
1.23	15.57
1.85	16.95

Table 7: Critical buckling compressive force for cantilevered boundary condition with varying end moment.

Moment (MN.m)	Buckling Force (MN)
0	-2.057
3.07	-1.900
6.14	-1.750
9.21	-0.900

Figure 5 through Figure 8 illustrate the variation of the fundamental frequency when both tensile force and end moment is acting on the beam, for various classical boundary conditions.

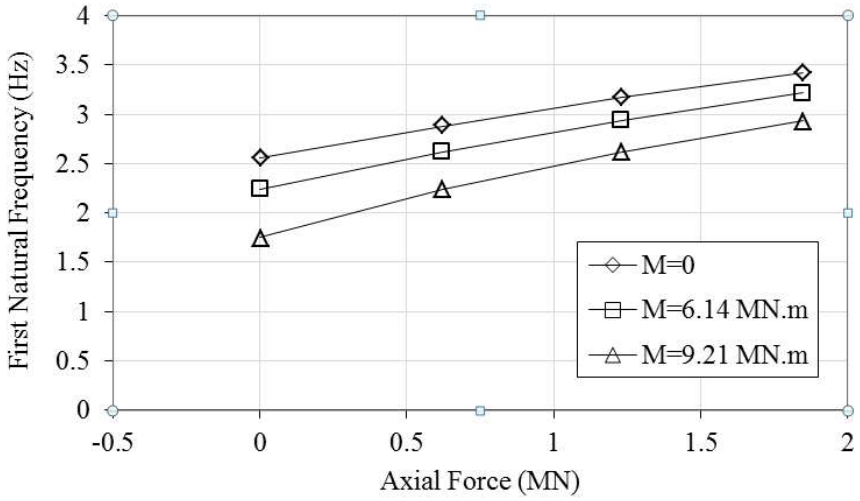

Figure 5: Variation of fundamental frequency with applied tensile force and end moment, for cantilevered boundary condition.

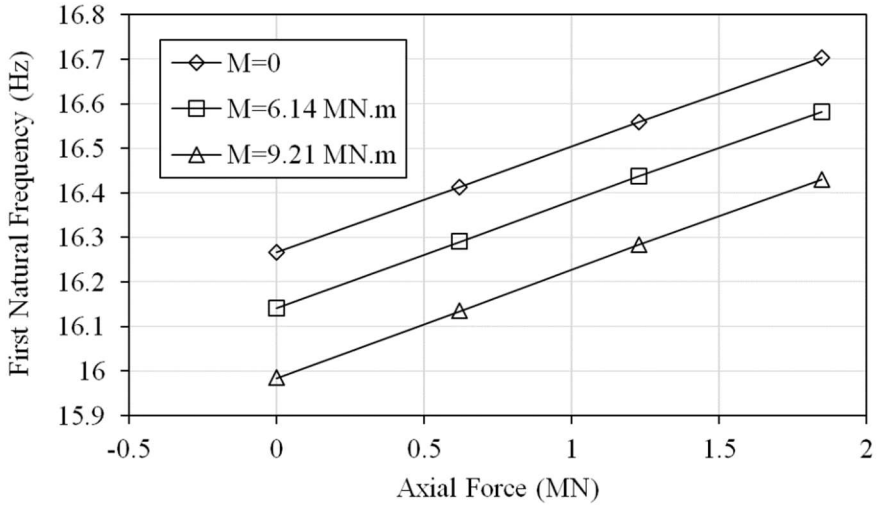

Figure 6: Variation of fundamental frequency with applied tensile force and end moment, for clamped-clamped boundary condition.

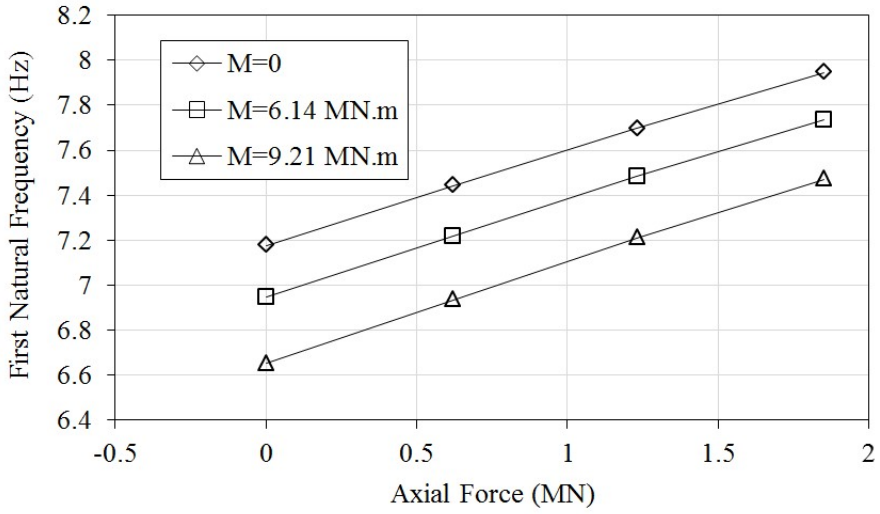

Figure 7: Variation of fundamental frequency when tensile force and end moment are applied for pinned-pinned boundary condition.

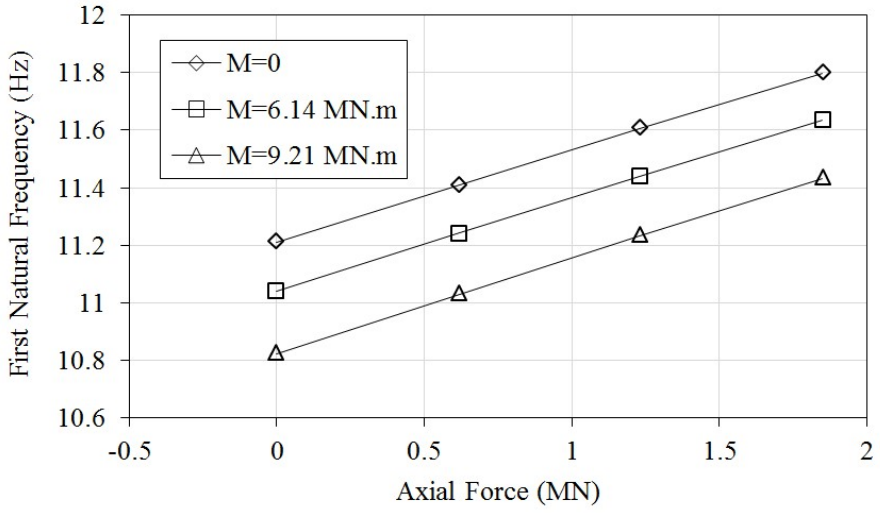

Figure 8: Variation of fundamental frequency when tensile force and end moment are applied for clamped-pinned boundary condition.

Figure 9 shows the critical buckling axial force versus end moment. As can be seen, buckling force decreases as end moment increases. Figure 10 depicts critical buckling moment with respect to the change in axial force. Here as the axial compressive force decreases or tensile axial force increases the buckling moment increases. In this study negative sign of axial force means the force is compressive and positive sign means it is tensile.

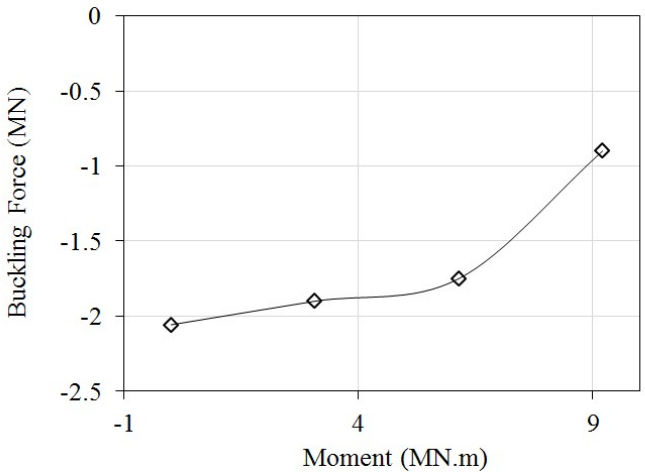

Figure 9: Variation of critical buckling compressive force with end moment.

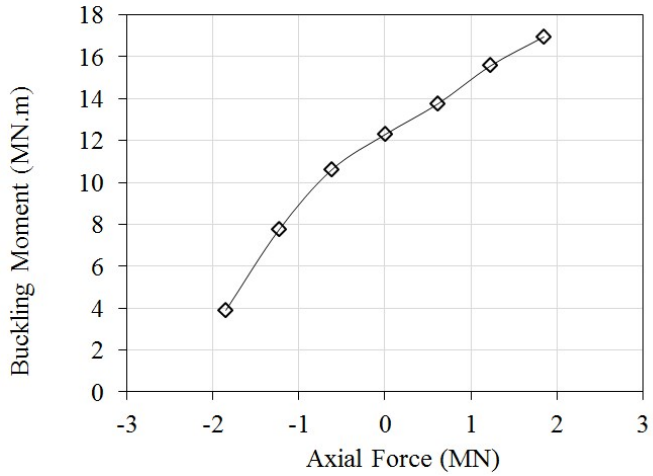

Figure 10: Variation of critical buckling end moment with axial force.

In Figure 11 and Figure 12 the bending and torsion components of the first five natural modes for the cantilevered beam subjected to a tensile force of 1.85MN and end moment of 9.21MN.m are

shown, respectively. From Figure 12 it is inferred that the 4th mode shape is the first torsion dominant mode.

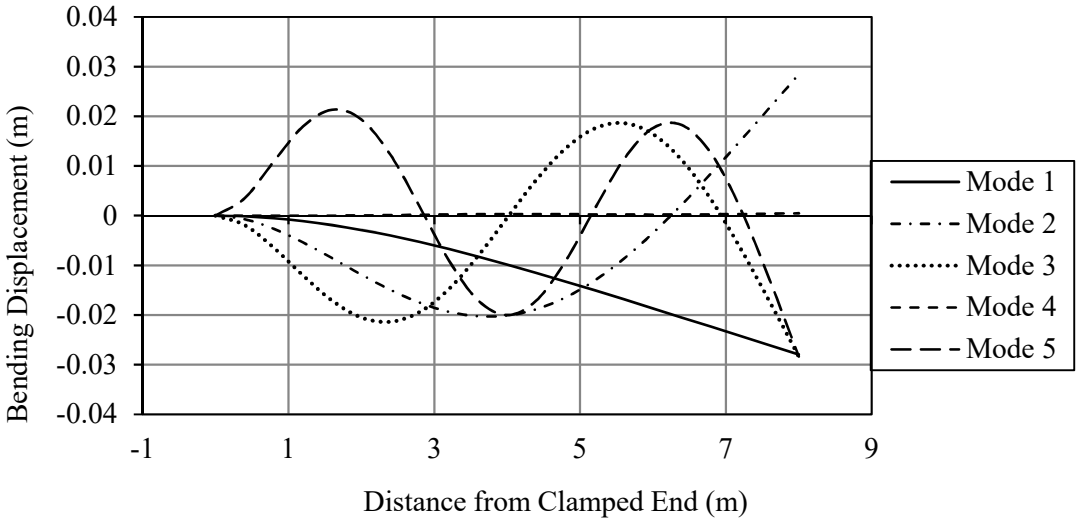

Figure 11: First five FEM bending components of mode shapes.

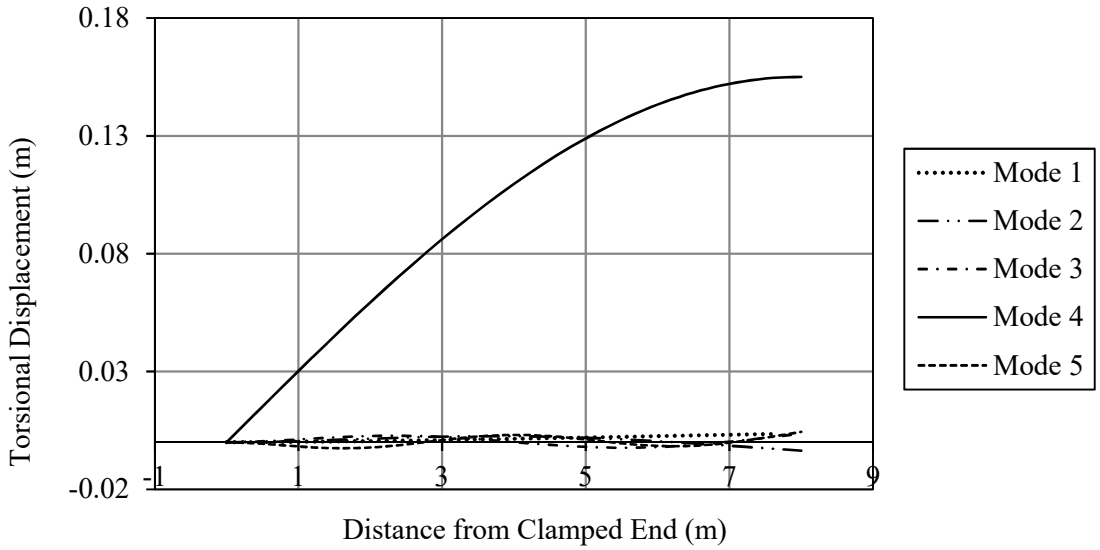

Figure 12: First five FEM torsion components of mode shapes.

2.4 The dynamic finite element (DFE)

Dynamic Finite Element (DFE), as mentioned in introduction section, is an intermediate approach between Classic Finite Element (FEM) and Dynamic Stiffness Matrix (DSM) Methods, leading to a better finite element method with higher convergence rates. For this purpose, DFE implements frequency-dependent trigonometric shape functions from DSM and develops interpolation functions with averaged value parameters, if variable, over each element. In order to find the dynamic shape functions, the solutions of uncoupled governing differential equations are used as basis functions and then these frequency dependent shape functions are utilized to find the element dynamic stiffness matrix. In formulation development, geometric and material parameters are all assumed to be constant per element [41]. In what follows, the development of a new DFE formulation for the free vibration analysis of pre-stressed beams, subjected to combined axial force and end moment is presented. Starting with discretized element weak form equations from the conventional FEM (20 and 21) repeated here:

$$\bar{W}_f^k = \int_{x_j}^{x_{j+1}} (EIW''\delta W'' - PW'\delta W' + M_{zz}\theta'\delta W' - \rho A\omega^2 W\delta W)dx \tag{41}$$

$$\bar{W}_t^k = \int_{x_j}^{x_{j+1}} (GJ\theta'\delta\theta' + \frac{PI_P}{A}\theta'\delta\theta' + M_{zz}W'\delta\theta' - \rho I_P\omega^2\theta\delta\theta)dx \tag{42}$$

two more integrations by parts will then be applied on the first two terms of the equation for flexure and one more integration by parts will be carried out on the first two terms of the torsion equation which result in the following form of the equations:

$$\begin{aligned}\bar{W}_f^k &= \int_{x_j}^{x_{j+1}} (EIW\delta W'''' - PW\delta W'' - \rho A\omega^2 W\delta W)dx + \int_{x_j}^{x_{j+1}} M_{zz}\theta'\delta W'dx \\ &+ \left[EIW'\delta W'' - EIW\delta W''' + PW\delta W'\right]_{x_j}^{x_{j+1}},\end{aligned} \tag{43}$$

$$\bar{W}_t^k = \int_{x_j}^{x_{j+1}} -(GJ\theta\delta\theta'' + \frac{PI_p}{A}\theta\delta\theta'' + \rho I_p\omega^2\theta\delta\theta)dx + \int_{x_j}^{x_{j+1}} M_{zz}W'\delta\theta' dx$$
$$+\left[GJ\theta\delta\theta' + \frac{PI_p}{A}\theta\delta\theta' \right]_{x_j}^{x_{j+1}}. \tag{44}$$

Substituting, $\xi = \frac{x}{l}$ in both equations above will results in their following non-dimensionalized form, written as:

$$\bar{W}_f^k(\xi) = \int_0^1 W(\underbrace{\frac{1}{l^3}EI\delta W'''' - \frac{1}{l}P\delta W'' - \rho A\omega^2 l\delta W}_{*})d\xi + \int_0^1 \frac{1}{l}M_{zz}\theta'\delta W' d\xi$$
$$+\left[\frac{1}{l^3}\left[EIW'\delta W'' - EIW\delta W''' \right] + \frac{1}{l}\left[PW\delta W' \right] \right]_0^1, \tag{45}$$

$$\bar{W}_t^k(\xi) = \int_0^1 -\theta(\underbrace{\frac{1}{l}GJ\delta\theta'' + \frac{1}{l}\frac{PI_p}{A}\delta\theta'' + \rho I_p\omega^2 l\delta\theta}_{**})d\xi + \int_0^1 \frac{1}{l}M_{zz}W'\delta\theta' d\xi$$
$$+\frac{1}{l}\left[GJ\theta\delta\theta' + \frac{PI_p}{A}\theta\delta\theta' \right]_0^1. \tag{46}$$

The interpolation functions, used to express element variables in terms of the nodal properties, are chosen to be evaluated in terms of the closed form solutions to the integral terms marked as (*) and (**), obtained respectively as:

$$W(\xi) = c_1\cos(\alpha\xi) + c_2\sin(\alpha\xi) + c_3\cosh(\beta\xi) + c_4\sinh(\beta\xi) \tag{47}$$

$$\theta(\xi) = c_5\cos(\tau\xi) + c_6\sin(\tau\xi) \tag{48}$$

Expressions 47 and 48 are used as the basis functions of approximation space. Thus, the non–nodal solution approximation functions, W, and θ, and the test functions, δW, and $\delta\theta$, written in terms of generalized parameters$\langle a\rangle$,$\langle \delta a\rangle$,$\langle b\rangle$ and $\langle \delta b\rangle$, are as follows:

$$W = \langle P(\xi)\rangle_f * \{a\}, \qquad \delta W = \langle P(\xi)\rangle_f * \{\delta a\}, \tag{49}$$

$$\theta = \left\langle P(\xi) \right\rangle_t * \{b\}, \qquad \delta\theta = \left\langle P(\xi) \right\rangle_t * \{\delta b\}, \tag{50}$$

where the basis functions are defined as:

$$\left\langle P(\xi) \right\rangle_f = \left\langle \cos(\alpha\xi); \frac{\sin(\alpha\xi)}{\alpha}; \frac{\cosh(\beta\xi) - \cos(\alpha\xi)}{\alpha^2 + \beta^2}; \frac{\sinh(\beta\xi) - \sin(\alpha\xi)}{\alpha^3 + \beta^3} \right\rangle, \tag{51}$$

$$\left\langle P(\xi) \right\rangle_t = \left\langle \cos(\tau\xi); \sin(\tau\xi)/\tau \right\rangle. \tag{52}$$

with the roots, α, β, and τ, defined as:

$$\alpha = \sqrt{|X_2|}, \qquad \beta = \sqrt{|X_1|}, \; \tau = \sqrt{\frac{\rho I_p \omega^2 l^2 A}{AGJ + PI_p}}. \tag{53}$$

and

$$X_1 = \frac{\left\{-B + \sqrt{B^2 - 4\bar{A}C}\right\}}{2\bar{A}}, \qquad X_2 = \frac{\left\{-B - \sqrt{B^2 - 4\bar{A}C}\right\}}{2\bar{A}}, \tag{54}$$

where:

$$\bar{A} = \frac{EI}{l^3}, \qquad B = -\left(\frac{P}{l}\right), \qquad C = -(ml\omega^2). \tag{55}$$

These basis function are the solutions to the characteristic equations (*) and (**). The Basis Functions (47) and (48) have been designed and defined as linear combinations of above-mentioned closed form solutions (53) and (54), such that when the roots, α, β, and τ, of the characteristic equations tend to zero, the resulting basis functions are similar to those of a standard beam element in the classical FEM, where flexure and torsion are approximated using cubic Hermite polynomials (31) and linear functions (32), respectively.

Replacing the generalized parameters,$\langle a \rangle$, $\langle \delta a \rangle$, $\langle b \rangle$ and $\langle \delta b \rangle$, in equations 45 and 46 with the nodal variables, $\langle W_1 W_1' W_2 W_2' \rangle$, $\langle \delta W_1 \; \delta W_1' \; \delta W_2 \; \delta W_2' \rangle$, $\langle \theta_1 \theta_2 \rangle$, and $\langle \delta\theta_1 \delta\theta_2 \rangle$, respectively, and re-writing equations 45 and 46 will result in the following Equations:

$$\{W_n\} = [P_n]_f \{a\} \qquad \{\delta W_n\} = [P_n]_f \{\delta a\} \tag{56}$$

$$\{\theta_n\} = [P_n]_t \{b\} \qquad \{\delta \theta_n\} = [P_n]_t \{\delta b\} \tag{57}$$

The matrices, $[P_n]_f$ and $[P_n]_t$, are defined as:

$$[P_n]_f = \begin{bmatrix} 1 & 0 & 0 & 0 \\ 0 & 1 & 0 & \dfrac{(\beta-\alpha)}{(\alpha^3+\beta^3)} \\ \cos(\alpha) & \dfrac{\sin(\alpha)}{\alpha} & \dfrac{[\cosh(\beta)-\cos(\alpha)]}{(\alpha^2+\beta^2)} & \dfrac{[\sinh(\beta)-\sin(\alpha)]}{(\alpha^3+\beta^3)} \\ -\alpha\sin(\alpha) & \cos(\alpha) & \dfrac{[\beta\sinh(\beta)+\alpha\sin(\alpha)]}{(\alpha^2+\beta^2)} & \dfrac{[\beta\cosh(\beta)-\alpha\cos(\alpha)]}{(\alpha^3+\beta^3)} \end{bmatrix} \tag{58}$$

$$[P_n]_t = \begin{bmatrix} 1 & 0 \\ \cos(\tau) & \dfrac{\sin(\tau)}{\tau} \end{bmatrix} \tag{59}$$

Thus expressions 56, 57 and the $[P_{n,f}]$ and $[P_{n,t}]$ matrices above are then combined in the following manner to construct nodal approximations for flexural displacement, $W(\xi)$, and torsion displacement, $\theta(\xi)$, written as:

$$W(\xi) = \langle P(\xi) \rangle_f [P_n]_f^{-1} \{W_n\} = \langle N(\xi) \rangle_f \{W_n\} \tag{60}$$

$$\theta(\xi) = \langle P(\xi) \rangle_t [P_n]_t^{-1} \{\theta_n\} = \langle N(\xi) \rangle_t \{\theta_n\} \tag{61}$$

In expressions 60 and 61, $\langle N(\xi) \rangle_f$ and $\langle N(\xi) \rangle_t$, are the frequency-dependent trigonometric shape functions for flexure and torsion, respectively. Expressions 60 and 61 can also be re-written as:

$$\begin{Bmatrix} W(\xi) \\ \theta(\xi) \end{Bmatrix} = [N]\{w_n\} \tag{62}$$

where,

$$[N]=\begin{bmatrix} N_{1f}(\omega) & N_{2f}(\omega) & 0 & N_{3f}(\omega) & N_{4f}(\omega) & 0 \\ 0 & 0 & N_{1t}(\omega) & 0 & 0 & N_{2t}(\omega) \end{bmatrix} \tag{63}$$

and

$$\{w_n\} = \langle W_1 W_1^{'} \theta_1 W_2 W_2^{'} \theta_2 \rangle^T \tag{64}$$

The definitions of the frequency-dependent trigonometric shape functions for flexure, as also reported by [41] are as follows:

$$\begin{aligned} N_{1f}(\omega) &= \frac{(\alpha\beta)}{D_f} * \{-\cos(\alpha\xi) + \cos(\alpha(1-\xi)) * \cosh(\beta) + \cos(\alpha) * \cosh(\beta(1-\xi)) \\ &- \cosh(\beta\xi) - \frac{\beta}{\alpha} * \sin(\alpha(1-\xi)) * \sinh(\beta) + \frac{\alpha}{\beta} * \sin(\alpha) * \sinh(\beta(1-\xi))\}, \end{aligned} \tag{65}$$

$$\begin{aligned} N_{2f}(\omega) &= \frac{1}{D_f} * \{\beta * [\cosh(\beta(1-\xi)) * \sin(\alpha) - \cosh(\beta) * \sin(\alpha(1-\xi)) - \sin(\alpha\xi)] \\ &+ \alpha * [\cos(\alpha(1-\xi)) * \sinh(\beta) - \cos(\alpha) * \sinh(\beta(1-\xi)) - \sinh(\beta\xi)]\}, \end{aligned} \tag{66}$$

$$\begin{aligned} N_{3f}(\omega) &= \frac{(\alpha\beta)}{D_f} * \{-\cos(\alpha(1-\xi)) + \cos(\alpha\xi) * \cosh(\beta) - \cosh(\beta(1-\xi)) + \cos(\alpha) \\ &* \cosh(\beta\xi) - \frac{\beta}{\alpha} * \sin(\alpha\xi) * \sinh(\beta) + \frac{\alpha}{\beta} * \sin(\alpha) * \sinh(\beta\xi)\}, \end{aligned} \tag{67}$$

$$\begin{aligned} N_{4f}(\omega) &= \frac{1}{D_f} * \{\beta * [-\cosh(\beta\xi) * \sin(\alpha) + \sin(\alpha(1-\xi)) + \cosh(\beta) * \sin(\alpha\xi)] \\ &+ \alpha * [-\cos(\alpha\xi) * \sinh(\beta) + \sinh(\beta(1-\xi)) + \cos(\alpha) * \sinh(\beta\xi)]\}. \end{aligned} \tag{68}$$

where,

$$D_f = (\alpha\beta) * \left\{-2 * (1 - \cos(\alpha) * \cosh(\beta)) + \left(\frac{\alpha^2 - \beta^2}{\alpha\beta}\right) * \sin(\alpha) * \sinh(\beta)\right\} \tag{69}$$

The trigonometric shape functions for torsion, as also presented in [35] are:

$$N_{1t}(\omega) = \cos(\tau\xi) - \cos(\tau) * \frac{\sin(\tau\xi)}{D_t} \tag{70}$$

$$N_{2t}(\omega) = \frac{\sin(\tau\xi)}{D_t} \tag{71}$$

where,

$$D_t = \sin(\tau) \tag{72}$$

Using non-dimensionalized, element, virtual work expressions 45, 46, stating the approximate element displacements in terms of nodal values and the shape functions 65 through 72, the element dynamic (frequency-dependent) stiffness matrix is obtained. The resulting frequency-dependent, Dynamic element stiffness matrix, $[K(\omega)]^k$ consists of two coupled dynamic stiffness matrices, $[K(\omega)]^k_{BT,c}$ and $[K(\omega)]^k_{TB,c}$, symbolized collectively as $[K(\omega)]^k_c$, and four uncoupled dynamic stiffness matrices, $[K(\omega)]^k_{u1}$, $[K(\omega)]^k_{u2}$, $[K(\omega)]^k_{u3}$ and $[K(\omega)]^k_{u4}$, jointly denoted as $[K(\omega)]^k_u$. The four uncoupled element stiffness matrices are as follows:

$$[K(\omega)]^k_{u1} = \frac{EI}{L^3}\left[\begin{matrix} N'_{1f}N''_{1f} & N'_{1f}N''_{2f} & N'_{1f}N''_{3f} & N'_{1f}N''_{4f} \\ N'_{2f}N''_{1f} & N'_{2f}N''_{2f} & N'_{2f}N''_{3f} & N'_{2f}N''_{4f} \\ N'_{3f}N''_{1f} & N'_{3f}N''_{2f} & N'_{3f}N''_{3f} & N'_{3f}N''_{4f} \\ N'_{4f}N''_{1f} & N'_{4f}N''_{2f} & N'_{4f}N''_{3f} & N'_{4f}N''_{4f} \end{matrix}\right]_0^1 \tag{73}$$

$$[K(\omega)]^k_{u2} = \frac{-EI}{L^3}\left[\begin{matrix} N_{1f}N'''_{1f} & N_{1f}N'''_{2f} & N_{1f}N'''_{3f} & N_{1f}N'''_{4f} \\ N_{2f}N'''_{1f} & N_{2f}N'''_{2f} & N_{2f}N'''_{3f} & N_{2f}N'''_{4f} \\ N_{3f}N'''_{1f} & N_{3f}N'''_{2f} & N_{3f}N'''_{3f} & N_{3f}N'''_{4f} \\ N_{4f}N'''_{1f} & N_{4f}N'''_{2f} & N_{4f}N'''_{3f} & N_{4f}N'''_{4f} \end{matrix}\right]_0^1 \tag{74}$$

$$[K(\omega)]_{u3}^{k}=\frac{P}{L}\left[\begin{array}{cccc} N_{1f}N_{1f}^{'} & N_{1f}N_{2f}^{'} & N_{1f}N_{3f}^{'} & N_{1f}N_{4f}^{'} \\ N_{2f}N_{1f}^{'} & N_{2f}N_{2f}^{'} & N_{2f}N_{3f}^{'} & N_{2f}N_{4f}^{'} \\ N_{3f}N_{1f}^{'} & N_{3f}N_{2f}^{'} & N_{3f}N_{3f}^{'} & N_{3f}N_{4f}^{'} \\ N_{4f}N_{1f}^{'} & N_{4f}N_{2f}^{'} & N_{4f}N_{3f}^{'} & N_{4f}N_{4f}^{'} \end{array}\right]_{0}^{1} \tag{75}$$

$$[K(\omega)]_{u4}^{k}=\frac{1}{L}\left(GJ+\frac{PI_{P}}{A}\right)\left[\begin{array}{cc} N_{1t}N_{1t}^{'} & N_{1t}N_{2t}^{'} \\ N_{2t}N_{1t}^{'} & N_{2t}N_{2t}^{'} \end{array}\right]_{0}^{1} \tag{76}$$

the two coupled element matrices are as follows:

$$[K(\omega)]_{BT,c}^{k}=\int_{0}^{1}\frac{M}{L}\left[\begin{array}{cccc} N_{1t}^{'}N_{1f}^{'} & N_{1t}^{'}N_{2f}^{'} & N_{1t}^{'}N_{3f}^{'} & N_{1t}^{'}N_{4f}^{'} \\ N_{2t}^{'}N_{1f}^{'} & N_{2t}^{'}N_{2f}^{'} & N_{2t}^{'}N_{3f}^{'} & N_{2t}^{'}N_{4f}^{'} \end{array}\right]d\xi \tag{77}$$

$$[K(\omega)]_{TB,c}^{k}=\int_{0}^{1}\frac{M}{L}\left[\begin{array}{cc} N_{1f}^{'}N_{1t}^{'} & N_{1f}^{'}N_{2t}^{'} \\ N_{2f}^{'}N_{1t}^{'} & N_{2f}^{'}N_{2t}^{'} \\ N_{3f}^{'}N_{1t}^{'} & N_{3f}^{'}N_{2t}^{'} \\ N_{4f}^{'}N_{1t}^{'} & N_{4f}^{'}N_{2t}^{'} \end{array}\right]d\xi \tag{78}$$

The element dynamic stiffness matrix $[K(\omega)]^{k}$ is determined by adding these six coupled and uncoupled sub-matrices and the global dynamic stiffness matrix $[K(\omega)]$ is then obtained by assembling all the element stiffness matrices (this assembling process is done using a code developed in MATLAB). By applying the principle of virtual work, for arbitrary virtual displacement $\langle\delta U_{n}\rangle$, the resulting non-linear eigenvalue problem is obtained as follows:

$$\left[K(\omega)\right]\left\{U_{n}\right\}=\left\{0\right\}. \tag{79}$$

Applying the relevant boundary conditions, the system's natural frequencies ω, are then evaluated by setting the determinant of the global dynamic stiffness matrix, i.e., $|K(\omega)|=0$. This is done by sweeping the frequency domain using visual inspection to find particular values of ω that produce a zero determinant, and mode shapes can be found by extracting data from corresponding eigenvectors

$\{U_n\}$. Alternatively, the natural frequency can be found by any standard determinant search method, or Wittrick–Williams (W-W) algorithm [98].

2.5 DFE Numerical Results; Simple Beam

In order to validate the developed DFE model, in the illustrative example cases studied below, the same properties as those used in the FEM examples presented earlier, are used; Young modulus E=200GPa, density ρ=7800kg/m^3 (steel), beam length of 8m, width of 0.4m and depth of 0.2m. In order to optimize the number of elements, a convergence study for the 5th natural frequency is carried out, as depicted in Figure 13. The error is found in comparison with the exact values found from analytical closed form solution by Joshi and Suryanarayan [13]. A comparison between the DFE method and conventional FEM with regards to the efficiency in convergence is illustrated in Figure 14. For the 5th natural frequency, the DFE method produces an error less than 0.2 percent, whereas FEM shows 1.3% error, compared to the exact result with just 5 elements or an error less than 0.1 percent using 8 DFE elements and 0.3% error using the same number of FEM element, which shows that a specific degree of accuracy could be achieved with less number of elements using DFE.

Table 8 through Table 11 represent the FEM and DFE results for the system's fundamental frequency, for different preloads and boundary conditions. As in absence of end moment the equations of motion are uncoupled, and as a result the DFE method in this case yields exact results. Therefore, for M=0, there is no difference between analytical method and DFE data.

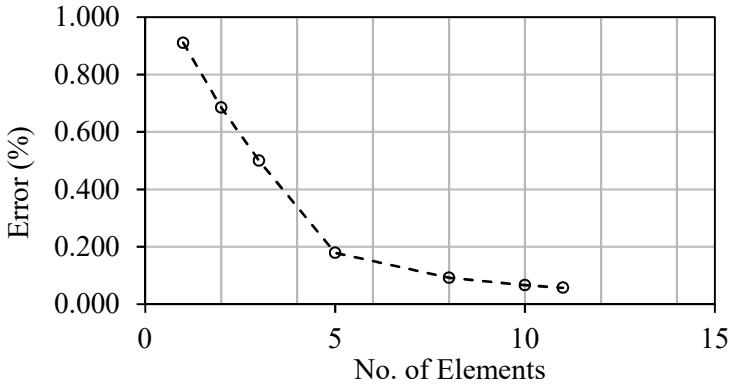

Figure 13: Convergence analysis for the fifth natural frequency results, obtained from DFE method for cantilevered beam.

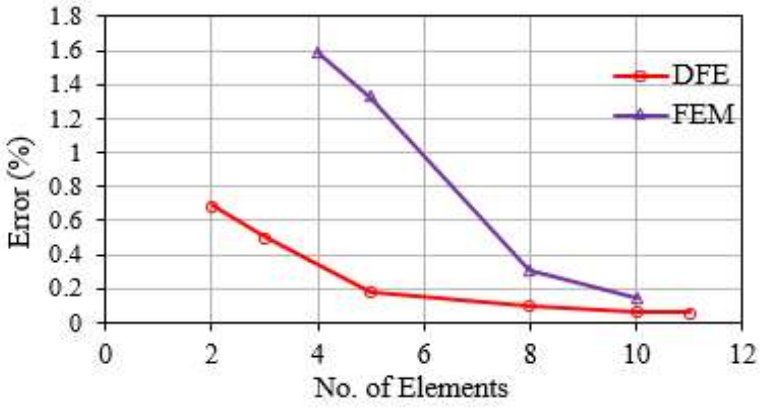

Figure 14: Comparison of convergence efficiency between DFE method and conventional FEM for cantilevered beam, the fifth natural frequency.

Table 8: First natural frequencies of DFE for cantilever boundary condition.

C-F	End Moment (MN.m)					
	0		6.14		9.21	
	Fundamental Frequency (Hz)					
Force (MN)	DFE (1 element)	Exact [97]	DFE (5 elements)	FEM (5 elements)	DFE (5 elements)	FEM (5 elements)
0	2.556	2.556	2.237	2.345	1.730	1.836
0.62	2.884	2.884	2.617	2.710	2.219	2.327
1.23	3.169	3.169	2.935	3.082	2.603	2.725
1.85	3.422	3.422	3.213	3.306	2.925	3.047

Table 9: First natural frequencies of DFE for clamped-clamped boundary condition.

C-C	End Moment (MN.m)					
	0		6.14		9.21	
	FEM Fundamental Frequency (Hz)					
Force (MN)	DFE (1 element)	Exact [97]	DFE (5 elements)	FEM (5 elements)	DFE (5 elements)	FEM (5 elements)
0	16.266	16.266	16.157	16.243	16.019	16.082
0.62	16.413	16.413	16.306	16.399	16.170	16.230
1.23	16.559	16.559	16.451	16.530	16.316	16.386
1.85	16.703	16.703	16.597	16.685	16.464	16.533

Table 10: First natural frequencies of DFE for pinned-pinned boundary condition.

P-P	End Moment (MN.m)					
	0		6.14		9.21	
	FEM Fundamental Frequency (Hz)					
Force (MN)	DFE (1 element)	Exact [97]	DFE (5 element)	FEM (5 elements)	DFE (5 element)	FEM (5 elements)
0	7.175	7.175	6.955	7.058	6.669	6.783
0.62	7.440	7.440	7.228	7.398	6.954	7.067
1.23	7.695	7.695	7.488	7.552	7.223	7.370
1.85	7.942	7.942	7.743	7.847	7.487	7.521

Table 11: First natural frequencies of DFE for pinned-clamped boundary condition.

P-C	End Moment (MN.m)					
	0		6.14		9.21	
	FEM Fundamental Frequency (Hz)					
Force (MN)	DFE (1 element)	Exact [97]	DFE (5 elements)	FEM (5 elements)	DFE (5 elements)	FEM (5 elements)
0	11.209	11.209	11.051	11.183	10.851	10.987
0.62	11.408	11.408	11.254	11.321	11.058	11.163
1.23	11.604	11.604	11.451	11.574	11.257	11.353
1.85	11.796	11.796	11.646	11.724	11.456	11.556

In order to investigate the effect of combined axial force and end moment on the stability of beam, a buckling analysis is carried out. Table 12 represents the values of buckling moment for different applied axial forces and Table 13 shows the buckling forces for different applied end moments.

Table 12: Critical buckling moment for cantilevered boundary condition with varying compressive force.

Force (MN)	Buckling Moment (MN.m) DFE (5 element)
-1.85	3.91
-1.23	7.82
-0.62	10.31
0	12.33
0.62	14.07
1.23	15.59
1.85	17.00

Table 13: Critical buckling compressive force for cantilevered boundary condition with varying end moment.

Moment (MN.m)	Buckling Force (MN) DFE (5 elements)
0	-2.06
3.07	-1.93
6.14	-1.55
9.21	-0.91

A comparison between different methods is also made for buckling loads (using 5 elements for DFE, 5 elements for FEM, and 40 elements for ANSYS) and the results are presented in Table 14.

Table 14: Comparison of buckling results for different methods.

Moment	Buckling Force (N)		
(N.m)	DFE	FEM	ANSYS
0	707	708	698
50	665	669	661
100	539	551	549
150	330	354	346
205	0	47	35

Figure 15 through Figure 18 are graphical representations of the results in Table 8 through Table 11. These figures illustrate the variation of the first fundamental frequency with tensile axial force and end moment.

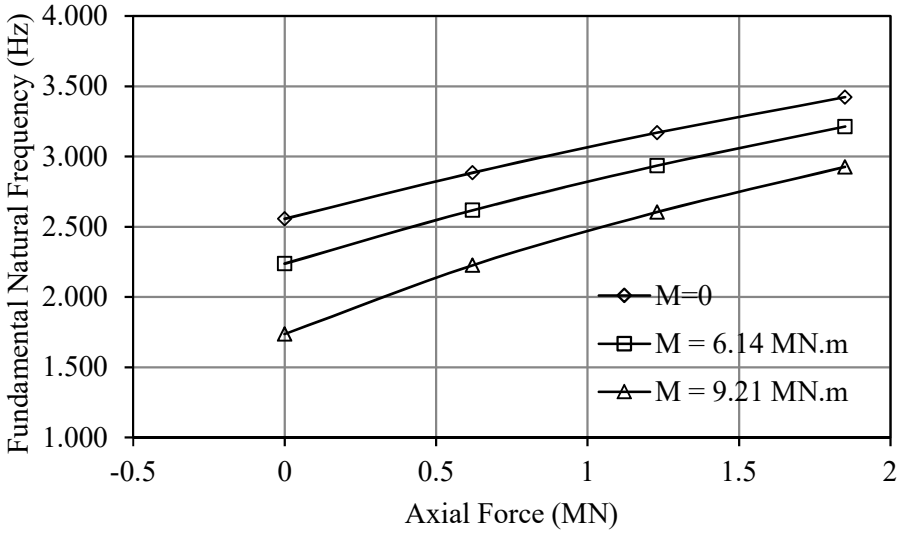

Figure 15: Variation of natural frequencies when tensile force and end moment is applied for cantilevered boundary condition.

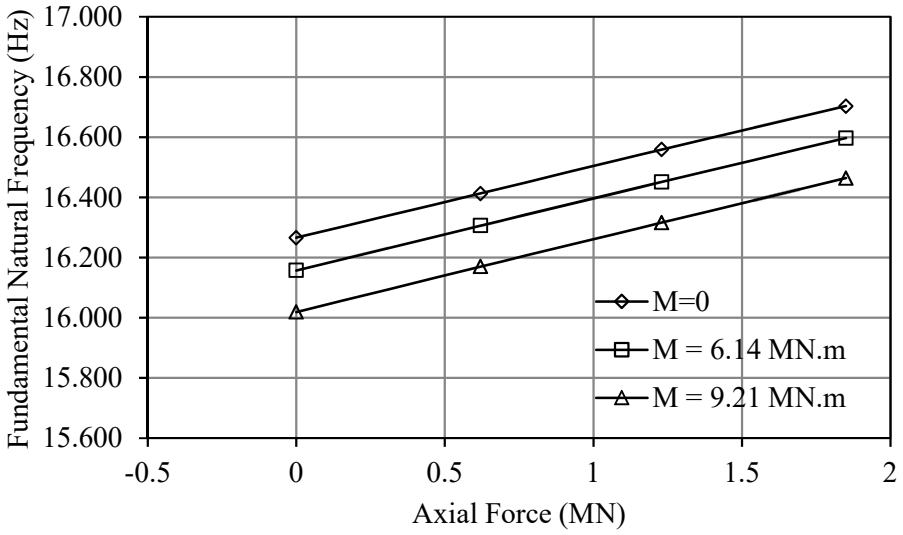

Figure 16: Variation of natural frequencies when tensile force and end moment is applied for clamped-clamped boundary condition.

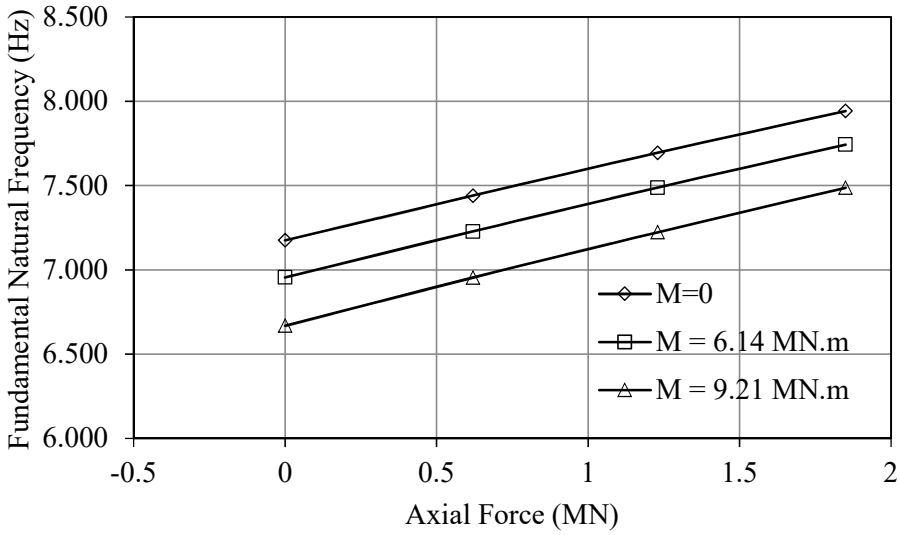

Figure 17: Variation of natural frequencies when tensile force and end moment is applied for pinned-pinned boundary condition.

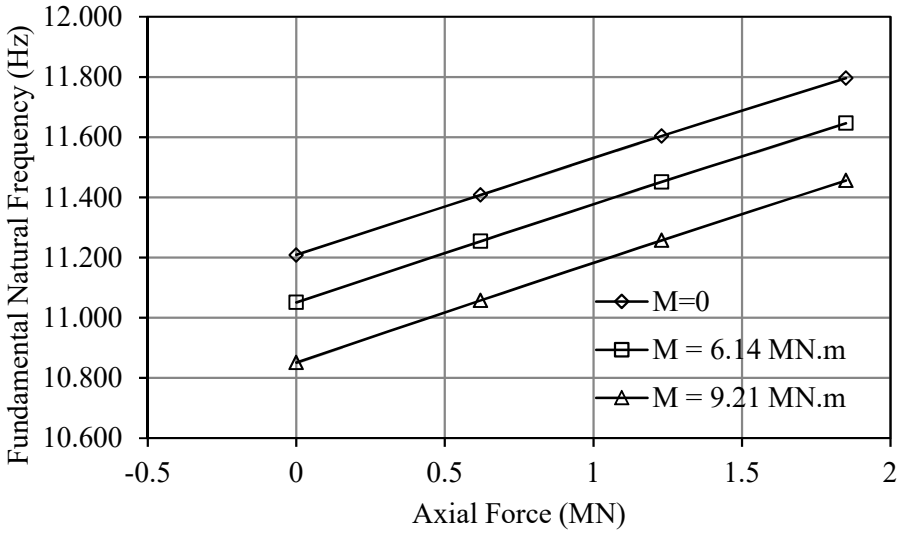

Figure 18: Variation of natural frequencies when tensile force and end moment is applied for pinned-clamped boundary condition.

Figure 19 illustrates how the critical buckling end moment varies with axial force, and Figure 20 depicts the variation of the critical buckling compressive force with changing end moment.

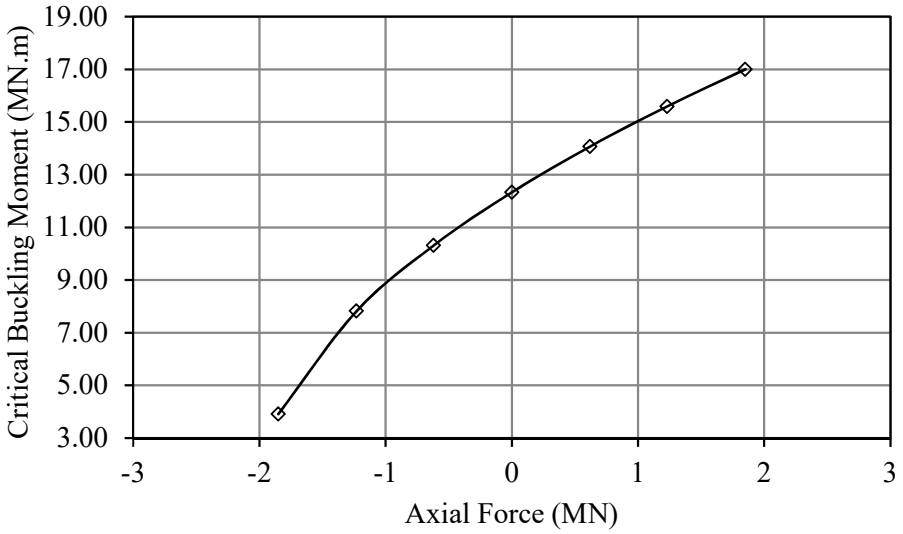

Figure 19: Variation of critical buckling end moment with axial force for cantilevered boundary condition.

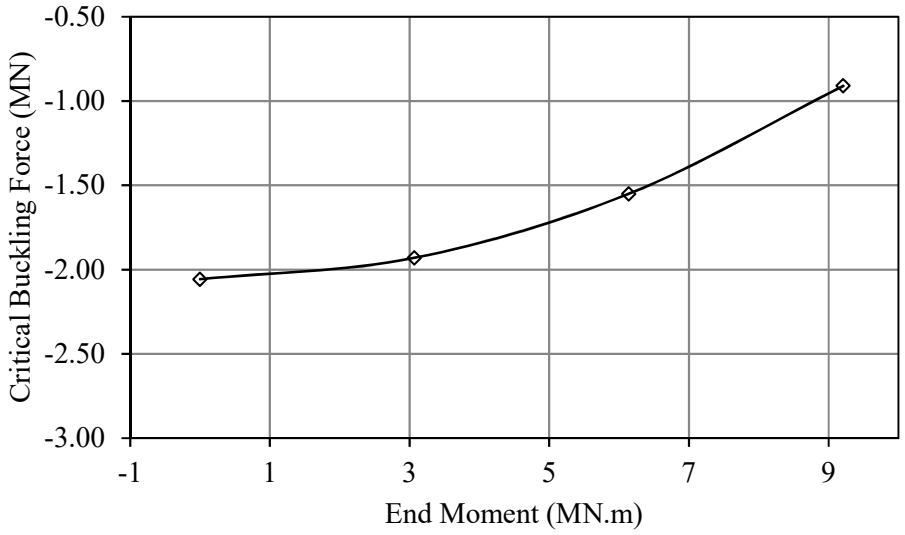

Figure 20: Variation of critical buckling compressive force with end moment for cantilevered boundary condition.

Figure 21 and Figure 22 show bending and torsion components of the system's first five mode shapes, respectively, for a cantilevered system subjected to a tensile force of 1.85MN and end moment of 9.21MN.m.

For further validation, all methods are compared with the limited experimental data available in the open literature [99]. In this experiment, carried out in the absence of end moment, the beam is made of aluminium with ρ=2700 kg/m^3, G=26GPa, E=70GPa, and beam dimensions are $L\times H\times B$= 1290×75×35. It is worth mentioning that in this case, due to the absence of end moment, the two governing differential equations become uncoupled. As a result, and as it was mentioned earlier in this thesis, the DFE formulation results in exact values of the system's frequencies (within the limits of the theory). In other words, a 1-element DFE model becomes equivalent to the exact DSM model, leading to infinite natural frequencies. The results are shown in Table 15.

Table 15: Comparison of different methods (DFE, FEM and ANSYS models using 5 elements).

Load (N)	Natural Frequency (Hz)											
	1st				2nd				3rd			
	DFE	Experiment	FEM	ANSYS	DFE	Experiment	FEM	ANSYS	DFE	Experiment	FEM	ANSYS
1962	36.0	35.9	36.1	36.1	93.1	92.8	94.0	94.1	177.0	176.2	180.3	180.5
4022	40.0	39.9	40.1	40.1	98.9	98.5	99.8	99.8	184.0	183.3	187.7	187.7
6671	44.5	44.3	44.6	44.6	106.6	106.3	107.4	107.4	193.9	192.2	196.5	196.7
7750	46.4	45.3	46.5	46.5	109.6	109.4	110.5	110.6	197.6	196.8	200.9	201.2
9810	49.5	49.4	49.6	49.6	114.9	114.7	115.7	115.6	204.4	203.8	207.4	207.4

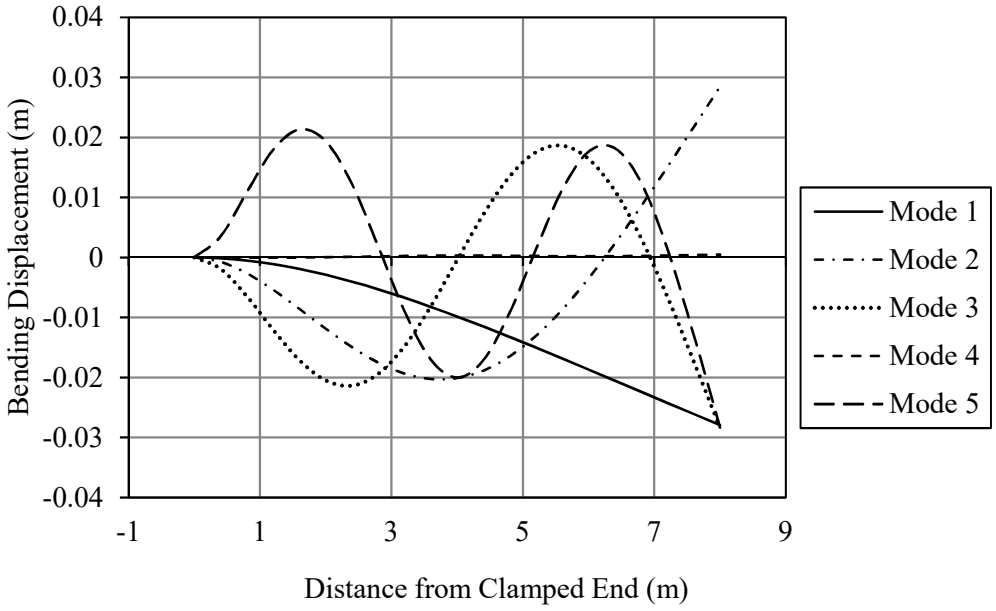

Figure 21: Bending component of mode shapes using DFE.

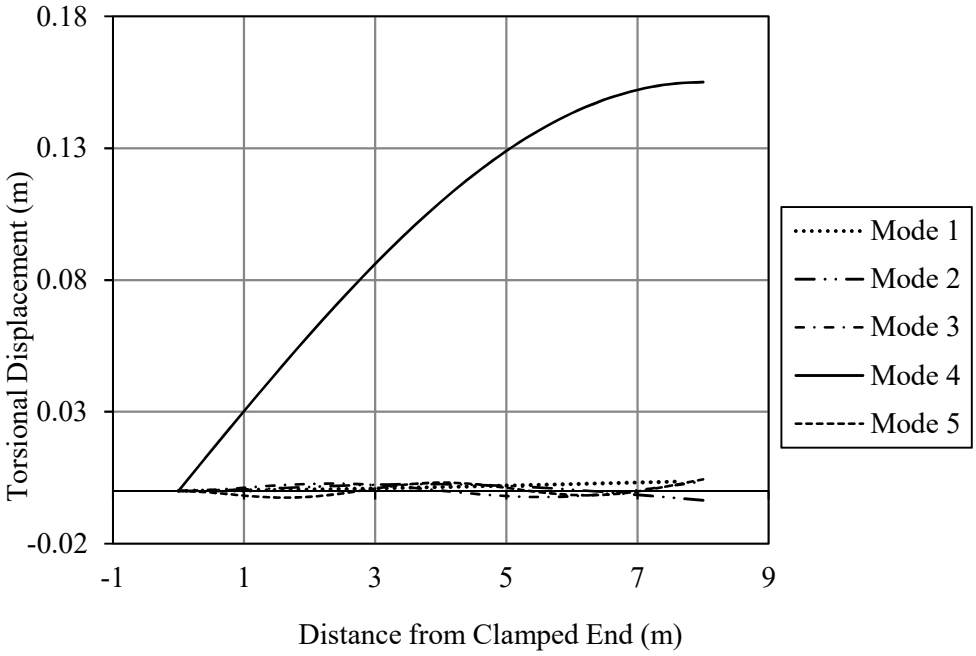

Figure 22: Torsional component of mode shapes using DFE.

2.6 Discussions and Concluding remarks

In this chapter, free vibration analysis of a pre-stressed isotropic beam was presented using conventional FEM and frequency dependent numerical method DFE. Later, the numerical results for a still beam with different loadings and boundary conditions was reported. Followed by, convergence tests and buckling analysis.

For all the classical boundary conditions, using same number of elements, DFE was proven to have higher rate of convergence (e.g. see Figure 13). This higher rate of convergence in large scale designs can results in saving hours of processing time. DFE is especially advantageous at the preliminary design/analysis stage. For the detailed design and analysis stage, however, an elaborated FEM model will be a better option. Concerning buckling analysis, results show that the tensile forces increase the natural frequencies and stiffness of the beam while compressive forces and end moments reduces the natural frequencies and stiffness of the beam for all four investigated classical boundary

conditions. As expected, tensile axial load increases the natural beam frequencies, indicating an increase in the beam stiffness (see e.g. Figure 5). When the end moment is increased, the natural frequencies reduce, indicating a reduction in stiffness of the beam. If the end moment is held constant and the tensile load is increased, the natural frequencies increase indicating an increase in the beam stiffness. Conversely, if the tensile load is held constant and the end moment is increased, the beam stiffness reduces. A compressive axial load has the opposite effect and the critical buckling moment reduces with a progressive increase in the compressive load.

Even though the trend of fundamental natural frequency versus axial force seems linear in Figures 16 through 18 (for all boundary conditions except cantilevered), the curves fitted to the results are not linear. The linear look of the curves is due to the considered interval of axial force not being large enough to show the non-linear trend of the variations. However, by choosing a larger interval non-linear curves similar to those in Figure 15 (cantilevered beam) will be observed for all the classic boundary conditions.

The coupled vibration of the beam is found to be predominantly flexural in the first few natural frequencies (the first four, for the case studied here) and torsion becomes predominant at higher natural frequencies.

3 Free Vibration of Pre-stressed Layered Beams

3.1 Introduction

In this Chapter, the free vibration of pre-stressed layered beams made of different materials, subjected to axial force and end moment is investigated. First, homogenization method which is a common method in dealing with layered beams, is introduced followed by its numerical results. Later, these results are used as a benchmark where both axial force and end moment are applied on the beam where there are no other results in open literature to be used as benchmark. Next, exploiting the layer-wise theory and the differential equations governing system's coupled flexural-torsional vibrations, a layered beam finite element is developed. The linear Eigenvalue problem resulting from the discretization along the length is solved to determine the Eigensolutions of two- and three-layer illustrative beam examples, exhibiting geometric bending-torsion coupling caused by the end moment, and various classical boundary conditions are investigated. The layered nature of beams are considered in the modeling using a novel layer-wise formulation by discretizing the beam along the thickness together with the method of homogenization. Natural frequencies and mode shapes resulting from the proposed method are found to be in good agreement with the results obtained from the homogenization method, and those found from FEM simulations in ANSYS. A preliminary stability analysis is also carried out to illustrate the effects of axial load and end moment on the system's stiffness and fundamental frequencies. Enforcing inter-element displacement continuity, the layers' matrices are then assembled through the beam thickness to form the Layered Beam Finite Element (LBFE) matrices. Assembly of the resulting LBFE matrices along the beam length and applying the boundary conditions then leads to the system's linear eigenvalue problem. The resulting eigenproblem is then solved to determine the natural frequencies and modes (eigensolutions) of the system. The application of the proposed LBFE method is demonstrated through the vibration

analysis of cantilevered two- and three-layer illustrative beam examples, exhibiting geometric bending-torsion coupling caused by the end moment. The axial load and end moment are varied and their effects on the beam stiffness and natural frequencies are examined. The natural frequencies and mode shapes obtained from the LBFE are validated against those obtained from the homogenization method - Equivalent Single Layer (ESL) theory- and FEM simulations in the commercial software package ANSYS. The frequency results show good agreement with those obtained from both ESL theory and ANSYS. A preliminary stability analysis is also carried out to illustrate the effects of axial load and end moment on the system's stiffness and fundamental frequencies. The presented LBFE formulation is adaptable to many complex systems, including those with geometric variations, e.g., non-uniform geometry.

A layer-wise beam DFE (LBDFE) formulation is also developed and tested against LBFE, method of homogenization and ANSYS. The investigated models include: two layer aluminium-steel, two layer glass/epoxy composite, steel-rubber-steel sandwich, fiber-metal laminate and three layer laminated composite beams. The frequency dependent LBDFE method is shown to have the highest convergence rates. Finally, in the discussions and concluding remarks section, a summary of Chapter 3 as well as discussions on the numerical tests are presented.

3.2 Method of Homogenization

In this section, a two-layered, linearly elastic, homogeneous, isotropic slender beam subjected to two equal and opposite end moments, M_{zz}, about z-axis and an axial load, P is considered. Figure 23, depicts the schematic of the problem, where L, h and t stand for the beam's length, width and height, respectively. Homogeneous layers are considered to be made of different materials and classic lamination theory (CLT) [65] is implemented to find the equivalent properties of a single layer

equivalent beam. After finding the equivalent (i.e., apparent) properties one can then treat the problem as a uniform beam. The equivalent properties are found using following equations [65]:

$$E_1 = E_f V_f + V_m E_m, \tag{80}$$

$$E_2 = \frac{E_f E_m}{V_f E_m + V_m E_f}, \tag{81}$$

$$G_{12} = \frac{G_f G_m}{V_f G_m + V_m G_f}, \tag{82}$$

$$\nu_{12} = V_f \nu_f + V_m \nu_m. \tag{83}$$

where ν is the Poisson's ratio and indices m and f represent properties of layer 1 and layer 2 respectively.

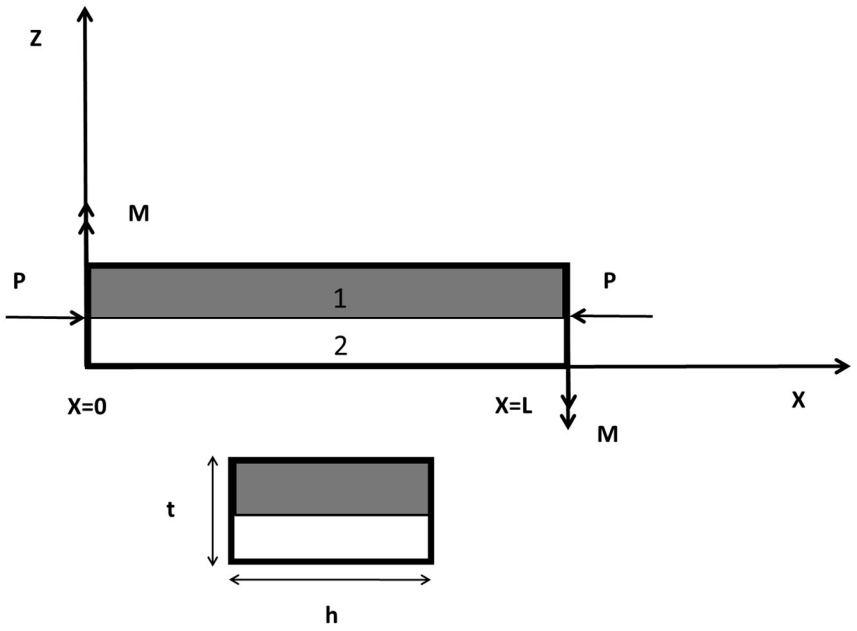

Figure 23: Schematic and coordinate system of the problem, with axial load and end-moment applied at x=0, and x=L.

3.3 Layer-wise Formulation of Pre-stressed Layered Beams

The differential equations governing the linear bending-torsion coupled vibrations of a pre-stressed single-layer beam subjected to end moment, was presented in the previous Chapter, where the development and application of conventional FEM and Dynamic Finite Element (DFE) formulations were demonstrated. In what follows, the presented theories are extended to an *n*-layer beam configuration, where each layer is, or can be readily modeled as an equivalent, homogeneous beam. The latter can be achieved by using the CLT briefly discussed in the previous Section (2.1). Consider an n-layered beam subjected to two equal and opposite end moments, M_{zz}, about z-axis and an axial load, P, loaded in the plane of greater bending rigidity, undergoing linear coupled torsion and lateral vibrations along z-axis. Figure 24 depicts the schematic of the problem, where L, h and t stand for the beam's length, width and height, respectively. Governing differential equations of motion can be developed by defining an infinitesimal element, and by using the following assumptions:

1. The displacements are small;
2. The stresses induced are within the limit of proportionality;
3. The cross section of the beam has one axes of symmetry;
4. The cross-sectional dimensions of the beam are small compared to the span.
5. The transverse cross sections of the beam remain plane and normal to the neutral axis during bending, and
6. The beam's torsional rigidity (GJ) is assumed to be very large compared with its warping rigidity (EI), and ends are free to warp; i.e., state of uniform torsion.

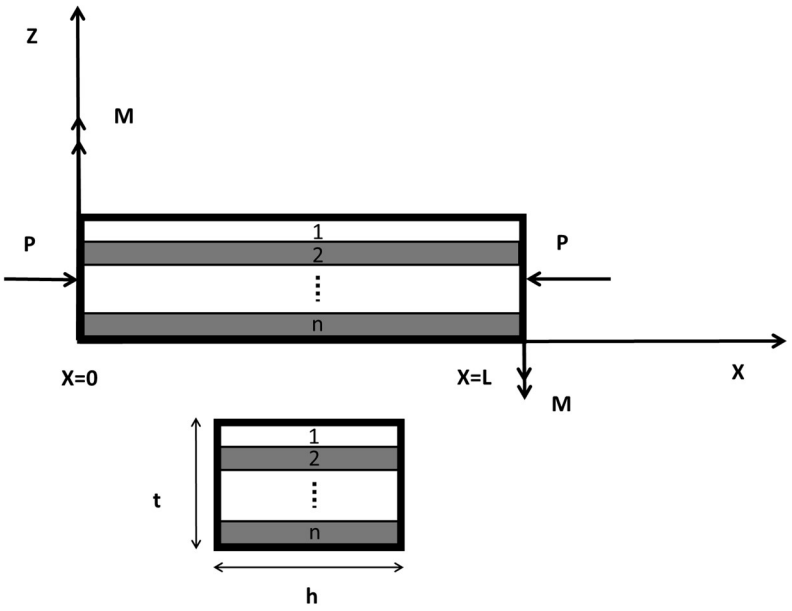

Figure 24: n-layered beam, with axial load and end-moment applied at *x=0* and *x=L*.

Reminding from Chapter 2, Equations of motion for a prismatic Euler-Bernoulli beam (*EI*=constant) subjected to constant axial force (*P*) and end moment (M_{zz}), undergoing coupled flexural-torsional vibrations (caused by end moment), are as follows:

$$EIw'''' + Pw'' + M_{zz}\theta'' + \rho A\ddot{w} = 0, \tag{84}$$

$$GJ\theta'' + \frac{PI_P}{A}\theta'' + M_{zz}w'' - \rho I_P\ddot{\theta} = 0, \tag{85}$$

where $()'$, stand for derivative with respect to x and $(\dot{})$ denotes derivative with respect to t (time). With the beam's torsional rigidity (GJ) assumed to be very large compared with its warping rigidity (EI), and ends free to warp; i.e., state of uniform torsion.

The Equations 84 and 85 are coupled by the end-moments, M_{zz}. Exploiting the simple harmonic motion assumption, displacements, w and θ, are written as:

$$w(x,t) = \widehat{W}\sin(\omega t), \qquad \theta(x,t) = \hat{\theta}\sin(\omega t), \tag{86-87}$$

where ω denotes the frequency, $\widehat{W}$ and $\hat{\theta}$ are the amplitudes of flexural and torsional displacements, respectively. Substituting equations (86-87 into equations 84 and 85 leads to:

$$EI\hat{W}'''' + P\hat{W}'' + M_{zz}\hat{\theta}'' - \rho A\omega^2\hat{W} = 0, \tag{88}$$

$$GJ\hat{\theta}'' + PI_P\hat{\theta}'' + M_{zz}\hat{W}'' + \rho I_P A\omega^2\hat{\theta} = 0. \tag{89}$$

As there are n layers with different materials, one will have n sets of equations for the whole system, i.e., two for each layer and $2n$ equations in total, written as ($i=1,2,3\ldots,n$):

$$E_i I_i \hat{W}_i'''' + P_i \hat{W}_i'' + M_{zz,i}\hat{\theta}''_i - \rho_i A_i \omega^2 \hat{W}_i = 0, \tag{90}$$

$$G_i J_i \hat{\theta}_i'' + P_i I_{P,i}\hat{\theta}_i'' + M_{zz,i}\hat{W}_i'' + \rho_i I_{P,i} A_i \omega^2 \hat{\theta}_i = 0. \tag{91}$$

where i represent the properties, displacements and loadings of i^{th} layer. Second moment of inertia and polar moment of inertia for each layer are calculated about the neutral axis of the whole (beam) cross section, and the applied axial load, P, and end moment, M_{zz}, can be written in terms of layers' contributions, P_i and $M_{zz,i}$, respectively, as follows:

$$P = \sum_{i=1}^{n} P_i, \quad \text{and } M_{zz} = \sum_{i=1}^{n} M_{zz,i}. \tag{92}$$

Enforcing the interlayer linear continuity for lateral and torsional displacements, similar to ANSYS 'constraint rigid link' element [100], the summation of n bending equations describes the bending equation of the whole beam and the summation of n torsion equations describes the torsion equation of the whole beam, resulting in the following two equations:

$$(\sum_{i=1}^{n} E_i I_i)\hat{W}'''' + (\sum_{i=1}^{n} P_i)\hat{W}'' + (\sum_{i=1}^{n} M_{zz,i})\hat{\theta}'' - (\sum_{i=1}^{n} \rho_i A_i)\omega^2 \hat{W} = 0, \tag{93}$$

$$(\sum_{i=1}^{n} G_i J_i)\hat{\theta}'' + (\sum_{i=1}^{n} P_i I_{P,i})\hat{\theta}'' + (\sum_{i=1}^{n} M_{zz,i})\hat{W}'' + (\sum_{i=1}^{n} \rho_i I_{P,i} A_i)\omega^2 \hat{\theta} = 0. \tag{94}$$

It is worth noting that in the above expressions, (93) and (94), $\hat{W}$ and $\hat{\theta}$ stand for the overall system's equivalent lateral and torsional displacements; i.e., those the entire system would undergo, if the it is modeled and treated as a single layer equivalent pre-stressed beam (similar to homogenization method).

3.4 The Layer-wise Beam Finite Element (LBFEM) formulation

The Galerkin method of weighted residuals is employed to develop the integral form of the above Expressions (93) and (94), written as:

$$\bar{W}_f = \int_0^L \delta W((\sum_{i=1}^{n} E_i I_i)W'''' + (\sum_{i=1}^{n} P_i)W'' + (\sum_{i=1}^{n} M_{zz,i})\theta'' - (\sum_{i=1}^{n} \rho_i A_i)\omega^2 W)dx = 0 \tag{95}$$

$$\bar{W}_t = \int_0^L \delta\theta((\sum_{i=1}^{n} G_i J_i)\theta'' + (\sum_{i=1}^{n} P_i I_{P,i})\theta'' + (\sum_{i=1}^{n} M_{zz,i})W'' + (\sum_{i=1}^{n} \rho_i I_{P,i} A_i)\omega^2 \theta)dx = 0 \tag{96}$$

where δW and $\delta\theta$ (i.e. weighting functions) represent the transverse and torsional virtual displacements, respectively. Performing integration by parts on equations 95 and 96 leads to the weak integral form of the governing equations, and by setting the boundary terms equal to zero based on the boundary conditions and definitions of shear force, bending moment and torsional torque, the beam is then discretized along its length, leading to the following element integral equations:

$$\bar{W}_f^k = \int_0^l ((\sum_{i=1}^{n} E_i I_i)W''\delta W'' - (\sum_{i=1}^{n} P_i)W'\delta W' + (\sum_{i=1}^{n} M_{zz,i})\theta'\delta W' - (\sum_{i=1}^{n} \rho_i A_i)\omega^2 W\delta W)dx \tag{97}$$

$$\bar{W}_t^k = \int_0^l ((\sum_{i=1}^{n} G_i J_i)\theta'\delta\theta' + (\sum_{i=1}^{n} P_i I_{P,i})\theta'\delta\theta' + (\sum_{i=1}^{n} M_{zz,i})W'\delta\theta' - (\sum_{i=1}^{n} \rho_i I_{P,i} A_i)\omega^2\theta\delta\theta)dx \qquad (98)$$

The total work satisfies the principle of virtual work ($\bar{W} = \bar{W}_f + \bar{W}_f = 0$, with $\bar{W}_{EXT} = 0$, for free vibrations), and

$$\bar{W} = \bar{W}_{INT} = \sum_{k=1}^{No.ofElements} \bar{W}^k = \sum_{k=1}^{No.ofElements} \bar{W}_f^k + \bar{W}_t^k \qquad (99)$$

The Layer-wise Beam FEM (LBFEM) formulation is attained by introducing linear and cubic Hermite polynomial interpolation functions to express the field and virtual variables (W, θ, δW and $\delta\theta$), expressed in terms of nodal variables, subsequently introduced in expressions 97 and 98. This process leads to the LBFE, with through-the-thickness mass $[m]^k$ and stiffness $[k]^k$ matrices written as:

$$[k]^k = [k]^k_{flex} + [k]^k_{tor} + [k]^k_{Coupling} \qquad (100)$$

where $[k]^k_{flex}$ and $[k]^k_{tor}$ are the *element* uncoupled flexural and torsional stiffness matrices, respectively, and $[k]^k_{Coupling}$ is the element coupling stiffness matrix, resulting from the end moment, M_{zz}. Furthermore, each of the $[k]^k_{flex}$ and $[k]^k_{tor}$ are written as:

$$[k]^k_{flex} = [k]^k_{flex\text{-}Static} + [k]^k_{flex\text{-}Geo} \quad \text{and} \quad [k]^k_{tor} = [k]^k_{tor\text{-}Static} + [k]^k_{tor\text{-}Geo} \qquad (101)$$

where $[k]^k_{flex\text{-}Static}$ and $[k]^k_{tor\text{-}Static}$ are the *element* uncoupled (constant) static flexural and torsional stiffness matrices respectively, and $[k]^k_{flex\text{-}Geo}$ and $[k]^k_{tor\text{-}Geo}$ are the corresponding geometric stiffness matrices resulting from the axial load P, respectively.

Assembly of the through-the-thickness mass $[m]^k$ and stiffness $[k]^k$ matrices along the beam length and the application of system boundary conditions leads to the following linear eigenvalue problem:

$$\langle \delta W_n \rangle \left(K - \omega^2 M\right) \{W_n\} = 0 \qquad \text{or} \qquad [K(\omega)]\{W_n\} = 0, \text{ where } K(\omega) = ([K] - \omega^2[M]) \quad (102)$$

where [K] and [M] are the system's (global) stiffness and mass matrices respectively, and [$K(\omega)$] is the so-called system Dynamic Stiffness Matric (DSM). Finally, the system's eigenvalues (i.e., natural frequencies) and their corresponding eigenvectors (i.e., natural modes) are extracted by setting:

$$\det[K(\omega)] = 0 \quad (103)$$

3.5 The Layer-wise Beam Dynamic Finite Element (LBDFE)

As mentioned in the introduction Chapter, section 1.1, DFE is an intermediate approach between the conventional FEM and Dynamic Stiffness Matrix (DSM) Methods, with proven higher convergence rates. In the DFE formulation the frequency-dependent trigonometric shape functions adopted from DSM are used. In order to develop the problem-specific dynamic shape functions, the solutions of uncoupled portions of the governing differential equations are used as the basis functions approximation space. The resulting frequency dependent shape functions are then utilized to find the element frequency dependent dynamic stiffness matrix. To this end, further integrations by parts are applied on the discretized (element) flexural integral Equation 97 and torsional integral Equation 98, leading to the following forms:

$$\begin{aligned} \bar{W}_f^k = & \int_{x_j}^{x_{j+1}} ((\sum_{i=1}^{n} E_i I_i) W \delta W'''' - (\sum_{i=1}^{n} P_i) W \delta W'' - (\sum_{i=1}^{n} \rho_i A_i) A\omega^2 W \delta W) dx + \int_{x_j}^{x_{j+1}} (\sum_{i=1}^{n} M_{zz,i}) \theta' \delta W' dx \\ & + \left[(\sum_{i=1}^{n} E_i I_i) W' \delta W'' - (\sum_{i=1}^{n} E_i I_i) W \delta W''' + (\sum_{i=1}^{n} P_i) W \delta W' \right]_{x_j}^{x_{j+1}} \end{aligned} \quad (104)$$

$$\bar{W}_t^k = \int_{x_j}^{x_{j+1}} -((\sum_{i=1}^{n} G_i J_i)\theta\delta\theta'' + (\sum_{i=1}^{n} P_i I_{P,i})\theta\delta\theta'' + (\sum_{i=1}^{n} \rho_i I_{P,i} A_i)\omega^2\theta\delta\theta)dx + \int_{x_j}^{x_{j+1}} (\sum_{i=1}^{n} M_{zz,i})W'\delta\theta' dx$$
$$+ \left[(\sum_{i=1}^{n} G_i J_i)\theta\delta\theta' + (\sum_{i=1}^{n} P_i I_{P,i})\theta\delta\theta' \right]_{x_j}^{x_{j+1}} \tag{105}$$

Substituting, $\xi = \frac{x}{l}$ in both equations above results in the non-dimensionalized element integral equations written as:

$$\bar{W}_f^k(\xi) = \int_0^1 W(\frac{1}{l^3}(\sum_{i=1}^{n} E_i I_i)\delta W'''' - \frac{1}{l}(\sum_{i=1}^{n} P_i)\delta W'' - (\sum_{i=1}^{n} \rho_i A_i)\omega^2 l\delta W)d\xi + \int_0^1 \frac{1}{l}(\sum_{i=1}^{n} M_{zz,i})\theta'\delta W' d\xi$$
$$+ \frac{1}{l^3}\left[(\sum_{i=1}^{n} E_i I_i)W'\delta W'' - (\sum_{i=1}^{n} E_i I_i)W\delta W''' \right]_0^1 + \frac{1}{l}\left[(\sum_{i=1}^{n} P_i)W\delta W' \right]_0^1 \tag{106}$$

$$\bar{W}_t^k(\xi) = \int_0^1 -\theta(\frac{1}{l}(\sum_{i=1}^{n} G_i J_i)\delta\theta'' + \frac{1}{l}(\sum_{i=1}^{n} P_i I_{P,i})\delta\theta'' + (\sum_{i=1}^{n} \rho_i I_{P,i} A_i)\omega^2 l\delta\theta)d\xi + \int_0^1 \frac{1}{l}(\sum_{i=1}^{n} M_{zz,i})W'\delta\theta' d\xi$$
$$+ \frac{1}{l}\left[(\sum_{i=1}^{n} G_i J_i)\theta\delta\theta' + (\sum_{i=1}^{n} P_i I_{P,i})\theta\delta\theta' \right]_0^1 \tag{107}$$

The flexural and torsional basis functions used to develop the relevant dynamic interpolation functions are, respectively, the solutions to the first (uncoupled) integral terms in expressions 106 and 107. Thus, the non–nodal solution approximation functions, W, and θ, and the test functions, δW, and $\delta\theta$, written in terms of generalized parameters $\langle a \rangle$, $\langle \delta a \rangle$, $\langle b \rangle$ and $\langle \delta b \rangle$, are as follows:

$$W = \langle P(\xi) \rangle_f * \{a\}, \qquad \delta W = \langle P(\xi) \rangle_f * \{\delta a\}, \tag{108-109}$$

$$\theta = \langle P(\xi) \rangle_t * \{b\}, \qquad \delta\theta = \langle P(\xi) \rangle_t * \{\delta b\}, \tag{110-111}$$

where the basis functions are defined as:

$$\langle P(\xi) \rangle_f = \left\langle \cos(\alpha\xi); \frac{\sin(\alpha\xi)}{\alpha}; \frac{\cosh(\beta\xi) - \cos(\alpha\xi)}{\alpha^2 + \beta^2}; \frac{\sinh(\beta\xi) - \sin(\alpha\xi)}{\alpha^3 + \beta^3} \right\rangle, \tag{112}$$

$$\left\langle P(\xi)\right\rangle_t = \left\langle \cos(\tau\xi); \sin(\tau\xi)/\tau \right\rangle. \tag{113}$$

with the roots, α, β, and τ defined as:

$$\alpha = \sqrt{|X_2|}, \quad \beta = \sqrt{|X_1|}, \; \tau = \sqrt{\frac{(\sum_{i=1}^{n} \rho_i I_{P,i} A_i)\omega^2 l^2}{(\sum_{i=1}^{n} A_i G_i J_i) + (\sum_{i=1}^{n} P_i I_{P,i})}} \tag{114}$$

and

$$X_1 = \frac{\left\{-B + \sqrt{B^2 - 4\bar{A}C}\right\}}{2\bar{A}}, \qquad X_2 = \frac{\left\{-B - \sqrt{B^2 - 4\bar{A}C}\right\}}{2\bar{A}}, \tag{115}$$

where:

$$\bar{A} = \frac{(\sum_{i=1}^{n} E_i I_i)}{l^3}, \qquad B = -\left(\frac{(\sum_{i=1}^{n} P_i)}{l} \right), \quad C = -(\sum_{i=1}^{n} m_i) l\omega^2 \tag{116}$$

The basis functions 112 and 113 are the solutions to the characteristic equations. When the roots, α, β, and τ, of the characteristic equations tend to zero, the resulting basis functions are similar to those of a standard beam element in the classical FEM, where flexure and torsion are approximated using cubic Hermite polynomials and linear functions, respectively.

Replacing the generalized parameters, $\langle a \rangle$, $\langle \delta a \rangle$, $\langle b \rangle$ and $\langle \delta b \rangle$, in equations (108-109 and (110-111 with the nodal variables, $\langle W_1 W_1' W_2 W_2' \rangle$, $\langle \delta W_1 \; \delta W_1' \; \delta W_2 \; \delta W_2' \rangle$, $\langle \theta_1 \theta_2 \rangle$, and $\langle \delta\theta_1 \delta\theta_2 \rangle$, respectively, and re-writing equations (108-109 and (110-111 will result in [41]:

$$\{W_n\} = [P_n]_f \{a\} \qquad \{\delta W_n\} = [P_n]_f \{\delta a\} \tag{117-118}$$

$$\{\theta_n\} = [P_n]_t \{b\} \qquad \{\delta\theta_n\} = [P_n]_t \{\delta b\} \tag{119-120}$$

The matrices, $[P_n]_f$ and $[P_n]_t$, are defined as:

$$[P_n]_f = \begin{bmatrix} 1 & 0 & 0 & 0 \\ 0 & 1 & 0 & \dfrac{(\beta-\alpha)}{(\alpha^3+\beta^3)} \\ \cos(\alpha) & \dfrac{\sin(\alpha)}{\alpha} & \dfrac{[\cosh(\beta)-\cos(\alpha)]}{(\alpha^2+\beta^2)} & \dfrac{[\sinh(\beta)-\sin(\alpha)]}{(\alpha^3+\beta^3)} \\ -\alpha\sin(\alpha) & \cos(\alpha) & \dfrac{[\beta\sinh(\beta)+\alpha\sin(\alpha)]}{(\alpha^2+\beta^2)} & \dfrac{[\beta\cosh(\beta)-\alpha\cos(\alpha)]}{(\alpha^3+\beta^3)} \end{bmatrix} \tag{121}$$

$$[P_n]_t = \begin{bmatrix} 1 & 0 \\ \cos(\tau) & \dfrac{\sin(\tau)}{\tau} \end{bmatrix} \tag{122}$$

Expressions equations (117-118), (119-120) and the $[P_{n,f}]$, and $[P_{n,t}]$ matrices above are combined in the following form to construct nodal approximations for flexural displacement, $W(\xi)$, and torsion displacement, $\theta(\xi)$.

$$W(\xi) = \langle P(\xi)\rangle_f [P_n]_f^{-1} \{W_n\} = \langle N(\xi)\rangle_f \{W_n\} \tag{123}$$

$$\theta(\xi) = \langle P(\xi)\rangle_t [P_n]_t^{-1} \{\theta_n\} = \langle N(\xi)\rangle_t \{\theta_n\} \tag{124}$$

In expressions 123 and 124, $\langle N(\xi)\rangle_f$ and $\langle N(\xi)\rangle_t$ are the frequency-dependent trigonometric shape functions for flexure and torsion, respectively. Equations 123 and 124 could be re-written as:

$$\begin{Bmatrix} W(\xi) \\ \theta(\xi) \end{Bmatrix} = [N]\{w_n\} \tag{125}$$

where,

$$[N] = \begin{bmatrix} N_{1f}(\omega) & N_{2f}(\omega) & 0 & N_{3f}(\omega) & N_{4f}(\omega) & 0 \\ 0 & 0 & N_{1t}(\omega) & 0 & 0 & N_{2t}(\omega) \end{bmatrix} \tag{126}$$

and

$$\{w_n\} = \left\langle W_1 W_1^{'} \theta_1 W_2 W_2^{'} \theta_2 \right\rangle^T \tag{127}$$

The definitions of the frequency-dependent trigonometric shape functions for flexure are:

$$\begin{aligned} N_{2f}(\omega) &= \frac{1}{D_f} * \left\{ \beta * \left[\cosh(\beta(1-\xi)) * \sin(\alpha) - \cosh(\beta) * \sin(\alpha(1-\xi)) - \sin(\alpha\xi) \right] \right. \\ &\left. + \alpha * \left[\cos(\alpha(1-\xi)) * \sinh(\beta) - \cos(\alpha) * \sinh(\beta(1-\xi)) - \sinh(\beta\xi) \right] \right\}, \end{aligned} \tag{128}$$

$$\begin{aligned} N_{3f}(\omega) &= \frac{(\alpha\beta)}{D_f} * \{ -\cos(\alpha(1-\xi)) + \cos(\alpha\xi) * \cosh(\beta) - \cosh(\beta(1-\xi)) + \cos(\alpha) \\ &* \cosh(\beta\xi) - \frac{\beta}{\alpha} * \sin(\alpha\xi) * \sinh(\beta) + \frac{\alpha}{\beta} * \sin(\alpha) * \sinh(\beta\xi) \}, \end{aligned} \tag{129}$$

$$\begin{aligned} N_{4f}(\omega) &= \frac{1}{D_f} * \left\{ \beta * \left[-\cosh(\beta\xi) * \sin(\alpha) + \sin(\alpha(1-\xi)) + \cosh(\beta) * \sin(\alpha\xi) \right] \right. \\ &\left. + \alpha * \left[-\cos(\alpha\xi) * \sinh(\beta) + \sinh(\beta(1-\xi)) + \cos(\alpha) * \sinh(\beta\xi) \right] \right\}. \end{aligned} \tag{130}$$

where,

$$D_f = (\alpha\beta) * \left\{ -2 * (1 - \cos(\alpha) * \cosh(\beta)) + \left(\frac{\alpha^2 - \beta^2}{\alpha\beta} \right) * \sin(\alpha) * \sinh(\beta) \right\} \tag{131}$$

The trigonometric shape functions for torsion, as also presented in [41] are:

$$N_{1t}(\omega) = \cos(\tau\xi) - \cos(\tau) * \frac{\sin(\tau\xi)}{D_t} \tag{132}$$

$$N_{2t}(\omega) = \frac{\sin(\tau\xi)}{D_t} \tag{133}$$

where,

$$D_t = \sin(\tau) \tag{134}$$

Using element integral expressions 106, 107 and the dynamic shape functions, 128 through 134, the element through-the-thickness Layer-wise Beam Dynamic Finite Element (LBDFE) matrix is obtained. The element stiffness matrix $[K(\omega)]^k$ consists of two coupled dynamic stiffness matrices, $[K(\omega)]^k_{BT,c}$ and $[K(\omega)]^k_{TB,c}$, symbolized collectively as $[K(\omega)]^k_c$, and four uncoupled dynamic stiffness matrices, $[K(\omega)]^k_{u1}$, $[K(\omega)]^k_{u2}$, $[K(\omega)]^k_{u3}$ and $[K(\omega)]^k_{u4}$ jointly denoted as, $[K(\omega)]^k_u$. The four uncoupled element stiffness matrices are as follows:

$$[K(\omega)]^k_{u1} = \frac{EI}{L^3}\left[\begin{matrix} N'_{1f}N''_{1f} & N'_{1f}N''_{2f} & N'_{1f}N''_{3f} & N'_{1f}N''_{4f} \\ N'_{2f}N''_{1f} & N'_{2f}N''_{2f} & N'_{2f}N''_{3f} & N'_{2f}N''_{4f} \\ N'_{3f}N''_{1f} & N'_{3f}N''_{2f} & N'_{3f}N''_{3f} & N'_{3f}N''_{4f} \\ N'_{4f}N''_{1f} & N'_{4f}N''_{2f} & N'_{4f}N''_{3f} & N'_{4f}N''_{4f} \end{matrix}\right]\Bigg|_0^1 \tag{135}$$

$$[K(\omega)]^k_{u2} = \frac{-EI}{L^3}\left[\begin{matrix} N_{1f}N'''_{1f} & N_{1f}N'''_{2f} & N_{1f}N'''_{3f} & N_{1f}N'''_{4f} \\ N_{2f}N'''_{1f} & N_{2f}N'''_{2f} & N_{2f}N'''_{3f} & N_{2f}N'''_{4f} \\ N_{3f}N'''_{1f} & N_{3f}N'''_{2f} & N_{3f}N'''_{3f} & N_{3f}N'''_{4f} \\ N_{4f}N'''_{1f} & N_{4f}N'''_{2f} & N_{4f}N'''_{3f} & N_{4f}N'''_{4f} \end{matrix}\right]\Bigg|_0^1 \tag{136}$$

$$[K(\omega)]^k_{u3} = \frac{P}{L}\left[\begin{matrix} N_{1f}N'_{1f} & N_{1f}N'_{2f} & N_{1f}N'_{3f} & N_{1f}N'_{4f} \\ N_{2f}N'_{1f} & N_{2f}N'_{2f} & N_{2f}N'_{3f} & N_{2f}N'_{4f} \\ N_{3f}N'_{1f} & N_{3f}N'_{2f} & N_{3f}N'_{3f} & N_{3f}N'_{4f} \\ N_{4f}N'_{1f} & N_{4f}N'_{2f} & N_{4f}N'_{3f} & N_{4f}N'_{4f} \end{matrix}\right]\Bigg|_0^1 \tag{137}$$

$$[K(\omega)]^k_{u4} = \frac{1}{L}\left(GJ + \frac{PI_P}{A}\right)\left[\begin{matrix} N_{1t}N'_{1t} & N_{1t}N'_{2t} \\ N_{2t}N'_{1t} & N_{2t}N'_{2t} \end{matrix}\right]\Bigg|_0^1 \tag{138}$$

The two coupled element matrices are as follows:

$$[K(\omega)]^k_{BT,c} = \int_0^1 \frac{M}{L}\left[\begin{matrix} N'_{1t}N'_{1f} & N'_{1t}N'_{2f} & N'_{1t}N'_{3f} & N'_{1t}N'_{4f} \\ N'_{2t}N'_{1f} & N'_{2t}N'_{2f} & N'_{2t}N'_{3f} & N'_{2t}N'_{4f} \end{matrix}\right] d\xi \tag{139}$$

$$[K(\omega)]^{k}_{TB,c} = \int_0^1 \frac{M}{L} \begin{bmatrix} N'_{1f}N'_{1t} & N'_{1f}N'_{2t} \\ N'_{2f}N'_{1t} & N'_{2f}N'_{2t} \\ N'_{3f}N'_{1t} & N'_{3f}N'_{2t} \\ N'_{4f}N'_{1t} & N'_{4f}N'_{2t} \end{bmatrix} d\xi \tag{140}$$

The through-the-thickness element dynamic stiffness matrix $[K(\omega)]^k$ is determined by adding these six coupled and uncoupled sub-matrices. Finally, the system's global dynamic stiffness matrix $[K(\omega)]$ is obtained by assembling all the through-the-thickness element matrices along the beam length and applying the system boundary conditions (using a code developed in MATLAB). This procedure, also satisfying the principle of virtual work, leads to:

$$[K_{DFE}(\omega)]\{W_n\} = 0 \tag{141}$$

which is solved using any standard determinant search method or Wittrick–Williams (W-W) algorithm [98], to obtain the eigenvalue ω and eigenmodes, $\{W_n\}$ of the structure.

3.6 Method of Homogenization Numerical Results

To verify the validity of the homogenization method, a two-layer beam with length of 8 m and rectangular cross section is selected. The width is 0.4 m and height is 0.2 m. Layer 1 is aluminium with Young's modulus E=72GPa and density ρ=2800 kg/m^3, and layer 2 is Steel with E=200GPa and ρ=7800 kg/m^3. Thickness of aluminium and Steel layers are 0.0667 m and 0.1333 m, respectively, and the boundary conditions are clamped-free (cantilevered beam).

In order to validate the results, the layered beam is modeled in ANSYS. The results of the code and ANSYS for first six natural frequencies, end moment M_{zz}=0, and three different values of compressive axial force are presented in Table 16. By increasing the axial load from 0 to 0.9 MN, the first natural frequency changes form 2.3 Hz to 0.56 Hz. Table 17 presents the first six natural

frequencies for end moment M_{zz}=0 and three different values of tensile axial force. Changing the tensile force from 0 to 0.9 MN increases the first natural frequency from 2.3 Hz to 3.11 Hz. The effect of end moment in absence of axial force is also investigated and the results are shown in Table 18. Increasing the end moment from 0 to 4.5MN.m decreases the first natural frequency from 2.3 Hz to 1.44 Hz.

Table 16: First six natural frequencies for end moment M_{zz}=0 and different values of compressive axial force P.

	P=0, M_{zz}=0		P=-0.3MN, M_{zz}=0		P=-0.6MN, M_{zz}=0		P=-0.9MN, M_{zz}=0	
	ANSYS 20 elements (Hz)	Homog. FEM 5 elements (Hz)	ANSYS 20 elements (Hz)	Homog. FEM 5 elements (Hz)	ANSYS 20 elements (Hz)	Homog. FEM 5 elements (Hz)	ANSYS 20 elements (Hz)	Homog. FEM 5 elements (Hz)
1st	2.301	2.302	1.927	1.928	1.434	1.435	0.558	0.559
2nd	14.385	14.426	14.005	14.046	13.614	13.654	13.210	13.250
3rd	40.124	40.393	39.804	40.073	39.481	39.750	39.156	39.425
4th	74.474	74.705	74.540	74.699	74.601	74.694	74.672	74.688
5th	78.693	79.155	78.534	78.853	78.374	78.551	78.214	78.247
6th	128.370	130.850	128.080	130.559	127.780	130.267	127.490	129.975

Table 17: First six natural frequencies for end moment M_{zz}=0 and three different values of tensile axial force.

	P=0.3MN, M_{zz}=0		P=0.6MN, M_{zz}=0		P=0.9MN, M_{zz}=0	
	ANSYS 20 elements (Hz)	Homog. FEM 5 elements (Hz)	ANSYS 20 elements (Hz)	Homog. FEM 5 elements (Hz)	ANSYS 20 elements (Hz)	Homog. FEM 5 elements (Hz)
1st	2.610	2.611	2.876	2.878	3.113	3.114
2nd	14.754	14.795	15.112	15.154	15.461	15.503
3rd	40.441	40.711	40.756	41.026	41.068	41.339
4th	74.410	74.710	74.345	74.716	74.280	74.721
5th	78.852	79.455	79.011	79.754	79.169	80.052
6th	128.660	131.140	128.950	131.429	129.240	131.718

Table 18: First six natural frequencies for end Axial force P=0 and three different values of end moment.

	P=0, M_{zz}=1.5 MN.m		P=0, M_{zz}=3 MN.m		P=0, M_{zz}=4.5 MN.m	
	ANSYS 20 elements (Hz)	Homog. FEM 5 elements (Hz)	ANSYS 20 elements (Hz)	Homog. FEM 5 elements (Hz)	ANSYS 20 elements (Hz)	Homog. FEM 5 elements (Hz)
1st	2.195	2.226	1.936	1.976	1.361	1.441
2nd	14.292	14.343	14.006	14.090	13.502	13.657
3rd	40.010	40.322	39.664	40.108	39.070	39.749
4th	74.770	74.706	73.426	74.710	71.739	74.716
5th	78.693	79.087	79.416	78.885	80.181	78.546
6th	128.330	130.784	128.220	130.586	128.030	130.256

In Figure 25 and Figure 26, the bending and torsion mode shapes, for first five natural frequencies are shown, respectively. The critical (buckling) loads are also found. In Table 19 buckling end moments for ten different values of axial force (tension and compression) and in Table 20 buckling axial force for five different values of end moment are presented. These results are also illustrated in Figure 27 and Figure 28.

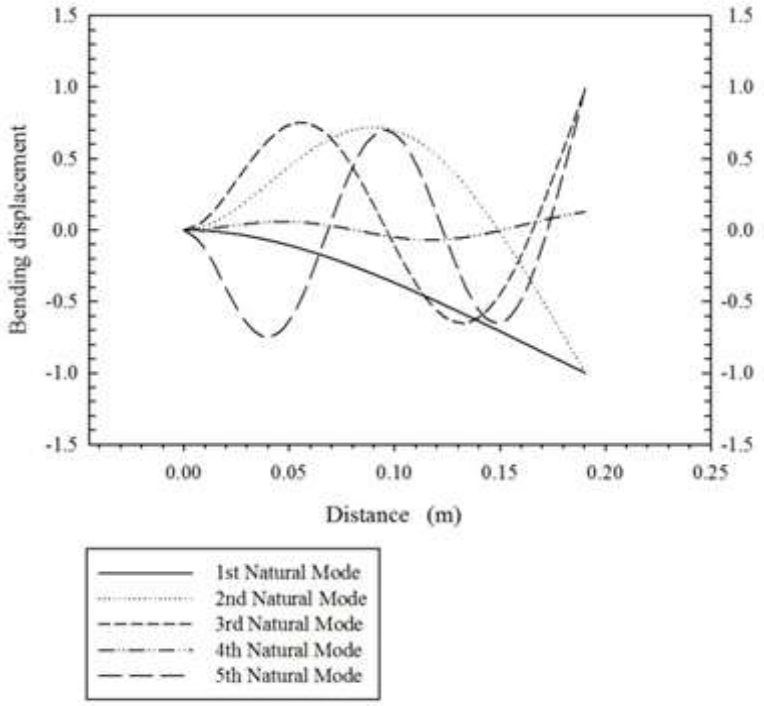

Figure 25: Bending components of the natural modes for M_{zz}=3MN and P=0.6MN homogenization method.

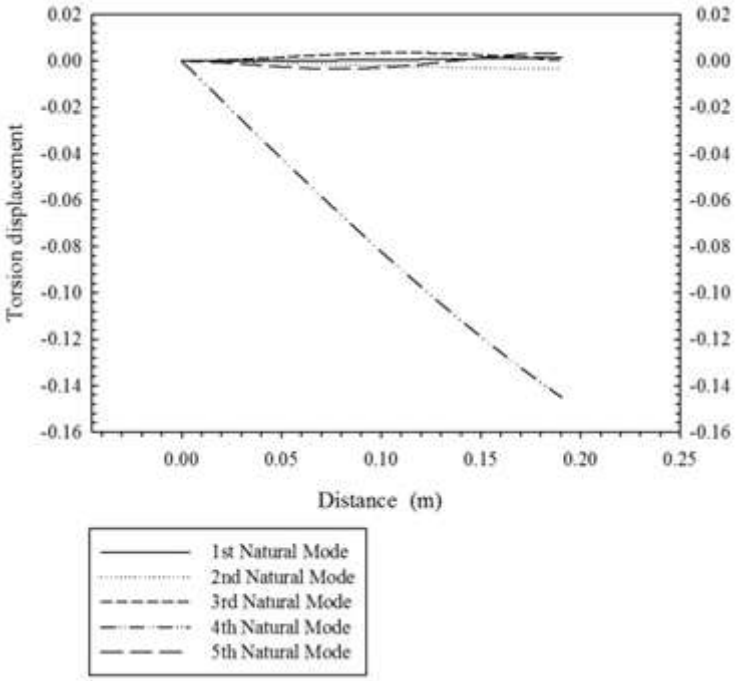

Figure 26: Torsion components of the natural modes for M_{zz}=3 MN and P=0.6 MN homogenization method.

Table 19: Buckling end moments for different values of axial force homogenization method.

Force (MN)	Buckling Moment, (MN.m)
-0.900	1.320
-0.750	2.660
-0.600	3.470
-0.450	4.140
-0.300	4.740
0.000	5.690
0.300	6.520
0.450	6.900
0.600	7.259
0.750	7.610

Table 20: Buckling axial force for different values of end moment homogenization method.

Moment (MN.m)	Buckling Force (MN)
0.000	-0.995
1.500	-0.896
2.250	-0.814
3.000	-0.695
3.750	-0.538

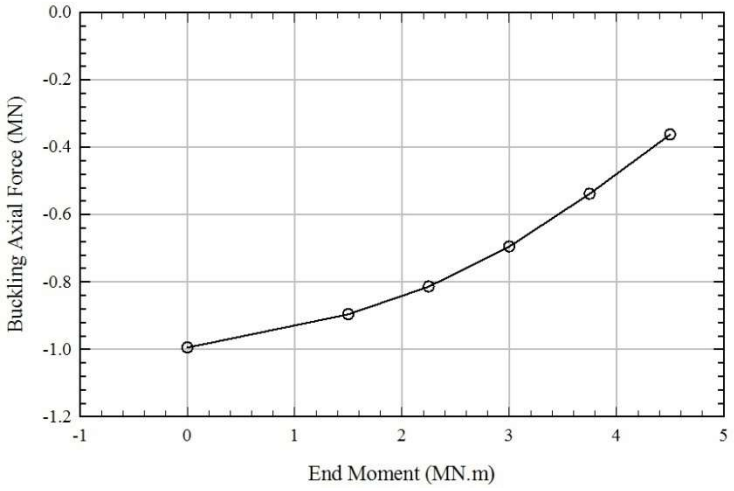

Figure 27: Buckling axial force vs. end moment homogenization method.

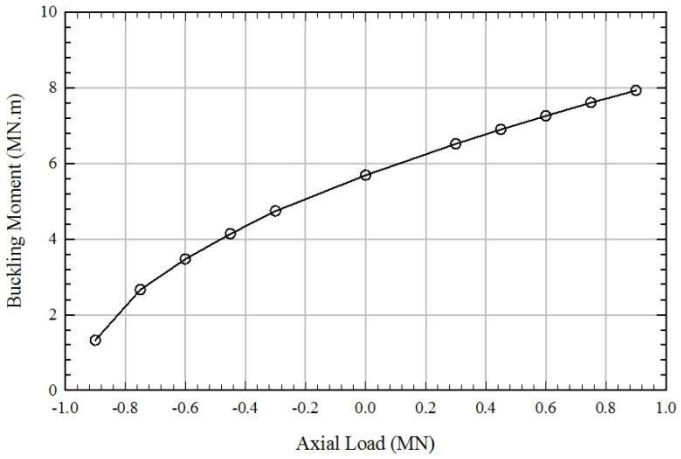

Figure 28: Buckling end moment vs. axial load using homogenization method.

3.7 Layer-wise formulation numerical tests; two-layer aluminium-steel beam

In order to test the layer-wise theory a two-layered beam made of aluminium (E=70 GPa and ρ=2700kg/m^3) and steel (E=200 GPa and ρ=7800 kg/m^3), with 8 m length, 0.12 m width and 0.06 m height is considered. The thickness of steel and aluminium layers are the same and equal to 0.03 m. Table 21 represents the fundamental frequencies using clamped-free boundary condition for the new method, method of homogenization and ANSYS. For comparing the accuracy of the new method and method of homogenization, the ANSYS results using 20 elements are used as benchmark.

Table 21: Fundamental frequencies for clamped-free boundary condition.

C-F	End Moment 52.5 (KN.m)			
	FEM Fundamental Frequency (Hz)			
Tensile Force (KN)	DFE (5 elements)	FEM (5 elements)	Homogenization (5 elements)	ANSYS (20 elements)
0	0.306	0.308	0.313	0.306
17.5	0.979	0.980	0.982	0.979
34.9	1.299	1.300	1.301	1.299
52.3	1.532	1.533	1.534	1.532

The buckling analysis is also carried out to investigate the effect of axial force and end moment on the stability of beam. Figure 29 illustrate the variation of the first fundamental frequency with tensile axial force and end moment and Table 22 shows the variation of buckling moment with axial force for M_{zz}=52.5KN.m, P=17.5KN using DFE.

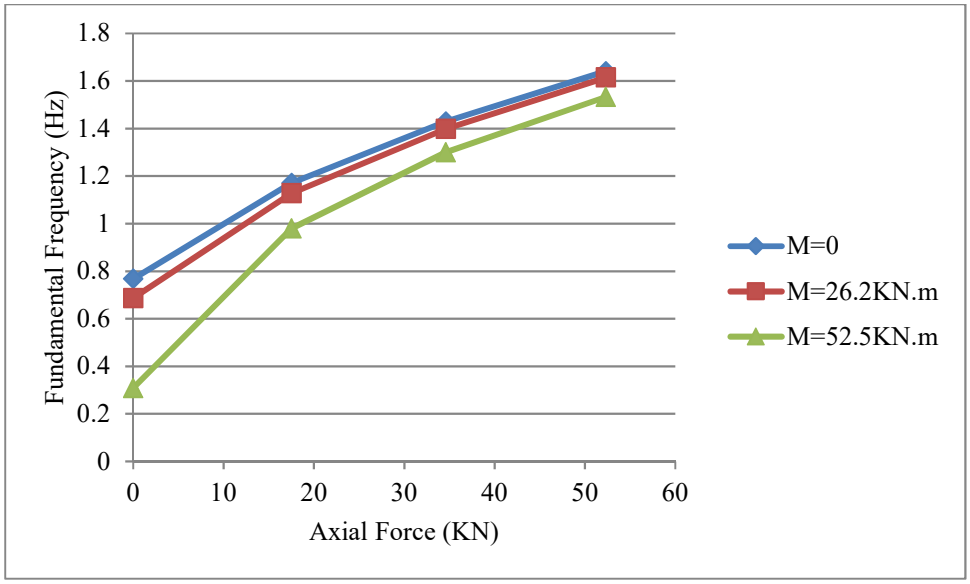

Figure 29: Variation of natural frequencies with tensile force and end moment for cantilevered boundary condition.

Table 22: Variation of buckling moment with axial force for two layered Aluminium-Steel beam

Force (KN)	Buckling Moment (KN.m) DFE (5 element)
0	118.61
0.62	135.33
1.23	160.52
1.85	183.32

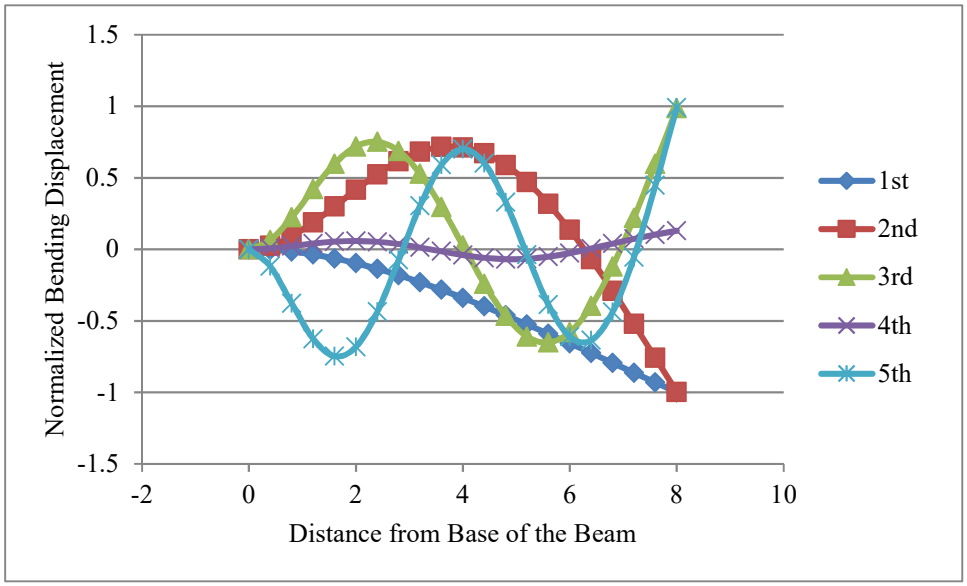

Figure 30: Bending components of mode shapes (DFE) *M*=52.5 KN.m, *P*=17.5KN

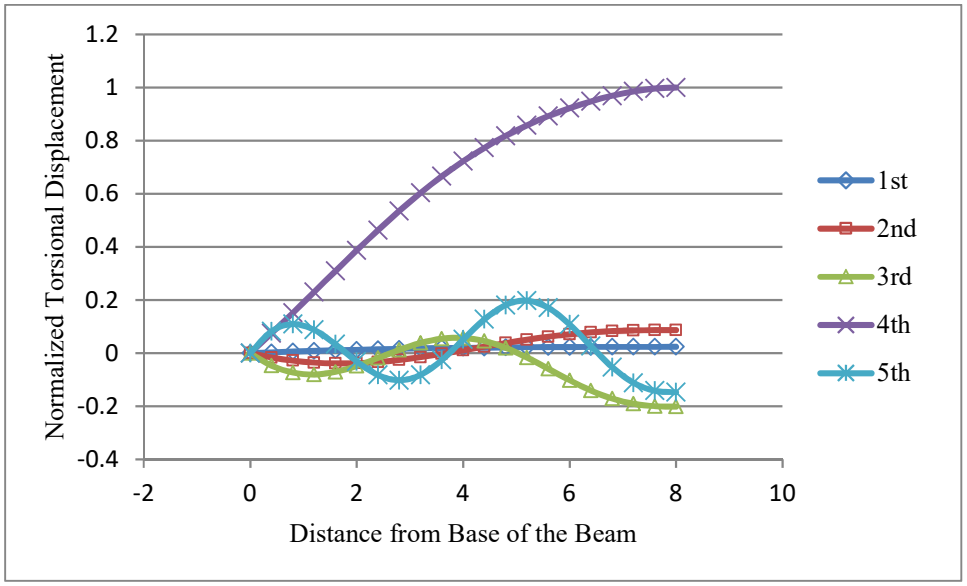

Figure 31: Torsion components of mode shapes (DFE) Moment=52.5KN.m, Force=17.5KN

3.8 Numerical tests; two-layer Glass/Epoxy composite beam

Consider a uniform two-layered cantilever beam, made of unidirectional plies of glass/epoxy composite material, with fibre angles of +90˚ and 0˚ for layer 1 and 2 respectively. The beam has a length of L=0.1905 m, thickness of 3.18 mm, width of 12.7 mm and thickness of each layer is 1.59 mm. The fibre properties include: E_f=275.6 GPa, G_f=114.8 GPa, v_f=0.2, ρ_f=1900 Kg/m^3 and matrix properties include: E_m=2.76 GPa, G_m=1.036 GPa, v_m=0.33, ρ_m=1600 Kg/m^3 and the volume fraction of both layers is considered 0.8. The schematic of the problem is presented in Figure 32. The free vibration analysis of the system is performed using, FEM, DFE and ANSYS.

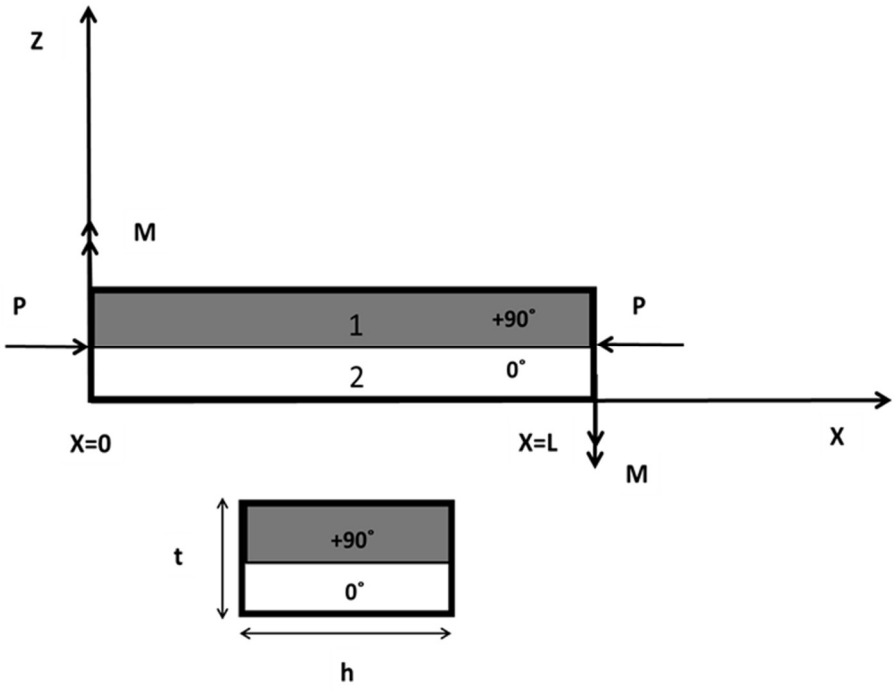

Figure 32: The schematic of two-layer composite beam.

Table 23: Fundamental frequencies for clamped-free boundary condition (DFE and FEM using 5 elements and ANSYS using 20 elements) for two-layer composite beam (M_{zz}=6.14MN.m, P=1.23MN).

Nat. Freq. [Hz]	DFE	FEM|	ANSYS
1st	76.45	76.51	76.42
2nd	316.35	318.98	314.46
3rd	758.84	763.78	755.71

As it could also be inferred from Table 23, the DFE frequency values are in excellent agreement with those obtained from ANSYS and standard FEM code. Stability analysis is also carried out for variable axial force and end moments and the results using both FEM and DFE are in good agreement. Figure 33 illustrate the variation of the first fundamental frequency with tensile axial force and end moment for cantilever boundary condition.

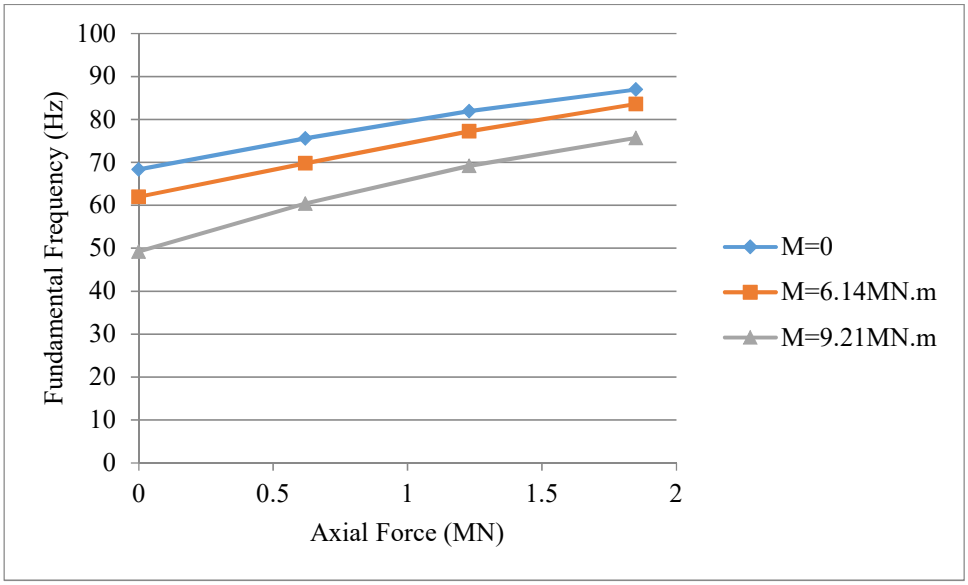

Figure 33: Fundamental frequency varying by different applied axial force and end moment for two-layer composite beam.

3.9 Numerical tests; steel-rubber-steel layered beam

In order to validate the results of sandwich beam models with a better benchmark, an experimental study by Banerjee *et al.* [101], is selected. The schematic of the sandwich beam is shown in Figure 34. The parameters of the steel-rubber-steel sandwich beam used in this study are as follows. Thicknesses are: steel (1.5 mm)–rubber (18 mm)–steel (2.4 mm), length of sandwich beam is 500 mm and width 50 mm for each layer. Their experimental modal testing set up includes an impact hammer kit and an accelerometer. In all of their tests, the sandwich beam is cantilevered with one end fully built-in in order to prevent any displacements. The accelerometer is set at a fixed position which is considered as the reference point while the hammer impact point is changed to a number of points in order to create the excitation forces on the test sample, corresponding to the allowed degrees of freedom in their model. Banerjee *et al.* [101] also developed a DSM model and confirmed their results with experimental results. The comparison between the experimental results, DSM, LBDFE, LBFEM and method of homogenization are presented in Table 24.

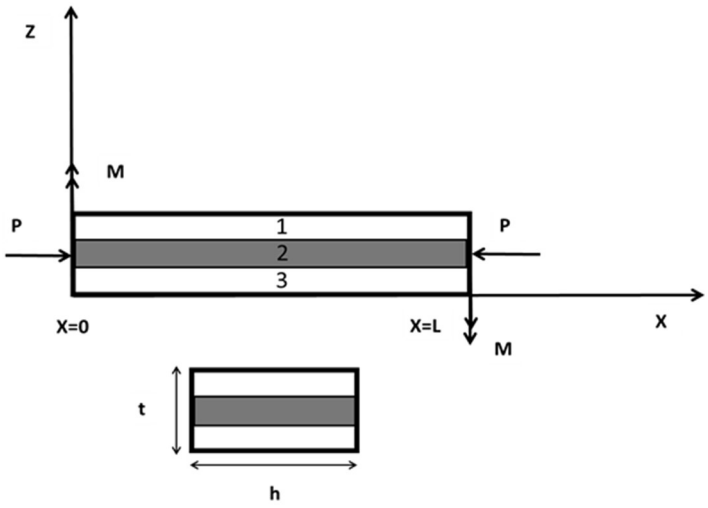

Figure 34: The schematic of steel-rubber-steel sandwich beam

Table 24: comparison between experimental results [101], DSM [101], LBDFE, LBFEM and homogenization methods with P=0 and M_{zz}=0 with cantilevered boundary condition.

Nat. Freq. No.	LBDFE (Hz) (5 elements)	LBFEM (Hz) (5 elements)	Homogen. (Hz) (5 elements)	Experiment (Hz) [101]	DSM (Hz) [101]
1	10.62	10.67	10.71	9.04	10.62
2	33.88	36.12	38.48	29.38	33.88
3	63.73	69.08	72.71	53.75	63.73

3.10 Numerical tests; fibre-metal laminated (FML) beam

Numerical tests were performed to confirm the predictability, accuracy and practical applicability of the proposed methods. Both the LBFEM and LBDFE formulations were first validated using the numerical examples of pre-stresses single-layer beams presented Chapter 2. In what follows, free vibration analysis of a pre-stressed three-layered Fibre-Metal Laminated (FML) and two unidirectional laminated glass/epoxy composite beams is presented.

The first numerical case is a three-layered (sandwich) Fibre-Metal Laminated (FML) beam of rectangular cross-section, length of 8m, width of 0.12m and 0.06 m of height (thickness). The top and bottom layers are assumed to be glass epoxy composite with fiber angle of +90˚. The fibre properties include: E_f=275.6 GPa, G_f=114.8 GPa, ν_f=0.2, ρ_f=1900 Kg/m^3 and matrix properties include: E_m=2.76 GPa, G_m=1.036 GPa, ν_m=0.33, ρ_m=1600 Kg/m^3 and the volume fraction of both layers is considered 0.8. The equivalent properties are found to be E_c=310 GPa and ρ_c=6100 kg/m^3. The middle layer is assumed to be aluminium (E_{Al}= 70 GPa and ρ_{Al} =2700 kg/m^3). The thickness of all the three FRP and Aluminium layers are the same and equal to 0.02m. Table 25 presents the

fundamental frequency of the system for clamped-free boundary condition, and various axial loads and end moment of 52.5KN.m, obtained from the proposed layer-wise DFE, FEM, homogenization method and ANSYS®. For comparison purposes, the ANSYS® results obtained using a 20-element model are used as benchmark. As can be observed from Table 25, excellent agreement is found between the LBDFE, LBFEM, and homogenization method and ANSYS® modeling results.

Table 25: Fundamental frequency of pre-stressed cantilevered FML beam, subjected to various axial loads and end moment of 52.5KN.m.

Tensile Force (KN)	LBDFE (5 elements)	LBFEM (5 elements)	ANSYS® (20 elements)	Homogenization (5 elements)
0	0.254	0.258	0.254	0.260
17.5	0.941	0.945	0.938	0.948
34.9	1.251	1.254	1.249	1.259
52.3	1.508	1.511	1.502	1.514

The convergence rates for the two proposed layer-wise LBFEM and LBDFE formulations are compared in Figure 35, where the DFE's rates of convergence surpassing FEM by almost a factor of five. An analysis is also carried out to investigate the effects of both axial force and end moment (combined) on the fundamental frequencies of the beam. Figure 36 illustrates the variation of the first natural frequency with tensile axial force and end moment using DFE method.

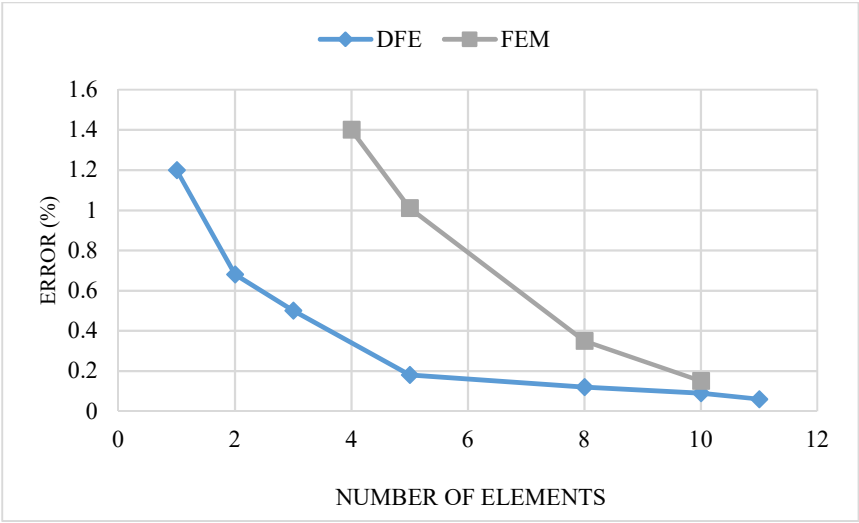

Figure 35: The convergence study for the two proposed layer-wise LBFEM and LBDFE formulations; fundamental frequency of cantilevered FML three-layer beam subjected to an axial load of 17.5MN and end moment of 52.5KN.m.

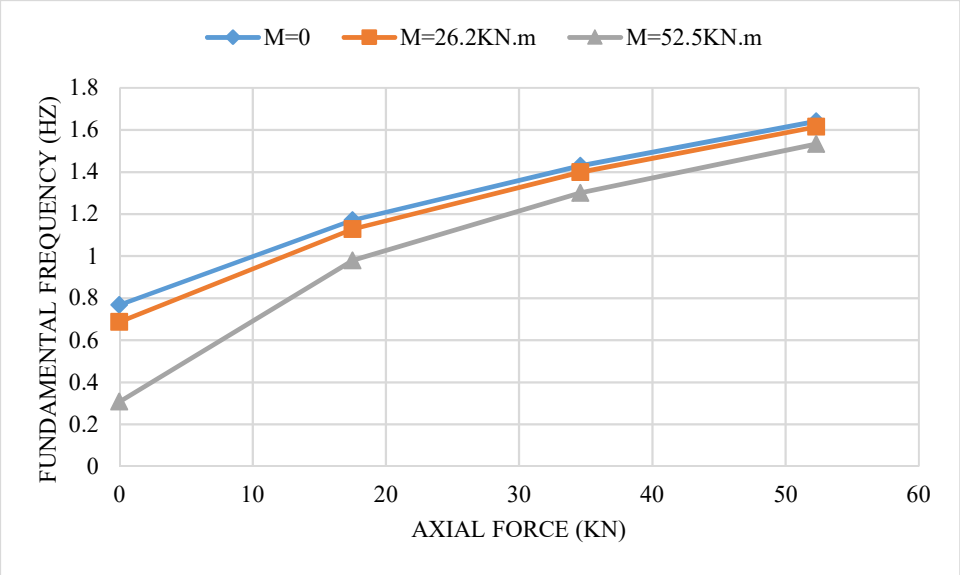

Figure 36: Fundamental frequency vs. tensile force and end moment for the cantilevered three-layer FML beam.

3.11 Numerical tests; three-layered laminated composite beam

In what follows, two cantilevered uniform three-layered composite beams made of unidirectional plies of glass/epoxy composite material, with fiber angles 0˚/+90˚/0˚ (layup 1) and +90˚/0˚/+90˚ (layup 2) are investigated. The beams have a length of L=0.1905 m, total thickness of 3.18 mm, width of 12.7 mm, and thickness of all three layers are equal. The fiber properties include: E_f=275.6 GPa, G_f=114.8 GPa, v_f=0.2, ρ_f=1900 Kg/m^3 and matrix properties include: E_m=2.76 GPa, G_m=1.036 GPa, v_m=0.33, ρ_m=1600 Kg/m^3 and the volume fraction of both layers is considered 0.8. The free vibration analysis of the system is performed using both LBFEM and LBDFE methods as well as ANSYS®. The first three natural frequencies of laminated composite beams are shown in Table 26.

Table 26: First three natural frequencies of cantilevered, preloaded, three-layer, unidirectional composite beams (Layups 1 and 2) obtained from 5-element LBDFE and LBFEM, and 20-element ANSYS® models, subjected to an axial load of 1.85MN and end moment of 6.14MN.m.

Nat. Freq. [Hz]	LBDFE (5 Elements)		LBFEM (5 Elements)		ANSYS® (20 Elements)	
	layup 1	layup 2	layup 1	layup 2	layup 1	layup 2
1^{st}	79.84	72.35	79.90	72.42	79.84	72.35
2^{nd}	328.05	299.75	342.62	312.04	326.91	298.73
3^{rd}	765.28	736.82	790.48	754.44	757.86	729.74

Based on the frequency results presented in Table 26, the LBDFE frequency values for both layups are in excellent agreement with those obtained from ANSYS® and LBFEM, with the DFE's rates of convergence surpassing FEM. As can be observed from Table 26, for the fundamental frequency the LBDFE and ANSYS® results match perfectly, whereas the LBFEM shows a minor difference of less than 0.1%. As expected, as the frequency number increases, the difference between the presented

methods and ANSYS® data increases. Finally, the maximum difference between the LBDFE and ANSYS® results (for the 3rd frequency) is less than 1%, whereas the LBFEM shows a larger difference of 3.3%.

A study is also carried out to find the variation of system's natural frequencies in terms of axial load and end moment. Variation of the fundamental frequency of cantilevered, preloaded, three-layer, unidirectional composite beam (Layup1) obtained from a 5-element LBDFE model, subjected to various axial loads and end moments is presented in Figure 37. As can be observed, when the axial force is increased, the natural frequency decreases. However, as the end moment is increased, the system's frequency decreases.

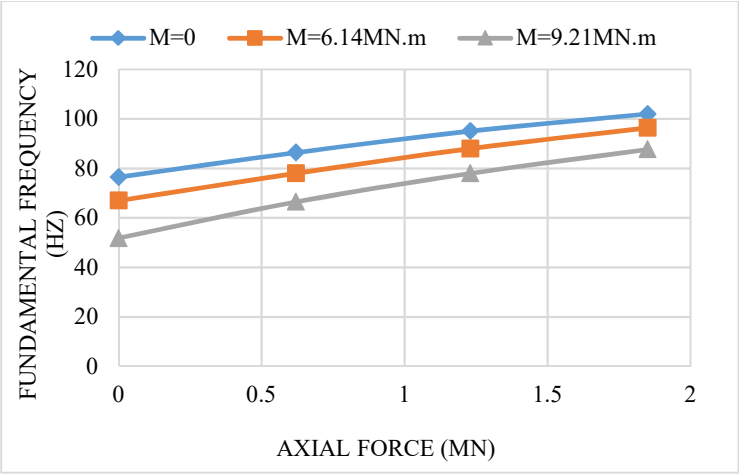

Figure 37: Fundamental frequency of cantilevered, preloaded, three-layer, unidirectional composite beam (Layup 1) obtained from a 5-element LBDFE model, subjected to various axial loads and end moments.

Figure 38 and Figure 39, respectively, show bending and torsional components of the first five mode shapes of the cantilevered, preloaded, three-layer, unidirectional composite beam (Layup1) obtained using a 20-element LBDFE model, subjected to an axial load of 1.85MN and end moment of

6.14MN.m. As it can be seen, the first three and fifth modes are predominantly bending with slight influence of torsion, whereas the third mode has a predominant torsional character.

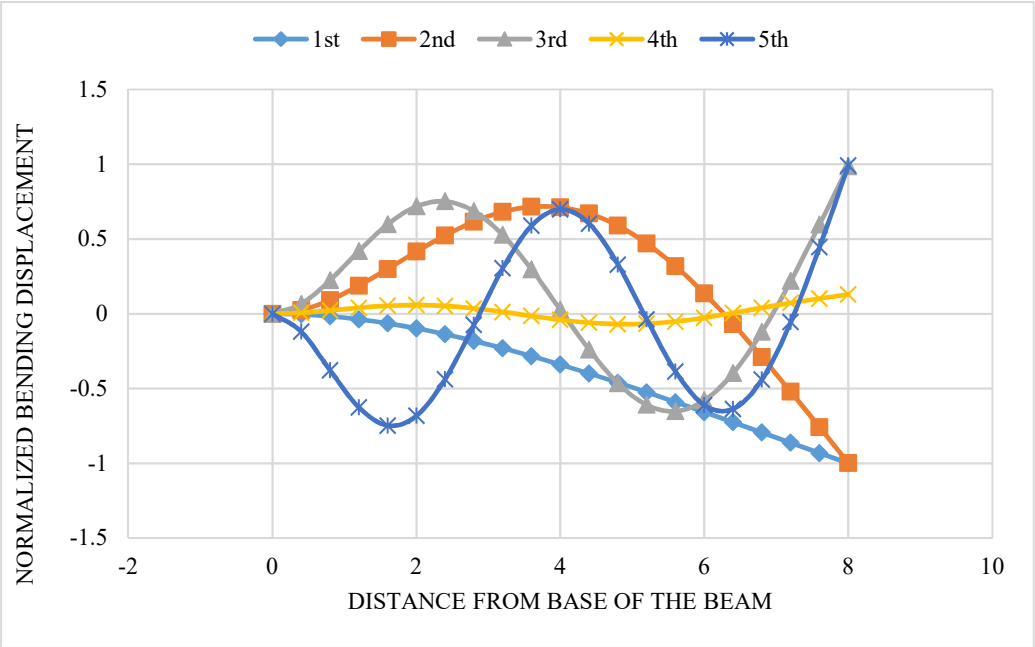

Figure 38: Bending component of the first five mode shapes of the cantilevered, preloaded, three-layer, unidirectional composite beam (Layup1) obtained using a 20-element LBDFE model, subjected to an axial load of 1.85MN and end moment of 6.14MN.m.

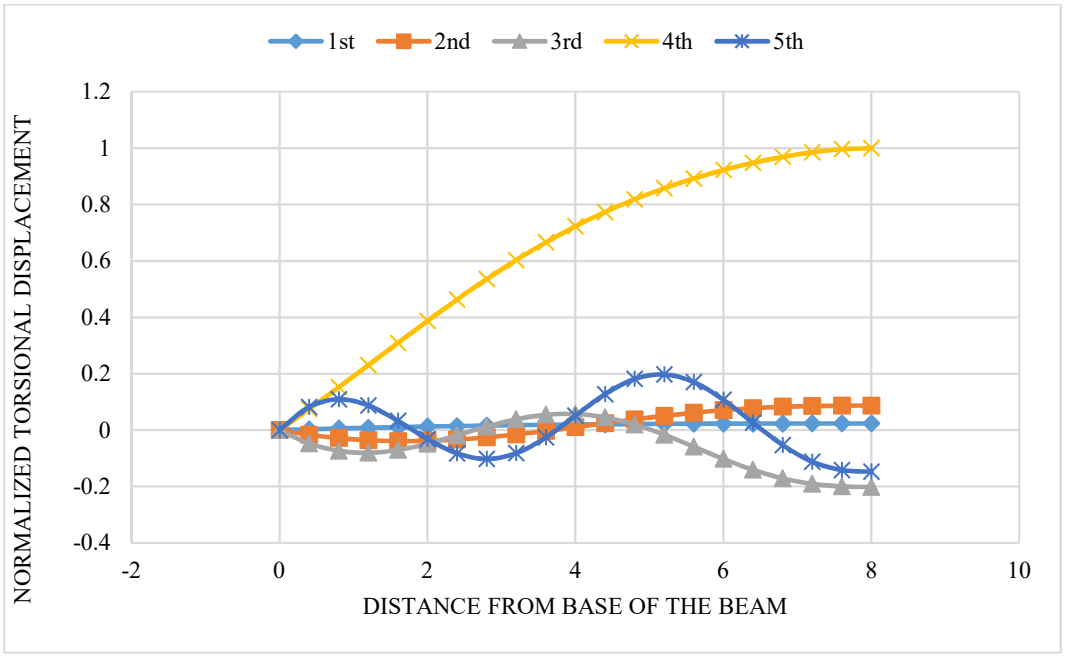

Figure 39: Torsion component of the first five mode shapes of the cantilevered, preloaded, three-layer, unidirectional composite beam (Layup1) obtained using a 20-element LBDFE model, subjected to an axial load of 1.85MN and end moment of 6.14MN.m.

3.12 Discussions and concluding remarks

Free vibration analysis of pre-stressed sandwich and layered beams including fiber-metal and unidirectional composite laminates, were presented in this Chapter. Method of homogenization, layer-wise Finite Element and layer-wise Dynamic Finite Element models were developed and used for numerical vibrational analysis of different configurations of layered, sandwich and composite beams. The results were compared to determine the method with highest rate of convergence and best accuracy. Based on the results shown in Table 25 and Figure 35, the presented layer-wise FEM method has higher rate of convergence comparing to method of homogenization while DFE has higher rate of convergence comparing to FEM method which makes DFE the most efficient method. Considering the benchmark (ANSYS 20 elements), error of the FML beam fundamental frequency

for DFE method using 5 elements along the beam length is almost zero. This error for layer-wise FEM method using 5 elements, is around 0.64% while for method of homogenization using same number of longitudinal elements it is 2.24%. As expected, and with reference to Figure 37 (three-layer unidirectional glass/epoxy composite beam, layup 1), tensile axial load increases the natural frequencies of the beam, indicating an increase in the stiffness of the beam. When the end moment is increased, the natural frequencies reduce, indicating a reduction in stiffness of the beam. If the end moment is held constant and the tensile load is increased, the natural frequencies increase indicating an increase in the beam stiffness. Conversely, if the tensile load is held constant and the end moment is increased, the beam stiffness reduces. Considering Figure 38 and Figure 39, the coupled vibration of the cantilevered three-layer, unidirectional composite beam (Layup1), is found to be predominantly flexural in the first few natural frequencies (the first three, for the case studied here) and torsion becomes predominant at a higher natural frequency starting from the fourth mode of vibration.

4 Modal analysis of laminated composite beams subjected to axial force and end moment

In this Chapter the free vibration analysis of a composite beam subjected to axial force and end moment is presented. In addition to the material coupling between bending and torsion displacements caused by end moment, encountered and treated in various cases of pre-stressed beam configurations studied the previous Chapters, a laminated composite beam (with general fibre angle) is characterized by another material coupling term appearing in the equations, which in turn, brings more complexity to free vibration analysis of composite beams. In what follows, the equations of motion are introduced and the mathematical models for FEM and DFE formulations are explained, followed by the numerical test for validation of results and comparison between the accuracy of proposed methods.

4.1 Finite element formulation (FEM)

Consider a laminated composite beam of length L and solid rectangular cross-section as shown in Figure 40. The material bending-torsion coupling behavior usually present in composite material is due to the unbalanced layup. The beam is characterized by the effective (equivalent) bending rigidity, EI, the torsional rigidity, GJ, and the bending-torsion coupling rigidity, K (see Appendix B for more information on coupling rigidity). A symmetric configuration consists of symmetry of fiber orientations and thickness with respect to the mid-plane of the laminate.

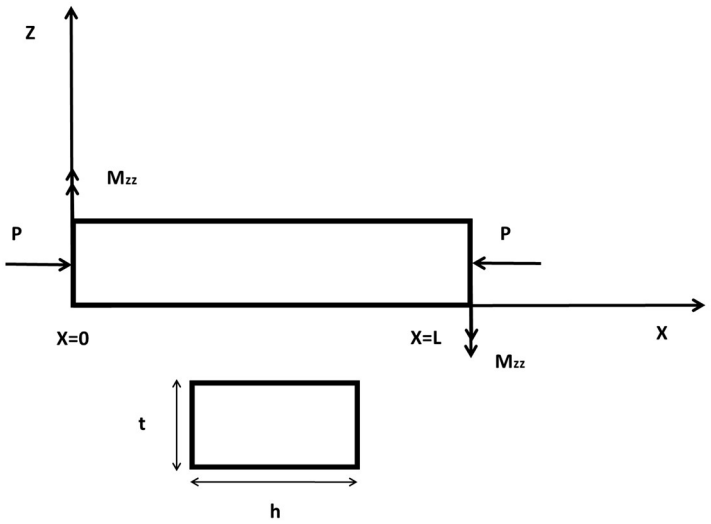

Figure 40: geometry and coordinate system of the model

The rigidities can be determined using classical lamination theory (CLT) [45]. Neglecting the shear, rotary inertia and warping effects, the Euler-Bernoulli bending and St. Venant torsion beam theories are used, where the flexural displacement is denoted by $w(x,t)$ whereas $\theta(x,t)$ is used to denote the twist angle. Governing differential equations of motion of the system can be developed by defining an infinitesimal element and assuming linearly elastic material, small displacements, rectangular cross-sectional area (i.e., two axes of symmetry), with dimensions small compared to the span and transverse cross sections of the beam remain plane and normal to the neutral axis during bending (Euler-Bernoulli bending beam theory). Further, the beam's torsional rigidity (*GJ*) is assumed to be very large compared with its warping rigidity (*EI*), and ends are free to warp; i.e., state of uniform torsion. The differential equations of motion governing the free vibration of a pre-stressed materially coupled bending-torsion beam, subjected to axial load and end moment, can be written as (for equations derivation refer to Appendix C):

$$EI\frac{\partial^4 w}{\partial x^4}+P\frac{\partial^2 w}{\partial x^2}+K\frac{\partial^3 \theta}{\partial x^3}+M_{zz}\frac{\partial^2 \theta}{\partial x^2}+(\rho A)\frac{\partial^2 w}{\partial t^2}=0. \tag{142}$$

$$GJ\frac{\partial^2\theta}{\partial x^2}+\frac{PI_P}{A}\frac{\partial^2\theta}{\partial x^2}+K\frac{\partial^3 w}{\partial x^3}+M_{zz}\frac{\partial^2 w}{\partial x^2}-\rho I_P\frac{\partial^2\theta}{\partial t^2}=0. \tag{143}$$

where x represents the distance spanning the beam and t is the time. Based on the simple harmonic motion assumptions, the displacements can be assumed to have a sinusoidal variation with frequency ω as:

$$w(x,t)=W\sin\omega t,\quad \text{and}\quad \theta(x,t)=\theta\sin\omega t \tag{144}$$

The sinusoidal variations from 144 are then substituted into equations 142 and 143 leading to:

$$EIW''''+PW''+K\theta'''+M_{zz}\theta''+\rho A\ddot{W}=0 \tag{145}$$

$$GJ\theta''+\frac{PI_P}{A}\theta''+KW'''+M_{zz}W''-\rho I_P\ddot{\theta}=0 \tag{146}$$

Based on the Galerkin weighted residual formulation, the weak integral forms associated with the equations 145 and 146, obtained after a number of integrations by parts, are then written as:

$$\begin{aligned}\bar{W}_f=&\int_0^L(EIW''\delta W''+PW'\delta W'+K\delta W''\theta'+M_{zz}\theta'\delta W'-\rho A\omega^2W\delta W)dx\\&+[(EIW'''+PW'+K\theta''+M_{zz}\theta')\delta W]_0^L-[(EIW''+K\theta')\delta W']_0^L=0\end{aligned} \tag{147}$$

$$\begin{aligned}\bar{W}_t=&\int_0^L(GJ\theta'\delta\theta'+\frac{PI_P}{A}\theta'\delta\theta'+KW''\delta\theta'+M_{zz}W'\delta\theta'-\rho I_P\omega^2\theta\delta\theta)dx\\&-[(GJ\theta'+\frac{PI_P}{A}\theta'+KW''+M_{zz}W')\delta\theta]_0^L=0\end{aligned} \tag{148}$$

Both Field variable (solution) and test weighting functions are defined in the same approximation space and appropriate boundary conditions are imposed at beam extremities, $x=0,\ L$. For example, zero displacements, $W=W'=\theta=0$, and virtual displacements, $\delta W=\delta W'=\delta\theta=0,$ at the clamped end ($x=0$) (i.e., where the displacements are imposed), and null resultant shear force, $S(x)$, bending moment, $M(x)$, and twisting moment $T(x)$ at the free end ($x=L$), etc. Here, we have:

$$M(x) = -EIW'' - K\theta' \tag{149}$$

$$S(x) = EIW''' + K\theta'' + M_{zz}\theta' + PW' \tag{150}$$

$$T(x) = GJ\theta' + \frac{PI_P}{A}\theta' + KW'' + M_{zz}W' \tag{151}$$

Consequently, the bracketed boundary terms in the integral expressions 147 and 148 will disappear. It can also be verified that the same is true regardless of the type of boundary conditions. Expressions 147 and 148 also satisfy the Principle of Virtual Work (PVW):

$$W = W_{INT} - W_{EXT} = 0 \tag{152}$$

where

$$W_{INT} = W_f + W_t, \tag{153}$$

and $W_{EXT} = 0$, for free vibrations. Then, the system is discretized along the beam span such that:

$$W = W_{INT} = \sum_{k=1}^{\text{Number of Elements}} W^k = \sum_{k=1}^{\text{Number of Elements}} W_f^k + W_t^k, \tag{154}$$

where the bending contribution into the elemental virtual work is obtained as:

$$W_f^k = \int_{x_j}^{x_{j+1}} \left(EIW''\delta W'' - PW'\delta W' + K\delta W''\theta' + M_{zz}\theta'\delta W' - \rho A\omega^2 W\delta W \right) dx \tag{155}$$

and the torsion contribution is:

$$W_t^k = \int_{x_j}^{x_{j+1}} \left(GJ\theta'\delta\theta' + \frac{PI_P}{A}\theta'\delta\theta' + KW''\delta\theta' + M_{zz}W'\delta\theta' - \rho I_P\omega^2\theta\delta\theta \right) dx \tag{156}$$

Each element is defined by nodes j and j+1 with corresponding coordinates and its length, l, where primes denote differentiation with respect to span wise Position x.

The field and virtual variables, W, θ, δW and $\delta\theta$, are then expressed in terms of nodal variables using the polynomial interpolation functions, and are subsequently introduced in expressions (155, 156).

This process leads to the Pre-stressed Composite Beam Finite Element (PCBFE) mass, $[m]^k$, and stiffness, $[k]^k$, matrices written as:

$$[k]^k = [k]^k{}_{Uncoupled} + + [k]^k{}_{P\text{-}Geometric} + [k]^k{}_{M\text{-}Coupling} + [k]^k{}_{G\text{-}Coupling} + [k]^k{}_{M\text{-}Geometric}\,, \qquad (157)$$

where:

$[k]^k{}_{Uncoupled}$ is the conventional static flexural and torsional stiffness matrices evaluated from the first terms, in expressions (155, 156), respectively,

$[k]^k{}_{P\text{-}Geometric}$ is the geometric stiffness matrix [80], caused by the axial force, P (2^{nd} terms),

$[k]^k{}_{M\text{-}Coupling}$ is the (Bending-Torsion and Torsion-Bending) material coupling stiffness matrices [47] resulting from the third terms including K factor,

$[k]^k{}_{G\text{-}Coupling}$ is the (Bending-Torsion and Torsion-Bending) geometric coupling stiffness matrices [80] caused by the end moment, M_{zz}, and evaluated from the third terms, and lastly

$[m]^k$, element mass matrix, is evaluated from the last terms in integral expressions (155,156).

Finally, assembly of the element matrices, $[k]^k$ and $[m]^k$, and the application of the system's boundary conditions leads to the following linear eigenvalue problem:

$$\langle \delta W_n \rangle \left([K] - \omega^2 [M] \right) \{U_n\} = 0, \qquad (158)$$

where $[K]$ stands for the global stiffness matrix, $[M]$ is global mass matrix, and $<\delta W_n>$ represents the vector of arbitrary virtual displacements. The nontrivial solution to the linear Eigenvalue problem (158) is then obtained by setting the determinant of the system's so-called dynamic stiffness matrix (DSM), $[K(\omega)]$, to zero; i.e., $\det([K] - \omega^2[M]) = 0;\ \det[K(\omega)] = 0$.

The above FEM formulation and modelling, consisting of the assembly of element matrices, application of the system's boundary conditions, and solution of the resulting eigenproblem is carried on using a code developed in MATLAB. The code gives the natural frequencies and also generates mode shapes for pre-stressed doubly coupled (material and geometric) beams by extracting data

from corresponding eigenvectors. The linear eigenproblem (158) can be solved using an inverse iteration procedure, subspace or Lanczos Method [41]. In this study, however, "eig" function in MATLAB was used to extract the natural frequencies and mode shapes of example problems.

4.2 Dynamic finite element (DFE) formulation

Alternatively, a Dynamic (frequency-dependent) Finite Element (DFE) formulation can be developed to analyze the free vibrations of the system at hand. In general, the DFE and FEM methods follow the same formulation that means the DFE approach starts with Galerkin weak formulation and integral form of equations, followed by the same integrations by parts to satisfy the natural (force) boundary conditions which results in Eqs. (155,156). The major difference between the two methods is the basis functions from which the shape functions are calculated. In the classic FEM, the cubic and linear polynomials shape functions are used for flexural and torsional displacements, respectively, which are the solutions of static deformation of a linear elastic beam. In the DFE, however, the solutions of the differential equations governing the uncoupled bending and torsion beam vibrations are chosen as the basis functions of approximation space, $\langle P(\xi) \rangle_f$ and $\langle P(\xi) \rangle_t$, leading to frequency dependent shape functions obtained with averaged value parameters over each element, where applicable; i.e., when the system's mechanical, and/or geometric, and/or material parameters are not constant. Therefore, the DFE can be considered as an intermediate approach, in which the FEM is combined to the exact DSM, to obtain a better numerical model.

In what follows, the DFE method is developed for the free vibration analysis of a pre-stressed, materially coupled, uniform composite beam element, where the geometric and material parameters are all assumed to be constant per element. The presented DFE can also be used to model the vibration behavior of piecewise uniform stepped composite beams. In addition, the present theory

can also be extended to include variable material and /or geometric parameters (e.g., tapered beam configurations), using the method presented by Hashemi, 1998 [19].

To obtain the DFE formulation, the element virtual work components W^k in expressions 155 and 156 are written in the following equivalent form, obtained after another set of integration by parts:

$$\begin{aligned}\bar{W}_f^k(\xi) &= \int_0^1 W(\underbrace{\frac{1}{l^3}EI\delta W'''' - \frac{1}{l}P\delta W'' - \rho A\omega^2 l\delta W}_{*})d\xi + \int_0^1 \frac{1}{l}M_{zz}\theta'\delta W' d\xi \\ &+ \int_0^1 \frac{1}{l^2}K\theta'\delta W'' d\xi + \left[\frac{1}{l^3}\left[EIW'\delta W'' - EIW\delta W'''\right] + \frac{1}{l}\left[PW\delta W'\right]\right]_0^1,\end{aligned} \tag{159}$$

$$\begin{aligned}\bar{W}_t^k(\xi) &= \int_0^1 -\theta(\underbrace{\frac{1}{l}GJ\delta\theta'' + \frac{1}{l}\frac{PI_p}{A}\delta\theta'' + \rho I_p\omega^2 l\delta\theta}_{**})d\xi + \int_0^1 \frac{1}{l}M_{zz}W'\delta\theta' d\xi \\ &+ \int_0^1 \frac{1}{l^2}KW''\delta\theta' d\xi + \frac{1}{l}\left[GJ\theta\delta\theta' + \frac{PI_p}{A}\theta\delta\theta'\right]_0^1.\end{aligned} \tag{160}$$

Then, the following non-nodal approximations (displacement functions) are introduced so that the integral terms (*) and (**) in the above equations vanish:

$$\begin{aligned}&\delta W = < P(\xi) >_f \{\delta a\}; \quad W = < P(\xi) >_f \{a\}; \\ &\delta\theta = < P(\xi) >_t \{\delta b\}; \quad \theta = < P(\xi) >_t \{b\},\end{aligned} \tag{161}$$

where the flexural and torsional basis functions of approximation space are defined as:

$$\left\langle P(\xi)\right\rangle_f = \left\langle \cos(\alpha\xi); \frac{\sin(\alpha\xi)}{\alpha}; \frac{\cosh(\beta\xi)-\cos(\alpha\xi)}{\alpha^2+\beta^2}; \frac{\sinh(\beta\xi)-\sin(\alpha\xi)}{\alpha^3+\beta^3}\right\rangle, \tag{162}$$

$$\left\langle P(\xi)\right\rangle_t = \left\langle \cos(\tau\xi); \sin(\tau\xi)/\tau\right\rangle, \tag{163}$$

with the roots, α, β, and τ, defined as:

$$\alpha = \sqrt{|X_2|}, \qquad \beta = \sqrt{|X_1|}, \; \tau = \sqrt{\frac{\rho I_p\omega^2 l^2 A}{AGJ + PI_p}}. \tag{164}$$

and

$$X_1 = \frac{\left\{-B + \sqrt{B^2 - 4\bar{A}C}\right\}}{2\bar{A}}, \qquad X_2 = \frac{\left\{-B - \sqrt{B^2 - 4\bar{A}C}\right\}}{2\bar{A}}, \tag{165}$$

where:

$$\bar{A} = \frac{EI}{l^3}, \qquad B = -\left(\frac{P}{l}\right), \qquad C = -(ml\omega^2). \tag{166}$$

The nodal approximations for element variables $w(\xi)$ and $\theta(\xi)$ can then be rewritten as:

$$\begin{aligned} W(\xi) &= < P(\xi)_f > [P_n]_f^{-1} \{W_n\} = < N(\xi)_f > \{W_1 \; W'_1 \; W_2 \; W'_2\}, \\ \theta(\xi) &= < P(\xi)_t > [P_n]_t^{-1} \{\theta_n\} = < N(\xi)_t > \{\theta_1 \; \theta_2\}. \end{aligned} \tag{167}$$

Similar expressions are also written for the test functions. Expressions 166 can then be rearranged as: $[W(\xi) \; \theta(\xi)]^T = [N]\{u_n\}$, where $\{u_n\} = < W_1 \; W'_1 \; \theta_1 \; W_2 \; W'_2 \; \theta_2 >^T$ is the element displacements (i.e., degrees of freedom) and [*N*] represents the dynamic shape functions in matrix form as:

$$[N] = \begin{Bmatrix} < N(\omega)_f > \\ < N(\omega)_t > \end{Bmatrix} = \begin{bmatrix} N_1(\omega)_f & N_2(\omega)_f & 0 & N_3(\omega)_f & N_4(\omega)_f & 0 \\ 0 & 0 & N_1(\omega)_t & 0 & 0 & N_2(\omega)_t \end{bmatrix}. \tag{168}$$

The four trigonometric shape functions, $Ni(\omega)_f$, pertaining to bending, and the two trigonometric interpolation functions, $Nj(\omega)_t$, pertaining to torsion, presented in (168) are then used to approximate the lateral and torsional displacements, respectively, introduced to the element integral expressions 158 and 159, leading to element DFE matrices, written as:

$$W^k = \left([k]^k_{Uncoupled} + [k]^k_{Coupled}\right)\{U_n\} = [k(\omega)]^k \{U_n\} \tag{169}$$

$$W^k = \left([k]^k_{Uncoupled} + [k]^k_{Coupled}\right)\{U_n\} = [k(\omega)]^k \{U_n\} \tag{170}$$

where $[k(\omega)]^k$ is the DFE matrix for a pre-stressed laminated composite beam element, $[k]^k_{Uncoupled}$ stands for the uncoupled portion of the element dynamic stiffness matrix, including the axial load

effect, resulting from the boundary (bracketed) terms in (158, 159), and $[k]^{k}_{Cncoupled}$ represents the element's coupling matrix which, in turn, consist of two parts, written as:

$$[k]^{k}_{Cncoupled} = [k]^{k}_{M\text{-}Cncoupled} + [k]^{k}_{G\text{-}Cncoupled}, \qquad (171)$$

$[k]^{k}_{M\text{-}Cncoupled}$ is the (Bending-Torsion) material coupling dynamic stiffness matrix resulting from the third integral terms in (158, 159) including *K* factor, and

$[k]^{k}_{G\text{-}Cncoupled}$ is the new geometric (Bending-Torsion) coupling stiffness matrix due to the end moment, M_{zz}, and evaluated from the second terms in (158, 159).

$$[k]^{k}_{Uncoupled} = \begin{bmatrix} \frac{EI}{l^3}\{N_1'''\}_0 & \frac{EI}{l^3}\{-N_1''\}_0 & 0 & \frac{EI}{l^3}\{-N_1'''\}_1 & \frac{EI}{l^3}\{N_1''\}_1 & 0 \\ \frac{EI}{l^3}\{N_2'''\}_0 & \frac{EI}{l^3}\{-N_2''\}_0 & 0 & \frac{EI}{l^3}\{-N_2'''\}_1 & \frac{EI}{l^3}\{N_1''\}_1 & 0 \\ 0 & 0 & \frac{GJ}{l}\{-N_{t1}'\}_0 & 0 & 0 & \frac{GJ}{l}\{N_{t1}'\}_1 \\ \frac{EI}{l^3}\{N_3'''\}_0 & \frac{EI}{l^3}\{-N_3''\}_0 & 0 & \frac{EI}{l^3}\{-N_3'''\}_1 & \frac{EI}{l^3}\{N_1''\}_1 & 0 \\ \frac{EI}{l^3}\{N_4'''\}_0 & \frac{EI}{l^3}\{-N_4''\}_0 & 0 & \frac{EI}{l^3}\{-N_4'''\}_1 & \frac{EI}{l^3}\{N_1''\}_1 & 0 \\ 0 & 0 & \frac{GJ}{l}\{-N_{t2}'\}_0 & 0 & 0 & \frac{GJ}{l}\{N_{t2}'\}_1 \end{bmatrix} \qquad (172)$$

and,

$$[k]^{k}_{Coupled} = \int_0^1 \frac{K}{l^2} \begin{bmatrix} 0 & 0 & \{N_1 "N_{t1}\} & 0 & 0 & \{N_1 "N_{t2}\} \\ 0 & 0 & \{N_2 "N_{t1}\} & 0 & 0 & \{N_2 "N_{t2}\} \\ \{N_1 "N_{t1}\} & \{N_2 "N_{t1}\} & 0 & \{N_3 "N_{t1}\} & \{N_4 "N_{t1}\} & 0 \\ 0 & 0 & \{N_3 "N_{t1}\} & 0 & 0 & \{N_3 "N_{t2}\} \\ 0 & 0 & \{N_4 "N_{t1}\} & 0 & 0 & \{N_4 "N_{t2}\} \\ \{N_1 "N_{t2}\} & \{N_2 "N_{t2}\} & 0 & \{N_3 "N_{t2}\} & \{N_4 "N_{t2}\} & 0 \end{bmatrix} d\xi$$

$$+ \int_0^1 \frac{M_{zz}}{l} \begin{bmatrix} 0 & 0 & \{N_1' N_{1t}'\} & 0 & 0 & \{N_1' N_{2t}'\} \\ 0 & 0 & \{N_2' N_{1t}'\} & 0 & 0 & \{N_2' N_{2t}'\} \\ \{N_{1t}' N_1'\} & \{N_{1t}' N_2'\} & 0 & \{N_{1t}' N_3'\} & \{N_{1t}' N_4'\} & 0 \\ 0 & 0 & \{N_3' N_{1t}'\} & 0 & 0 & \{N_3' N_{2t}'\} \\ 0 & 0 & \{N_4' N_{1t}'\} & 0 & 0 & \{N_4' N_{2t}'\} \\ \{N_{2t}' N_1'\} & \{N_{2t}' N_2'\} & 0 & \{N_{2t}' N_1'\} & \{N_{2t}' N_4'\} & 0 \end{bmatrix} d\xi \quad (173)$$

The element matrices are then assembled to form the system's global dynamic stiffness matrix of the structure. The resulting nonlinear eigenvalue problem, found to be similar to Expression 79 from Chapter 2, is then solved to find the natural frequencies and modes of vibration of the system.

4.3 Numerical tests

Let us consider a uniform cantilever beam, composed of glass/epoxy composite material and made up of unidirectional plies and fiber angles in each ply set to +15˚ subjected to end moment and axial force. The positive direction for fiber angle is defined counter clockwise from positive direction of X axis, as shown in Figure 41. The beam is assumed to be 0.1905 m long, and 12.7 mm wide. Based on Appendix B, the beam can be considered equivalent to a single thick ply, with a thickness of 3.18 mm and the following material and geometric properties are derived/considered: bending rigidity, EI=0.2865 Nm^2; torsion rigidity, GJ=0.1891 Nm^2; bending-torsion coupling rigidity, K=0.1143

Nm^2; mass per unit length, m=0.0544 kg/m; and mass moment of inertia per unit length, and I_α=7.77×10^{-7} kg.m.

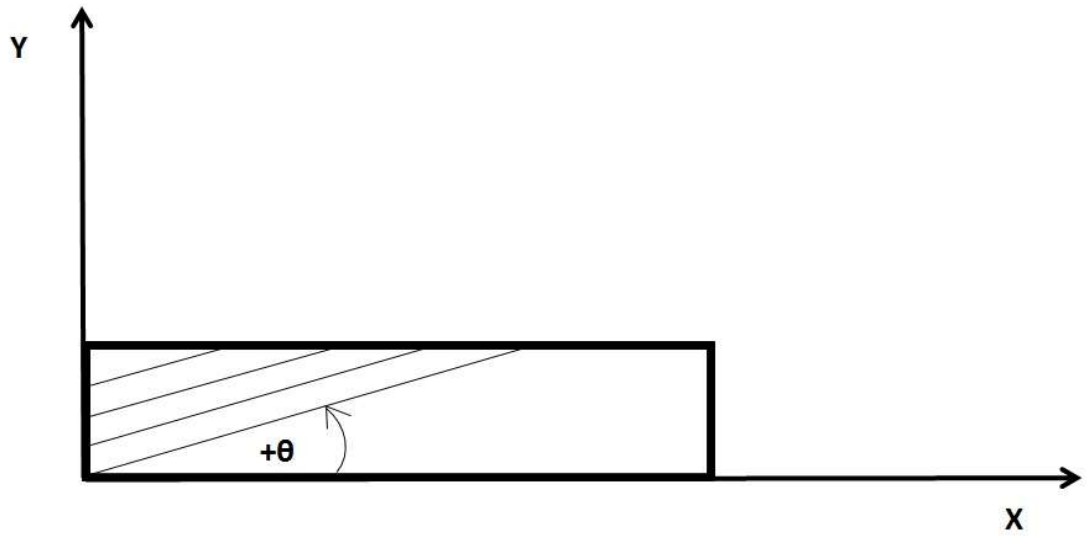

Figure 41: Positive direction of fiber angle

A free vibration analysis of the system is performed using FEM and DFE codes developed in MATLAB®, carrying out the assembly of the static (FEM) mass and stiffness and dynamic (DFE) matrices, application of the system's boundary conditions, and finally solving the resulting eigenvalue problems. There are no frequency data available in the open literature for such a pre-stressed composite beam subjected to axial load and end moment. Therefore, both the FEM and DFE codes are first validated for an unstressed composite beam m (i.e., M_{zz} and P set to zero) reported by Banerjee and Williams [45], for which exact DSM reference values are available. In the DSM theory, the element frequency dependent stiffness matrix is developed from the closed form solution to the governing coupled differential equations and, therefore, are exact within the limits of the theory. The conventional FEM theory and the corresponding element mass and stiffness matrices, as mentioned in previous sections, are developed based on cubic Hermite and linear interpolation functions for flexural and torsional displacements, respectively. In contrast, the DFE matrices are evaluated using

frequency-dependent trigonometric interpolation functions derived using basis functions presented in (162, 163).

The unstressed system's first five natural frequencies evaluated from a five-element mesh modelled using the presented FEM and DFE formulations are presented in Table 27 along with the (exact) DSM data from [44]. As can be seen from Table 27, the FEM frequencies are in excellent agreement with the DSM values [43], with a maximum error of less than 0.4% for the fifth frequency, and an average error of less than 0.14%. As expected, the 5-element FEM model predicts higher natural frequencies than the DSM values and the error is found to increase with the mode number, except for the fourth natural frequency. This can be associated with the fact that, in this case, 1st, 2nd, 3rd, and 5th modes exhibit bending-torsion material coupling, predominated by flexural displacement, whereas the 4th mode is predominantly torsional; i.e., exhibiting the first torsional mode's behavior. It is worth noting that all the DFE frequencies, in this case, are found to be in perfect match with the DSM data; i.e., 0% error. The FEM convergence test results for the unstressed beam's first five natural frequencies are shown in Figure 42.

The bending-torsion coupling behaviour in this model is in part caused by the fiber angle and in part by the applied end moment. Depending on the end moment and fiber angle directions, these two coupling sources either intensify or diminish one another's effects. It is worth noting that in most of composite materials applications, the resulting coupling between different displacements are undesired. Therefore, knowing the magnitude of the working end moment, the direction of fiber angle and stacking sequence can be tailored in such a way that resulting torsional displacement caused by the material coupling (K) is in the opposite direction of that resulting from end moment (M_{zz}), minimizing or ideally cancelling the coupling effects.

Table 27: Comparison of FEM and DFE natural frequency results for M_{zz}=0 and P=0 with the analytical DSM values [64].

Natural Frequency	FEM Using 5 Elements (Hz)	DFE Using 5 element (Hz)	Exact DSM (Hz) [64]
1st	30.82	30.82	30.82
2nd	192.87	192.72	192.72
3rd	538.47	537.38	537.38
4th	648.87	648.73	648.73
5th	1053.87	1049.73	1049.73

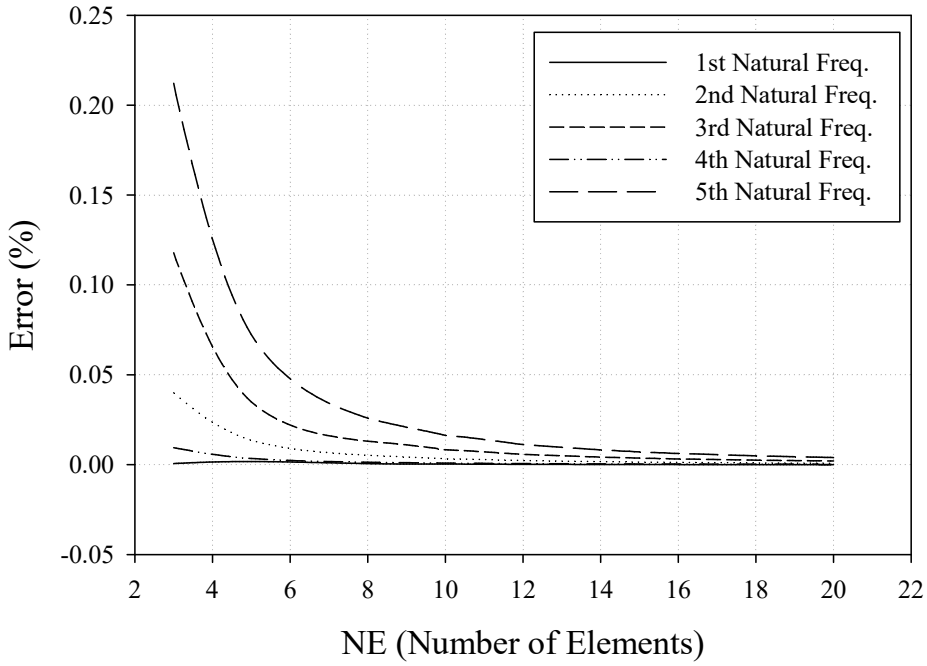

Figure 42: Error versus the number of elements for first five natural frequencies (percent error is relative to the exact values obtained from the DSM [26].

Once the validity of the FEM and DFE formulations for the unstressed composite beam is established, the vibrations of pre-stressed configurations subjected to combined axial load and end moment are investigated. The variation of the uniform cantilever composite beam's fundamental natural frequency versus axial compressive force obtained from 5-element FEM and DFE models for M_{zz}=6.14 MN.m and K=0.1143 Nm^2 is shown in Figure 43.

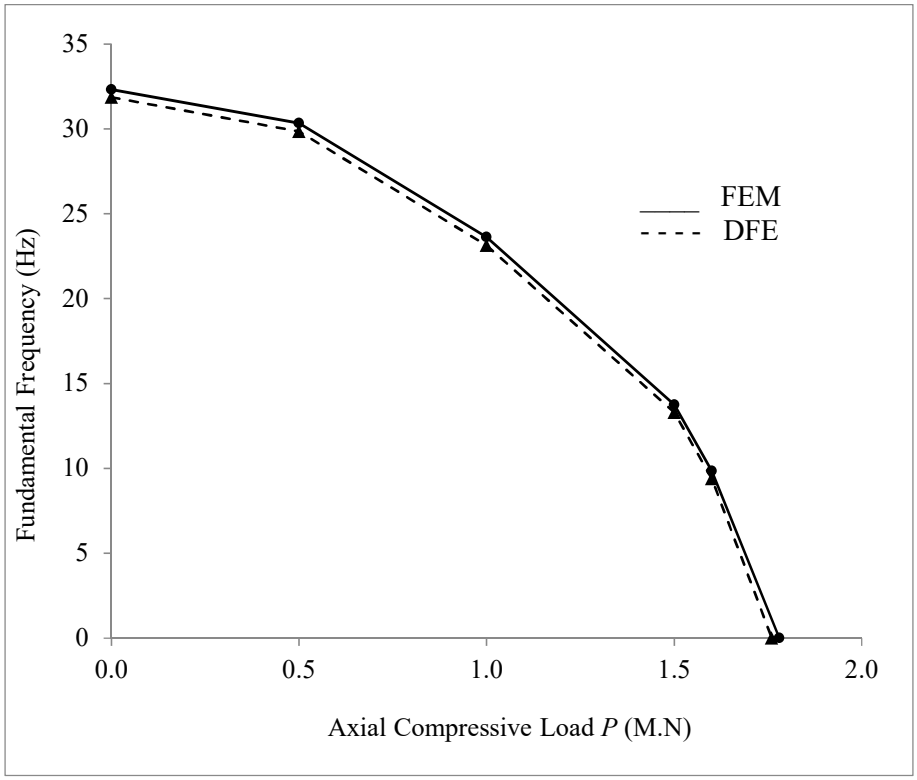

Figure 43: Variation of first natural frequency Vs. axial compressive force for FEM and DFE with M_{zz}=18.5MN.m and K=0.1143 Nm^2.

The effect of fiber angle on the vibrational behavior of the composite glass-epoxy beam is also investigated using a 5-element DFE model and the results are represented in Figure 44. As can be seen from Figure 44, at 45˚ fiber angle system exhibits the highest natural frequency, associated with the highest material bending-torsion coupling factor (K_{max}) at this fiber angle.

Buckling analysis for single layer glass-epoxy beam is also carried out using a 5-element DFE model and the results are presented in Figure 45. As can be observed from Figure 45, at zero axial force, P=0, the critical (buckling) end moment is found to be M_{zzCr} = 28.2 MN.m. An increase in the tensile (i.e., positive) axial force increases the critical (buckling) end moment. In contrast, increasing the compressive (i.e., negative) axial forces leads to a decrease in critical (buckling) end moment.

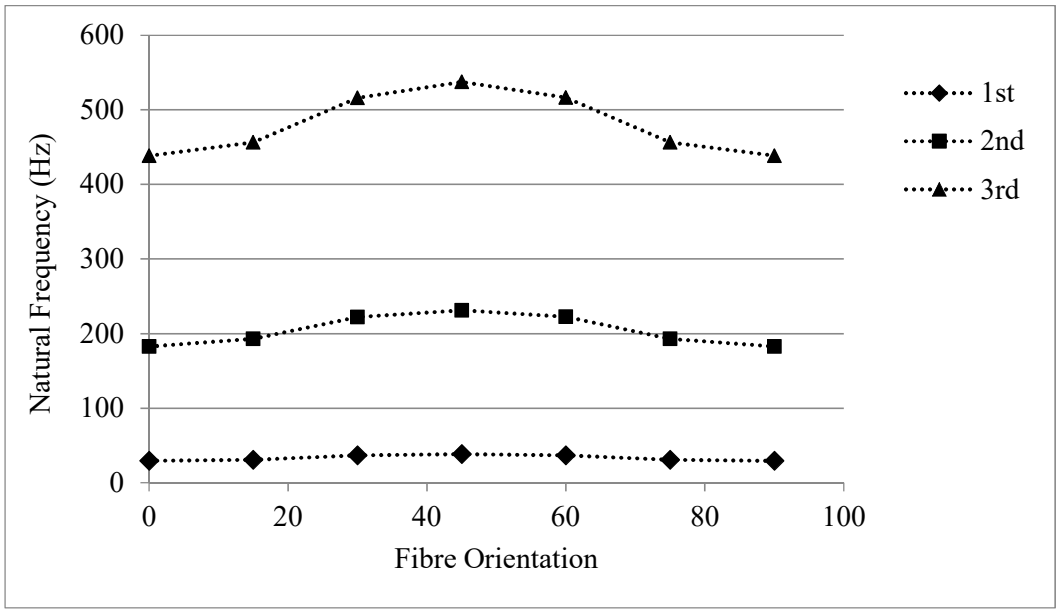

Figure 44: Variation of Natural frequencies with glass-epoxy composite ply angle, using a 5-element DFE model with M_{zz}=6.14 MN.m, P=1.23 MN and K=0.1143 Nm^2.

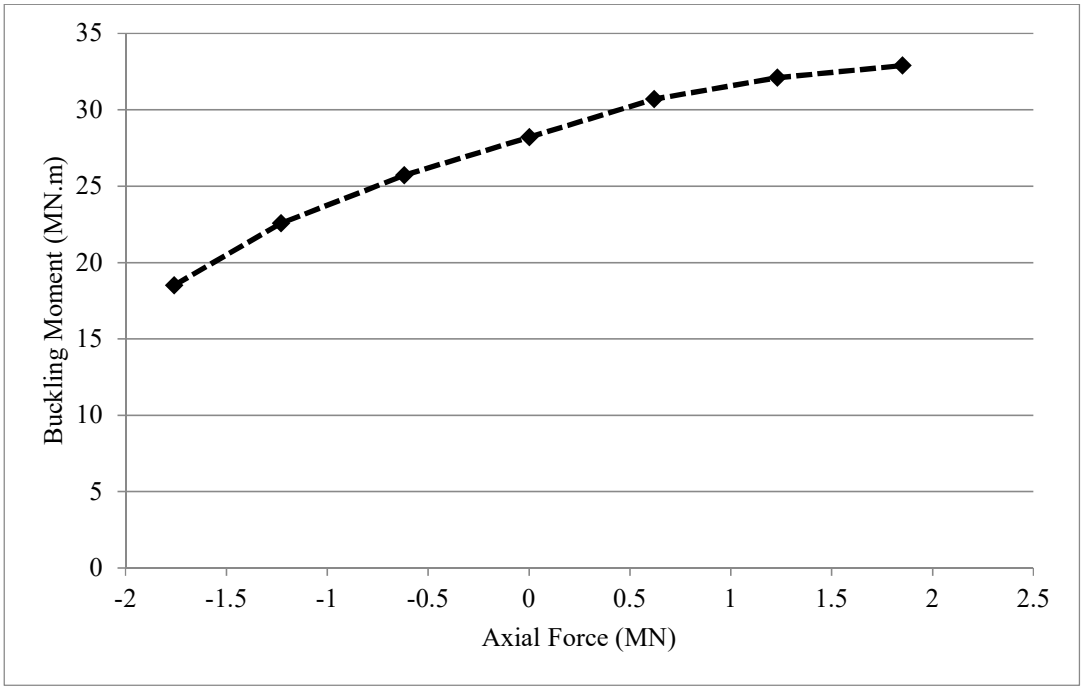

Figure 45: buckling analysis for single layer glass-epoxy composite cantilevered beam with fiber angle of +15˚, using a 5-elements DFE model.

In Figure 46 the first five natural modes shapes for bending and in Figure 47 the first five natural mode shapes for torsion using DFE method with Mzz=6.14 MN.m, P=1.23 MN and K=0.1143 N.m^2 are presented. Based on results, in 1st, 2nd, 3rd and 5th natural modes the bending is predominant while for the 4th natural mode the torsion contribution is more considerable.

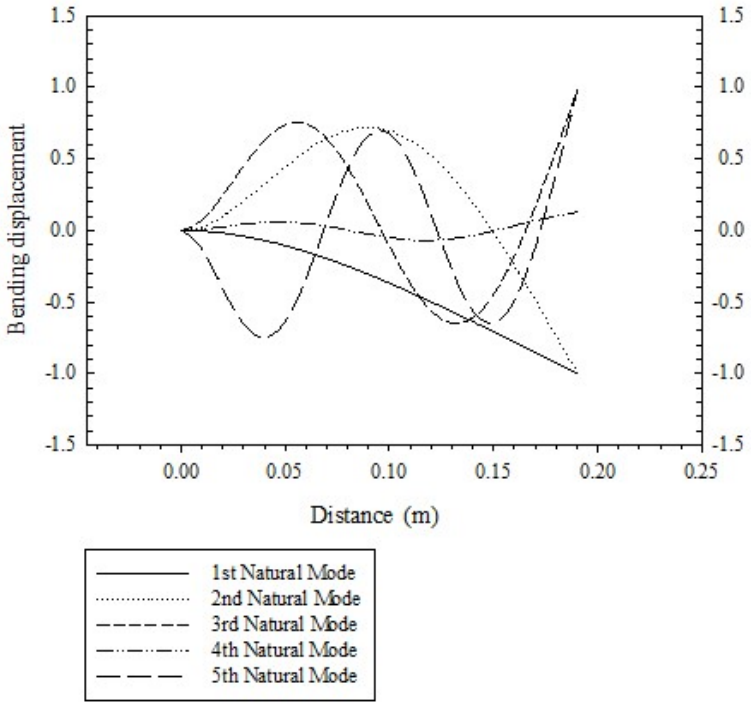

Figure 46: First five bending components of mode shapes using DFE method with M_{zz}=6.14 MN.m, P=1.23 MN and K=0.1143 Nm^2.

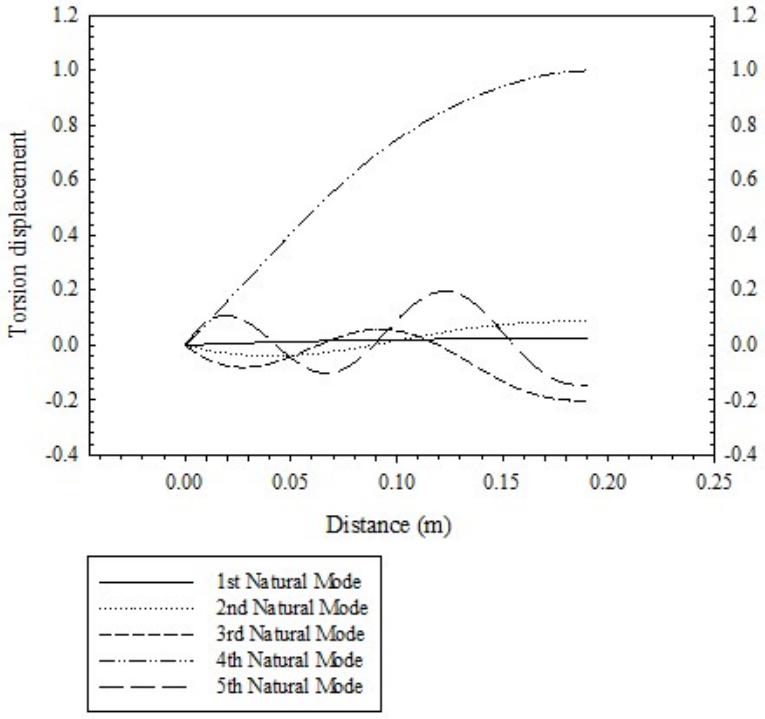

Figure 47: First five torsional components of mode shapes using DFE method with M_{zz}=6.14 MN.m, P=1.23 MN and K=0.1143 Nm^2.

3.2 Three-layer fiber-metal laminated (FML) beam

In order to further investigate the applicability of the presented formulation, FEM and DFE approaches together with a simple layer-wise formulation are used to investigate the free vibrations of an illustrative example of a cantilevered pre-stressed three-layer fiber-metal laminated (FML) beam subjected to axial force and end moment. The FML construction at hand, also known as GLARE (glass-reinforced aluminum laminate), is assumed to consist of two composite face layers, made of glass-epoxy with +15˚ fiber angle (similar to the previous example), and an Aluminium core, as shown in Figure 48.

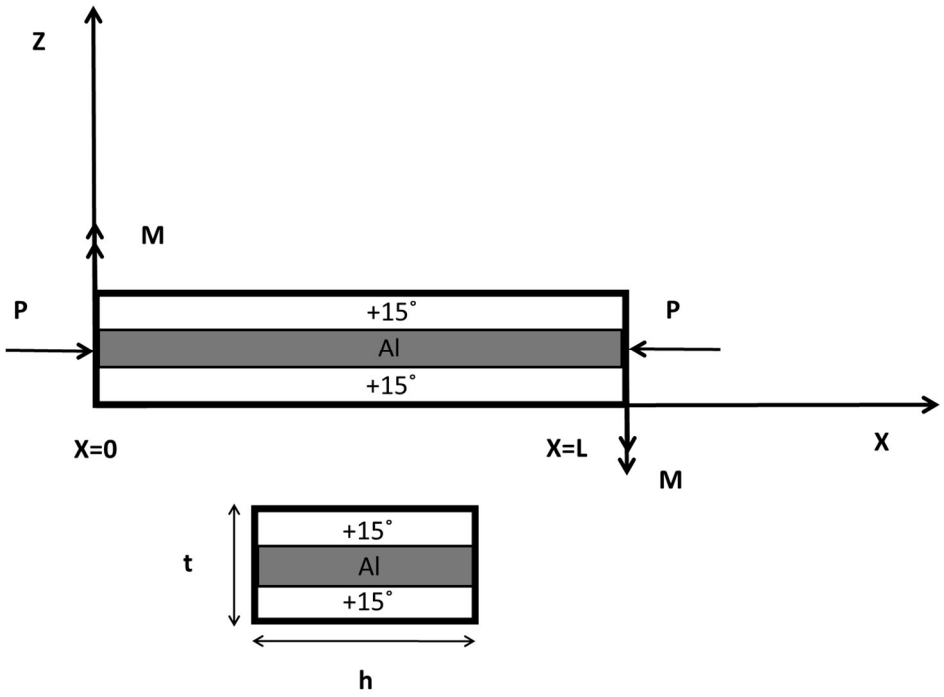

Figure 48: Three-layer Fiber-Metal Laminated (FML) beam schematic

Similar to the composite beam in previous example, the overall beam dimensions are; thickness of t=3.18 mm, width of w=12.7 mm and length of the L=0.1905 m. The Aluminium core has a mass density of ρ=2700 kg/m3, shear modulus of G=26GPa, and Young's modulus of E=70GPa and

thickness of all the three layers are considered equal (one-third of the total thickness; $t/3$). The pre-stressed FML beam exhibits coupled bending-torsion behavior, partly caused by the fiber angle in the face-layer (leading to the bending-torsion coupling stiffness, K), and in part by the applied end moment. These two couplings, depending on their directions, either alleviate or intensify each other's effects. In what follows, the simplified layer-wise formulation is briefly presented.

The variation of first natural frequency versus axial compressive force for FEM and DFE, both using 5 elements with M_{zz}=6.14 MN.m and K=0.1143 N.m^2, for sandwich beam is shown in Figure 49 and buckling analysis results are presented in Figure 50. The regular FEM overestimation is once again observed in Figure 49. This is mainly due to the constraints that polynomial basis functions put into system.

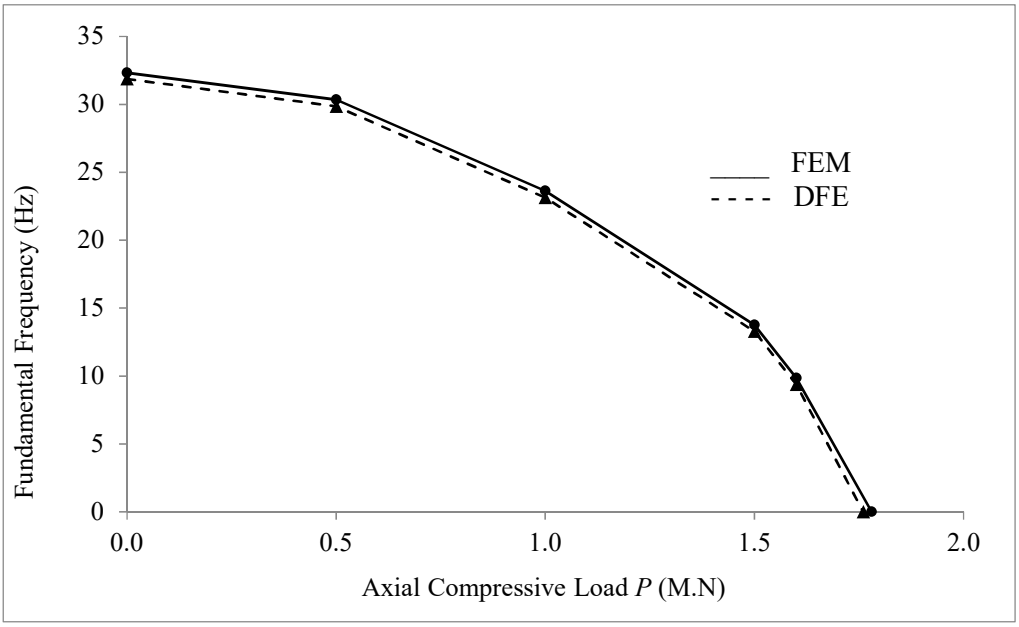

Figure 49: Variation of first natural frequency Vs. axial compressive force for three layer glass-epoxy and Aluminium sandwich beam using 5-element DFE and FEM models with M_{zz}=18.5 MN.m.

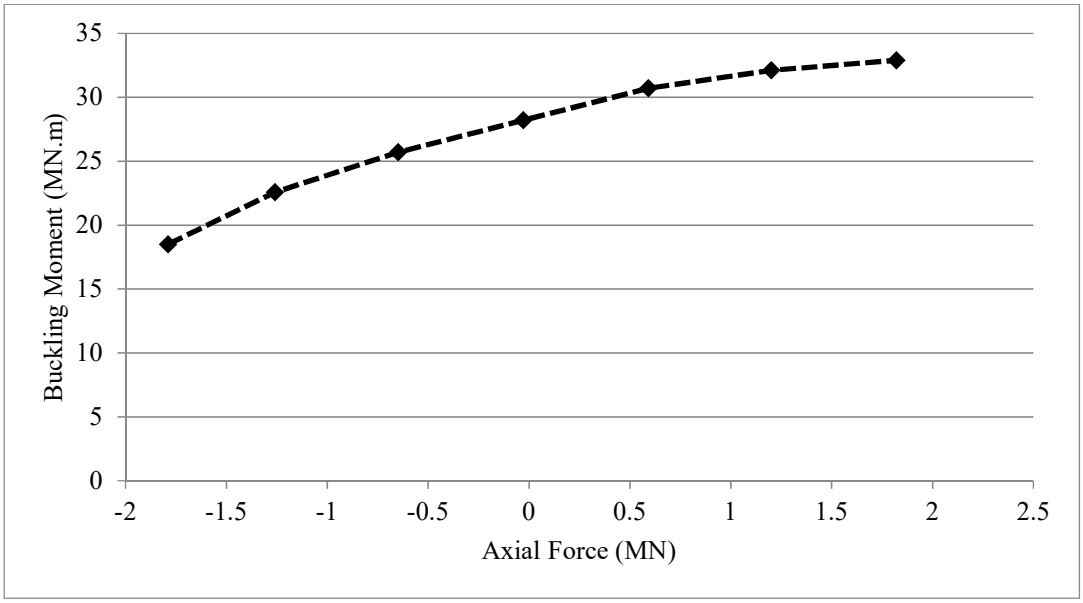

Figure 50: buckling analysis for three layer glass-epoxy and Aluminium sandwich cantilevered beam using 5-element DFE.

4.4 Conclusion

The vibration of a composite beam subjected to axial force and end moment is modeled using both FEM and DFE methods and the results are validated with analytical DSM results. In this modeling, the composite nature of beam material introduces one coupling term between bending and torsion displacements in bending differential equation of motion and one term in the torsion differential equation of motion while the applied end moment creates another coupling term in each equation, leading to total of four coupling terms in the system of differential equations. Because of theses coupling terms between the two differential equations, the system has no analytical solution which leads us to use numerical methods for modeling purposes.

Modeling results for the two numerical methods show that using same number of elements, DFE has higher rate of convergence compared to FEM method. Results also show that increase in tensile axial force and end moment increase the stiffness of system which leads to higher natural frequencies (Figure 43). All the vibration modes are coupled and include both torsion and bending components.

In the first three modes bending is dominant while in fourth one torsion becomes dominant (Figure 46 and Figure 47). From Table 27 it is inferred that in absence of end moment (M_{zz}=0) and material coupling (K=0), a single-element DFE model yields same results as the DSM method. The reason behind this is that in absence of these coupling terms the frequency dependent stiffness matrix in DFE method (without discretization) results in exactly the same formulation as the DSM analytical solution.

The effect of ply angle on the vibrational behavior of the composite glass-epoxy beam was investigated by the DFE method using 5 elements and based on Figure 44, all the first three natural frequencies increase from fiber angle of 0˚ to +45˚ and decrease from +45˚ to +90˚. This is justified by Equations A-10 to A-17 which estimates the highest rigidity for fiber angle of 45˚.

The composite-aluminium sandwich beam compared to thick single layer composite, was show to have almost same stiffness and buckling resistance. Also over prediction of natural frequencies by FEM method was once again observed (Figure 49) and can be justified by extra constraints on displacements, introduced in system by polynomial basis functions.

5 Free vibration of pre-stressed delaminated beam

5.1 Introduction

In this Chapter, free vibration analysis of single delaminated beams subjected to axial force and end moment and exhibiting bending-torsion coupling is modeled using traditional finite element technique as well as DFE. The Galerkin weighted residual method is applied to convert the coupled differential equations of motion into to a discrete problem. The Eigenvalue problem resulting from the discretization along the length of the beam is solved to determine the natural frequencies and mode shapes of free vibration. Both 'free mode' and 'constrained mode' models are considered in formulation and it is shown that the continuity (both kinematic and force) conditions at delamination tips, in particular, play a large role in formulation of 'free mode' model. Current trends in the literature are critically examined, and insight into different types of modeling techniques and constraint types are introduced. In addition, the data previously available from a commercial finite element suite are also utilized to validate the natural frequencies of the systems analyzed here. Finally, general concluding remarks are made on the usefulness of the presented theories.

5.2 Mathematical model

Figure 51 shows a pre-stressed two-layer beam of length L and thickness H_1 having a single through-the-width delamination with a length L_2, starting from $x=x_1$. This delamination divides the beam into four segments, which are assumed to have a slenderness ratio of greater than 10 and, as a result will be analyzed as four interconnected Euler–Bernoulli beams. Beam segments 2 and 3 have H_2 and H_3 thicknesses, respectively. The structure is subjected to axial force of P and constant end moment of M_{zz}, applied at its ends, $x=0$ and $x=L$.

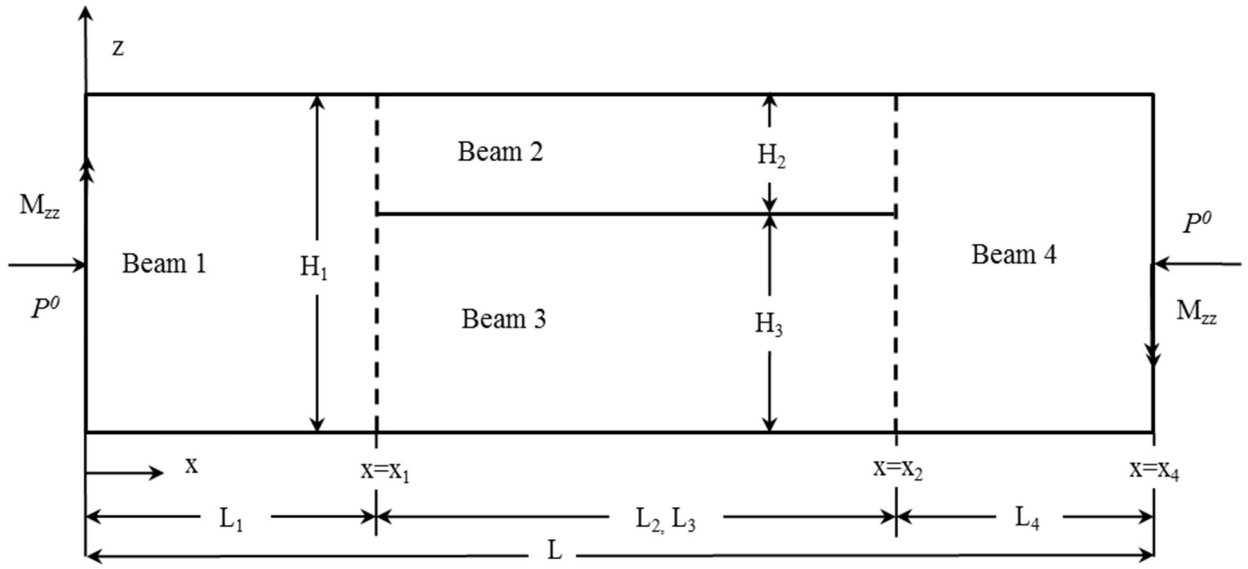

Figure 51: Schematic of a beam with single delamination under axial load and end moment

Assuming that each uniform beam segment is made of linearly elastic, homogeneous, isotropic material with constant mechanical, material and geometric properties, it can be shown that the partial differential equations of motion, governing free, linear, bending-torsion coupled vibrations of the i^{th} Euler-Bernoulli beam segment subjected to axial force and end moment are as follows [102]:

$$EI_i w_i'''' + P_i w_i'' + M_{zz,i}\phi_i'' + \rho A_i \ddot{w}_i = 0 \qquad (i = 1-4) \tag{174}$$

$$GJ_i\phi_i'' + P_i I_{P,i}\phi_i'' + M_{zz,i} w_i'' - \rho A_i I_{P,i}\ddot{\phi}_i = 0 \qquad (i = 1-4) \tag{175}$$

where w is the lateral displacement along z direction, ϕ stands for the torsional twist about x-axis, E is Young's modulus, G represents the shear modulus, J and I_p are, respectively, the torsion constant and the polar moment of inertia, and subscript i represents the beam segment's number, where i=1,2,3,4. P_i and $M_{zz,i}$ represent the components of axial force and end moment for i^{th} beam segment, respectively. ()′ stand for derivative with respect to x and ($\dot{}$) denotes derivative with respect to t (time). The beam's torsional rigidity (GJ) is assumed to be very large compared with its warping

rigidity (EI), and ends are free to warp; i.e., state of uniform torsion. As can be observed from equations 197 and 198, the system's bending and trorsional displacements are coupled by the end moment, $M_{zz,i}$. Exploiting the simple harmonic motion assumption and substituting $w_i(x,t) = W_i \sin(\omega t)$ and $\phi_i(x,t) = \theta_i \sin(\omega t)$ for lateral and torsional displacements, respectively, leads to:

$$EI_i W_i'''' + P_i W_i'' + M_{zz,i}\theta_i - \rho A_i \omega^2 W_i = 0 \qquad (i = 1-4) \tag{176}$$

$$GJ_i \theta_i'' + P_i I_{P,i} \theta_i'' + M_{zz,i} W_i'' + \rho I_{P,i} A_i \omega^2 \theta_i = 0 \qquad (i = 1-4) \tag{177}$$

where ω denotes the frequency and W_i and θ_i are the amplitudes of flexural and torsional displacements, respectively, of the beam segment i.

5.3 Free mode delamination model

The 'free mode' delamination model assumption, unlike 'constrained mode', considers no constraint or interaction between the top and bottom layers in the delaminated zone, i.e., segments 2 and 3 ([95] and [88]). The 'Free mode' model predicts the behavior of the beam more accurately but it also exhibits some physically impossible modes of vibration. In order to solve the four pairs of coupled equations as one system numerically, the boundary conditions at both ends of the beam and continuity conditions at the delamination tips are required. The continuity conditions for lateral deflection, slope, torsional displacement and axial force at the left delamination tip ($x=x_1$) are expressed as:

$$W_1(x = x_1) = W_2(x = x_1) = W_3(x = x_1) \tag{178}$$

$$W_1'(x = x_1) = W_2'(x = x_1) = W_3'(x = x_1) \tag{179}$$

$$\theta_1(x = x_1) = \theta_2(x = x_1) = \theta_3(x = x_1) \tag{180}$$

$$P_1 = P_2 + P_3 \tag{181}$$

Similarly, continuity conditions for the right delamination tip are written as:

$$W_4(x=x_2)=W_2(x=x_2)=W_3(x=x_2) \tag{182}$$

$$W_4'(x=x_2)=W_2'(x=x_2)=W_3'(x=x_2) \tag{183}$$

$$\theta_4(x=x_2)=\theta_2(x=x_2)=\theta_3(x=x_2) \tag{184}$$

$$P_4=P_2+P_3 \tag{185}$$

Additionally, the requirement for the delamination tip faces to remain planar after deformation, at the left delamination tip, results in:

$$u_2(x=x_1)-u_3(x=x_1)=\frac{H_1}{2}W_1'(x=x_1) \tag{186}$$

where u_i is the axial displacement of beam section i. Combining expression 186 with the similar expression from the right delamination tip leads to:

$$\left[u_3(x=x_2)-u_3(x=x_1)\right]-\left[u_2(x=x_2)-u_2(x=x_1)\right]=\frac{H_1}{2}\left[W_4'(x=x_2)-W_1'(x=x_1)\right] \tag{187}$$

It was originally assumed by Mujumdar [78], and was later shown in an exact way by Szekrényes [93], that (for small deformations of a beam with constant material and geometric properties along the length of the beam) the axial displacement will behave according to the following expression:

$$u_i(x_i=L_i)-u_i(x_i=0)=\int_0^{L_i}\frac{F_i(x_i)}{E_iA_i(x_i)}dx_i=\frac{F_iL_i}{E_iA_i} \tag{188}$$

where x_i represents the local position along the length and F_i is the axial force induced in the segment i. Compressive force during vibration, $P(x,t)$, is consisted of applied static axial force P and perturbed axial force, $P^t(x,t)$, which is induced in the delaminated layers during vibration to prevent inter-laminar slip. Knowing that the change in axial displacement for each segment is caused by induced perturbed component of axial force rather than its static component, substituting equation 188 into 187 yields:

$$\frac{P_2^tL_2}{EA_2}-\frac{P_3^tL_3}{EA_3}=\frac{H_1}{2}\left[W_4'(x=x_2)-W_1'(x=x_1)\right] \tag{189}$$

Taking the perturbation of equation 181 for continuity of axial force on the left delamination tip, one obtains:

$$P_2^t + P_3^t = P_1^t \tag{190}$$

Since $P_1 = P$, and P is constant, $P_1^t = 0$ which means: $P_2^t + P_3^t = 0.$ Substituting $P_3^t = -P_2^t$ into equation 189 results in:

$$P_3^t = \Lambda^* \left[W_4'(x = x_2) - W_1'(x = x_1) \right] \tag{191}$$

where the coefficient Λ^* is defined as:

$$\Lambda^* = \frac{H_1}{2L_2} \left(\frac{EA_2 EA_3}{EA_3 + EA_2} \right) \tag{192}$$

At the left and right delamination tips, respectively, continuity of bending moments leads to:

$$M_1(x = x_1) = M_2(x = x_1) + M_3(x = x_1) - P_2^t \frac{H_3}{2} + P_3^t \frac{H_2}{2} \tag{193}$$

and

$$M_4(x = x_2) = M_2(x = x_2) + M_3(x = x_2) - P_2^t \frac{H_3}{2} + P_3^t \frac{H_2}{2} \tag{194}$$

From beam theory, it can be shown that resulting internal bending moment, $M(x)$, shear force, $S(x)$, and torsional torque, $T(x)$, in each beam segment are related to displacements, through the following equations:

$$M_i(x) = EI_i W_i'' \tag{195}$$

$$S_i(x) = EI_i W_i''' + M_{zz,i} \theta_i' + P_i W_i' \tag{196}$$

$$T_i(x) = GJ_i \theta_i' + P_i I_{P,i} \theta_i' + M_{zz,i} W_i' \tag{197}$$

Using equation 193 and 195, the following continuity of bending moments is obtained:

$$EI_1W_1''\Big|_{x=x_1} = EI_2W_2''\Big|_{x=x_1} + EI_3W_3''\Big|_{x=x_1} + \Lambda\left[W_4'(x_4=0) - W_1'(x_1=L_1)\right] \tag{198}$$

where the parameter Λ is defined as:

$$\Lambda = \frac{H_1^{\,2}}{4L_2}\left(\frac{EA_2EA_3}{EA_3+EA_2}\right) \tag{199}$$

Likewise, to satisfy the continuity of shear forces (equation 196) at the left delamination tip, one should have:

$$EI_1W_1''' + P_1W_1' + M_{zz,1}\theta_1'\Big|_{x=x_1} = EI_2W_2''' + P_2W_2' + M_{zz,2}\theta_2'\Big|_{x=x_1} + EI_3W_3''' + P_3W_3' + M_{zz,3}\theta_3'\Big|_{x=x_1} \tag{200}$$

and finally, the continuity of torsional torque (equation 197) at left delamination tip yields:

$$GJ_1\theta_1' + P_1I_{P,1}\theta_1' + M_{zz,1}W_1'\Big|_{x=x_1} = GJ_2\theta_2' + P_2I_{P,2}\theta_2' + M_{zz,2}W_2'\Big|_{x=x_1} + GJ_3\theta_3' + P_3I_{P,3}\theta_3' + M_{zz,3}W_3'\Big|_{x=x_1} \tag{201}$$

5.4 Classical finite element method (FEM)

Using Galerkin weighted residual formulation, the integral forms of the governing differential equations 176 and 177, also representing the virtual flexural ($\bar{W}_f$) and torsional ($\bar{W}_t$) works are written as:

$$\bar{W}_f = \sum_{i=1}^{4}\left(\int_0^{L_i}\delta W_i(EI_iW_i'''' + P_iW_i'' + M_{zz,i}\theta_i'' - \rho A_i\omega^2W_i)dx\right) = 0 \tag{202}$$

$$\bar{W}_t = \sum_{i=1}^{4}\left(\int_0^{L_i}\delta\theta_i(GJ_i\theta_i'' + P_iI_{P,i}\theta_i'' + M_{zz,i}W_i'' + \rho I_{P,i}A_i\omega^2\theta_i)dx\right) = 0 \tag{203}$$

where δW_i and $\delta\theta_i$ are weighting functions corresponding to flexural and torsional displacements, respectively, for beam segment i. Then, performing integrations by parts twice on Eq. 202 and once on Eq. 203 leads to:

$$\bar{W}_f = \sum_{i=1}^{4}\left(\int_0^{L_i}(EI_iW_i''\delta W_i'' - P_iW_i'\delta W_i' + M_{zz,i}\theta_i'\delta W_i' - \rho A_i\omega^2 W_i\delta W_i)dx\right) + \underbrace{\sum_{i=1}^{4}[(EI_iW_i''' + P_iW_i' + M_{zz,i}\theta_i')\delta W_i]_0^{L_i} - \sum_{i=1}^{4}[(EI_iW_i'')\delta W_i']_0^{L_i}}_{\Delta} = 0 \tag{204}$$

$$\bar{W}_t = \sum_{i=1}^{4}\left(\int_0^{L}(G_iJ_i\theta_i'\delta\theta_i' + P_iI_{P,i}\theta'\delta\theta' + M_{zz,i}W_i'\delta\theta_i' - \rho_iI_{P,i}A_i\omega^2\theta_i\delta\theta_i)dx\right) - \underbrace{\sum_{i=1}^{4}[(G_iJ_i\theta_i' + P_iI_{P,i}\theta_i' + M_{zz,i}W_i')\delta\theta_i]_0^{L_i}}_{\Delta^*} = 0 \tag{205}$$

Considering expressions of shear force, $S_i(x)$, bending moment, $M_i(x)$, and torsion torque, $T_i(x)$, it can be shown that for all the system's global classic boundary conditions, i.e., at x=0 and x=L, the corresponding relationships in boundary terms (Δ) and (Δ^*) will go directly to zero. For example, for clamped-free boundary conditions, one has zero displacements, $W_1 = W_1' = \theta_1 = 0$, and zero virtual displacements, $\delta W_1 = \delta W_1' = \delta\theta_1 = 0$, at the clamped end ($x$=*0*), and null resultant shear force, $S_4(x)$, bending moment, $M_4(x)$, and torsion torque $T_4(x)$ at the free end (x=L). This leads to:

$$(EI_1W_1''' + P_1W_1' + M_{zz,1}\theta_1')\delta W_1\Big|_{x=0} - (EI_1W_1'')\delta W_1'\Big|_{x=0} = 0, \tag{206}$$

$$(EI_4W_4''' + P_4W_4' + M_{zz,4}\theta_4')\delta W_1\Big|_{x=x_4} - (EI_4W_4'')\delta W_4'\Big|_{x=x_4} = 0, \tag{207}$$

$$(GJ_1\theta_1' + P_1I_{P,1}\theta_1' + M_{zz,1}W_1')\delta\theta_1\Big|_{x=0} = 0, \tag{208}$$

$$(GJ_4\theta_4' + P_4I_{P,4}\theta_4' + M_{zz,4}W_4')\delta\theta_4\Big|_{x=x_4} = 0. \tag{209}$$

The remaining terms in (Δ), corresponding to delamination edges (i.e., $x=x_1$ and $x=x_2$), can be resolved by applying the continuity conditions 198 and 200, with the following as a result:

$$\sum_{i=1}^{4}[(EI_iW_i''' + P_iW_i' + M_{zz,i}\theta_i')\delta W_i]_0^{L_i} - \sum_{i=1}^{4}[(EI_iW_i'')\delta W_i']_0^{L_i} =$$
$$\delta W_2\big|_{x=x_1}\underbrace{\left(EI_1W_1''' + P_1W_1' + M_{zz,1}\theta_1'\Big|_{x=x_1} - EI_2W_2''' + P_2W_2' + M_{zz,2}\theta_2'\Big|_{x=x_1} - EI_3W_3''' + P_3W_3' + M_{zz,3}\theta_3'\Big|_{x=x_1}\right)}_{*}$$
$$-\delta W_2'\Big|_{x=x_1}\left(EI_1W_1''\Big|_{x=x_1} - EI_2W_2''\Big|_{x=x_1} - EI_3W_3''\Big|_{x=x_1}\right)$$
$$+\delta W_2\big|_{x=x_2}\underbrace{\left(EI_4W_4''' + P_4W_4' + M_{zz,4}\theta_4'\Big|_{x=x_2} - EI_2W_2''' + P_2W_2' + M_{zz,2}\theta_2'\Big|_{x=x_2} - EI_3W_3''' + P_3W_3' + M_{zz,3}\theta_3'\Big|_{x=x_2}\right)}_{**}$$
$$-\delta W_2'\Big|_{x=x_2}\left(EI_4W_4''\Big|_{x=x_2} - EI_2W_2''\Big|_{x=x_2} - EI_3W_3''\Big|_{x=x_2}\right) \tag{210}$$

The terms (*) and (**) go to zero directly as a result of shear force continuity conditions. The remaining terms, however do not vanish as the continuity of bending moment at the two delamination tips includes additional implicit bending-axial terms such that:

$$\sum_{i=1}^{4}[(EI_iW_i''' + P_iW_i' + M_{zz,i}\theta_i')\delta W_i]_0^{L_i} = \left(\delta W_2'\Big|_{x=x_1} - \delta W_2'\Big|_{x=x_2}\right)\left(\Lambda\left[W_4'(x_4=0) - W_1'(x_1=L_1)\right]\right) \tag{211}$$

Likewise, the remaining terms in (Δ^*) can be resolved by applying the continuity conditions 180 and 184:

$$\sum_{i=1}^{4}[GJ_i\theta_i' + P_iI_{P,i}\theta_i' + M_{zz,i}W_i')\delta\theta_i]_0^{L_i} = \tag{212}$$
$$\delta\theta_2\big|_{x=x_1}\underbrace{\left(GJ_1\theta_1' + P_1I_{P,1}\theta_1' + M_{zz,1}W_1'\Big|_{x=x_1} - GJ_2\theta_2' + P_2I_{P,2}\theta_2' + M_{zz,2}W_2'\Big|_{x=x_1} - GJ_3\theta_3' + P_3I_{P,3}\theta_3' + M_{zz,3}W_3'\Big|_{x=x_1}\right)}_{***}$$
$$+\delta\theta_2\big|_{x=x_2}\underbrace{\left(GJ_4\theta_4' + P_4I_{P,4}\theta_4' + M_{zz,4}W_4'\Big|_{x=x_2} - GJ_2\theta_2' + P_2I_{P,2}\theta_2' + M_{zz,2}W_2'\Big|_{x=x_2} - GJ_3\theta_3' + P_3I_{P,3}\theta_3' + M_{zz,3}W_3'\Big|_{x=x_2}\right)}_{****}$$

The terms (***) and (****) go to zero directly as a result of torsion torque continuity conditions for left delamination tip (see equation 201) and similar continuity condition for right tip. With the boundary and continuity conditions satisfied and knowing that the expressions 201 and 202 must satisfy the principle of virtual work which leads to $\bar{W}_f + \bar{W}_t = 0,$ the system can then be discretized into elements:

$$\begin{aligned}
&\Lambda\left(\delta W_2'\Big|_{x=x_1} - \delta W_2'\Big|_{x=x_2}\right)\left[W_4'(x_4=0) - W_1'(x_1=L_1)\right] \\
&+\sum_{i=1}^{4}\left[\sum_{m=1}^{n}\left(\int_{x_m}^{x_{m+1}} (EI_i W_i''\delta W_i'' - P_i W_i'\delta W_i' + M_{zz,i}\theta_i'\delta W_i' - \rho A_i\omega^2 W_i\delta W_i)dx\right)\right] \\
&+\sum_{i=1}^{4}\left[\sum_{m=1}^{n}\left(\int_{x_m}^{x_{m+1}} (G_i J_i\theta_i'\delta\theta_i' + P_i I_{P,i}\theta_i'\delta\theta_i' + M_{zz,i}W_i'\delta\theta_i' - \rho_i I_{P,i}A_i\omega^2\theta_i\delta\theta_i)dx\right)\right] = 0,
\end{aligned} \tag{213}$$

where n stands for the number of elements in beam segment i. Following the traditional Euler-Bernoulli finite element development, cubic Hermite shape functions for flexural displacement and linear shape functions for torsion displacement is used to relate the displacement within each element (m) to their corresponding nodal displacements:

$$W_i(x) = \langle N(x)\rangle\{W_p\}, \qquad \delta W_i(x) = \langle N(x)\rangle\{\delta W_p\}, \tag{214}$$

$$\theta_i(x) = \langle L(x)\rangle\{W_p\}, \qquad \delta\theta_i(x) = \langle L(x)\rangle\{\delta W_p\}, \tag{215}$$

where, $\langle N(x)\rangle$ and $\langle L(x)\rangle$ are row vectors of cubic shape functions and linear shape functions, respectively. $\{W_p\}$, $\{\delta W_p\}$, $\{\theta_p\}$ and $\{\delta\theta_p\}$ are vectors containing the nodal real and virtual displacements for each element (m), defined as:

$$\{W_p\} = \begin{Bmatrix} W_1 & W_1' & W_2 & W_2' \end{Bmatrix}^T, \qquad \{\delta W_p\} = \begin{Bmatrix} \delta W_1 & \delta W_1' & \delta W_2 & \delta W_2' \end{Bmatrix}^T, \tag{216}$$

$$\{\theta_p\} = \begin{Bmatrix} \theta_1 & \theta_2 \end{Bmatrix}^T, \qquad \{\delta\theta_p\} = \begin{Bmatrix} \delta\theta_1 & \delta\theta_2 \end{Bmatrix}^T. \tag{217}$$

Substituting the above approximate displacements in 213:

$$\langle \delta W_{n'} \rangle \left[\Lambda \left(\{N\}' \Big|_{x=x_2} - \{N\}' \Big|_{x=x_1} \right) \left(\langle N \rangle' \Big|_{x=x_2} - \langle N \rangle' \Big|_{x=x_1} \right) \right] \{W_{n'}\} \tag{218}$$

$$+\sum_{i=1}^{4} \left[\sum_{m=1}^{n} \langle \delta W_n \rangle \left(\int_{x_m}^{x_{m+1}} (EI_i \{N\}'' \langle N \rangle'' - P_i \{N\}' \langle N \rangle' + M_{zz,i} \{L\}' \langle N \rangle' - \rho A_i \omega^2 \{N\} \langle N \rangle) dx \right) \{W_n\} \right]$$

$$+\sum_{i=1}^{4} \left[\sum_{m=1}^{n} \langle \delta W_n \rangle \left(\int_{x_m}^{x_{m+1}} (G_i J_i \{L\}' \langle L \rangle' + P_i I_{P,i} \{L\}' \langle L \rangle' + M_{zz,i} \{N\}' \langle L \rangle' - \rho_i I_{P,i} A_i \omega^2 \{L\} \langle L \rangle) dx \right) \{W_n\} \right] = 0$$

where $\{W_{n'}\}$ and $\{\delta W_{n'}\}$ are real and virtual nodal displacement vectors for the two nodes at the two ends of the delamination while $\{W_n\}$ and $\{\delta W_n\}$ are the elemental nodal vectors of real and virtual displacements 216 and 217 rewritten as:

$$\{W_n\} = \begin{Bmatrix} W_1 & W_1' & \theta_1 & W_2 & W_2' & \theta_2 \end{Bmatrix}^T, \ \{\delta W_n\} = \begin{Bmatrix} \delta W_1 & \delta W_1' & \delta\theta_1 & \delta W_2 & \delta W_2' & \delta\theta_2 \end{Bmatrix}^T \tag{219}$$

Frequency-dependent and non-frequency-dependent terms in 218 are assembled and the system's global boundary conditions are enforced to form the delaminated system's linear Eigenvalue problem, written in the following form:

$$\langle \delta W_n \rangle K(\omega) \{W_n\} = 0; \text{ with } K(\omega) = \left[K_G - \omega^2 M \right] \tag{220}$$

where $K_G = K_B + K_{BT} + K_{TB} + K_T + K_D$.

In the last expressions, $K(\omega)$ is also known as the system's Dynamic Stiffness Matrix (DSM). K_B and K_T are the global bending and torsion stiffness matrices, respectively. K_{BT} and K_{TB} are global bending-torsion and torsion-bending stiffness matrices, respectively, resulting from coupled terms in bending and torsion equations. K_D is delamination stiffness matrix generated from the term outside the integral in equation 218, and K_G and M are the global overall stiffness and mass matrices, respectively. Finally the system's natural frequencies and mode shapes are evaluated from Eigenvalues and Eigenvectors of Eigenproblem 220; i.e., for arbitrary $<\delta W_n>$, $|K(\omega)|=0$. The above procedure is achieved through a code developed in Matlab®.

5.5 Constrained mode model

The 'constrained mode' model is simplified by the assumption that the delaminated layers are 'constrained' to have the same transverse deformations ([77] and [89]) The delaminated beam is analyzed as three beam segments I, II and III. In Figure 51, $0 \le x \le x_1$ is considered segment I, $x_1 \le x \le x_2$ is considered segment II, and $x_2 \le x \le L$ is considered segment III. For beam segment I, the governing equations are:

$$EI_1 W_I'''' + PW_I'' + M_{zz}\theta_I - \rho A_1 \omega^2 W_I = 0 \tag{221}$$

$$GJ_1 \theta_I'' + PI_{P,1}\theta_I'' + M_{zz} W_I'' + \rho I_{P,1} A_1 \omega^2 \theta_I = 0 \tag{222}$$

where I_2, I_3, J_2, J_3, $I_{P,2}$ and $I_{P,3}$ are all calculated with respect to the overall cross-section's neutral axis. For segment II:

$$E\left(I_2 + I_3\right) W_{II}'''' + PW_{II}'' + M_{zz}\theta_{II} - \rho\left(A_2 + A_3\right)\omega^2 W_{II} = 0 \tag{223}$$

$$G\left(J_2 + J_3\right)\theta_{II}'' + P\left(I_{P,2} + I_{P,3}\right)\theta_{II}'' + M_{zz} W_{II}'' + \rho\left(I_{P,2} A_2 + I_{P,3} A_3\right)\omega^2 \theta_{II} = 0 \tag{224}$$

and for segment III:

$$EI_4 W_{III}'''' + PW_{III}'' + M_{zz}\theta_{III} - \rho A_4 \omega^2 W_{III} = 0 \tag{225}$$

$$GJ_4 \theta_{III}'' + PI_{P,4}\theta_{III}'' + M_{zz} W_{III}'' + \rho I_{P,4} A_4 \omega^2 \theta_{III} = 0 \tag{226}$$

The continuity conditions for deflection, slope, shear force, bending moment and torsion torque at the left delamination tip, $x = x_1$, are:

$$W_I(x = x_1) = W_{II}(x = x_1) \tag{227}$$

$$W_I'(x = x_1) = W_{II}'(x = x_1) \tag{228}$$

$$\theta_{II}(x = x_1) = \theta_{II}(x = x_1) \tag{229}$$

$$EI_1 W_I''' + PW_I' + M_{zz}\theta_I'\Big|_{x=x_1} = E\left(I_2 + I_3\right) W_{II}''' + PW_{II}' + M_{zz}\theta_{II}'\Big|_{x=x_1} \tag{230}$$

$$EI_1 W_I''\Big|_{x=x_1} = E\left(I_2 + I_3\right) W_{II}''\Big|_{x=x_1} - P_2^t \frac{H_3}{2} + P_3^t \frac{H_2}{2} \tag{231}$$

$$GJ_1\theta_I' + PI_{P,1}\theta_I' + M_{zz}W_I'\Big|_{x=x_1} = G\left(J_2 + J_3\right)\theta_{II}' + P_2\left(I_{P,2} + I_{P,3}\right)\theta_{II}' + M_{zz}W_{II}'\Big|_{x=x_1} \quad (232)$$

The continuity conditions at the right delamination tip are also written in a similar way to expressions 227 through 232. The general solution steps, namely the assembly of element equations, application of boundary conditions, forming the system's linear Eigenproblem, and extraction of the natural frequencies and modes for the 'constrained mode' are identical to those stated above for the 'free mode' model.

5.6 Dynamic finite element

DFE is an intermediate approach between the conventional FEM and Dynamic Stiffness Matrix (DSM) Methods. In the DFE formulation the frequency-dependent trigonometric shape functions adopted from DSM are used. In order to develop the problem-specific dynamic shape functions, the solutions of uncoupled portions of the governing differential equations are used as the basis functions approximation space. The resulting frequency dependent shape functions are then utilized to find the element frequency dependent dynamic stiffness matrix. To this end, further integrations by parts are applied on the discretized equation 213, leading to the following forms:

$$
\begin{aligned}
&\Lambda\left(\delta W_2'\Big|_{x=x_1}-\delta W_2'\Big|_{x=x_2}\right)\left[W_4'(x_4=0)-W_1'(x_1=L_1)\right]\\
&+\sum_{i=1}^{4}\left[\sum_{m=1}^{n}\left(\int_{x_m}^{x_{m+1}}(\underbrace{EI_iW_i\delta W_i''''-P_iW_i\delta W_i''-\rho A_i\omega^2W_i\delta W_i}_{*}+M_{zz,i}\theta_i'\delta W_i')dx\right)\right.\\
&\left.+\left[E_iI_iW_i'\delta W_i''-E_iI_iW_i\delta W_i''+P_iW_i\delta W_i'\right]_{x_m}^{x_{m+1}}\right]\\
&+\sum_{i=1}^{4}\left[\sum_{m=1}^{n}\left(\int_{x_m}^{x_{m+1}}(\underbrace{G_iJ_i\theta_i\delta\theta_i''+P_iI_{P,i}\theta_i\delta\theta_i''+\rho_iI_{P,i}A_i\omega^2\theta_i\delta\theta_i}_{**}+M_{zz,i}W_i'\delta\theta_i')dx\right)\right.\\
&\left.+\left[G_iJ_i\theta_i\delta\theta_i'+\frac{P_iI_{P,i}}{A_i}\theta_i\delta\theta_i'\right]_{x_m}^{x_{m+1}}\right]=0.
\end{aligned}
\tag{233}
$$

Reminding from Chapter 2, the interpolation functions, used to express element variables in terms of the nodal properties, would be the solutions to the integral terms marked as (*) and (**). Thus, the non–nodal solution approximation functions, W, and θ, and the test functions, δW, and $\delta\theta$ are written in form of equations 49 and 50.

Following same procedure as explained in Section 4 of Chapter 2 for each equation, the frequency dependent stiffness matrix $K(\omega)$ is obtained and the natural frequencies are found by solving the eigenvalue problem $|K(\omega)|=0$. In this study, frequency was swept, searching a particular frequency, ω, which would make the determinant of the global dynamic stiffness matrix equal to zero.

5.7 Numerical Results

Numerical tests were performed to confirm the predictability, accuracy and practical applicability of the proposed delaminated FEM and DFE models. In the first example, the natural frequencies of the unloaded system (P=M_{zz}=0) with a central split, about the mid-section (L_1=L_4), of various lengths up to 60% of the span ($0 \leq L_2/L \leq 0.6$), occurring symmetrically along the mid-plane of the beam and surrounded by intact beam segments, are considered. This split beam configuration has also been presented and studied in [77] and [89]. The defective FEM and DFE models were then created and used to evaluate the natural frequencies and mode shapes of various pre-stressed delaminated beam configurations. As the benchmarks for comparison and validation purposes, the results from references [77] and [89] and reference [78] for the constrained mode were used.

5.7.1 Validation of presented formulation

Consider a steel beam with Young's modulus E=200GPa, density ρ=7800kg/m^3, length of 8m, and a rectangular cross-sectional area of width of 0.4m and depth of 0.2m. The delamination is assumed to be on the mid-plane (H_2=0.5H_1) and have the length of $0 \leq L_2/L \leq 0.6$. A sample of convergence study is presented in Figure 52 where the exact error of present solution is found using the analytical results of Wang *et al.* [77]. For validation of the present solution, the first two non-dimensional natural frequencies, λ^2, of a defective clamped–clamped beam with a through-the-width delamination occurring symmetrically about the mid-section (L_1=L_4) on the mid-plane (H_2=H_3) for various delamination lengths are compared with the analytical results reported by Wang *et al.* [77] as well as the DSM [89] and FEM data [90] by Erdelyi and Hashemi, where:

$$\lambda_i^4 = \frac{\omega_i^2 \rho A_1}{EI_1} L^4;\ i = 1,2,... \tag{234}$$

In the formulations presented by Wang *et al.* [77] and Erdelyi and Hashemi ([89] and [90]) no pre-stress effect and torsional vibration is investigated. Therefore, for comparison purposes, only bending equation is solved and applied axial force and end moment are set to zero; P=0 and M_{zz}=0. Erdelyi and Hashemi [90] presented FEM-based defective beam models and the frequency data calculated from six- and ten-element meshes of 2-node FEM elements. Table 28 and Table 29 summarize the system's first two natural frequencies obtained using the presented DFE method, in comparison with those reported in the literature [77], [79], [88] and [89]. Referring to Table 28 and Table 29 of reference [89], they show exact match between the 1st frequency values obtained from both meshes. The 2nd frequency values obtained from the 6- and 10-element meshes, however, are found to be slightly different. Therefore, in what follows frequency data obtained from the latter mesh are used for comparison.

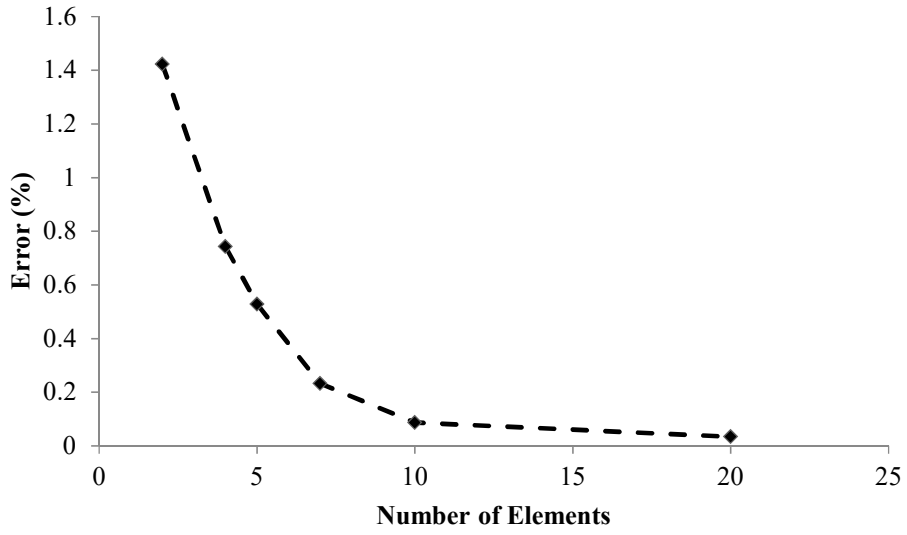

Figure 52: Convergence analysis for clamped–clamped isotropic beam, with P=0, M_{zz} =0, H_2/H=0.3, and L_2/L=0.4.

Table 28: Non-dimensional first natural frequency (λ_1^2) of a clamped–clamped isotropic beam with a mid-plane delamination.

Delamination Length (L_2/L)	1st Natural Freq.					
	DFE 10 Elements	Wang *et al.* [77]	FEM [90]	DSM [89]	Della & Shu [88]	Layer-wise FEM [79]
0.00	22.39	22.39	22.39	--	22.37	22.36
0.10	22.37	22.37	22.37	22.37	22.37	22.36
0.20	22.36	22.35	22.36	22.36	22.36	22.35
0.30	22.24	22.23	22.24	22.24	22.24	22.23
0.40	21.84	21.83	21.84	21.83	21.83	21.82
0.50	20.89	20.88	20.89	20.89	20.89	20.88
0.60	19.29	19.29	19.29	19.30	19.30	19.28

Table 29: Non-dimensional second natural frequency (λ_2^2) of a clamped–clamped isotropic beam with a mid-plane delamination.

Delamination Length (L_2/L)	2nd Natural Freq.					
	DFE 10 Elements	Wang *et al.* [77]	FEM [90]	DSM [89]	Della & Shu [88]	Layerwise FEM [79]
0.00	61.61	61.67	61.67	--	61.67	61.61
0.10	60.76	60.76	60.80	60.76	60.76	60.74
0.20	55.99	55.97	55.99	55.99	55.97	55.95
0.30	49.03	49.00	49.00	49.03	49.00	48.97
0.40	43.90	43.87	43.89	43.90	43.87	43.86
0.50	41.55	41.45	41.52	41.55	41.45	41.50
0.60	41.03	40.93	41.03	41.04	40.93	41.01

As can be observed from Table 28 and Table 29, natural frequencies obtained from the DFE method are in excellent agreement with the analytical results reported by Wang *et al.* [77], Della and Shu [88], as well as FEM [87] and layer-wise FEM [79] data, with discrepancies less than 0.1%.

5.7.2 Vibration analysis of delaminated pre-stressed beams

To further investigate the validity and practical applicability of the proposed formulation, and the effect of pre-load on the natural frequency of the defective beam structures, following illustrative examples of pre-stressed symmetrically delaminated beams, characterized by various delamination lengths, axial loads, and end moments are investigated. In each case, the change of normalized fundamental frequency, λ^2, versus the normalized end moment, M_{zz}/M_b, compressive axial load, P/P_{cr}, for 'free mode' is investigated, where:

$$\frac{P}{P_{cr}} = \frac{P}{4\pi^2 EI_1} L^4 \tag{235}$$

where P_{cr} and M_b, respectively, stand for the critical buckling load and buckling moment of an intact (non-delaminated) beam in absence of pre-load.

Figure 53 shows the system's fundamental natural frequency, λ^2, of an isotropic homogeneous beam with clamped-clamped boundary condition, M_{zz}/M_b=0.4, and central delamination located in mid-plane H_2/H=0.5, versus normalized axial force in 'free mode' model for different delamination sizes, L_2/L. As can be observed, when the load P approaches the buckling load, the natural frequency, λ^2, becomes zero, i.e., the structure has buckled. Moreover, as expected, the larger the delamination size, the smaller P_{cr} and the fundamental frequency. This reconfirms the fact that structural stiffness decreases when the delamination size increased.

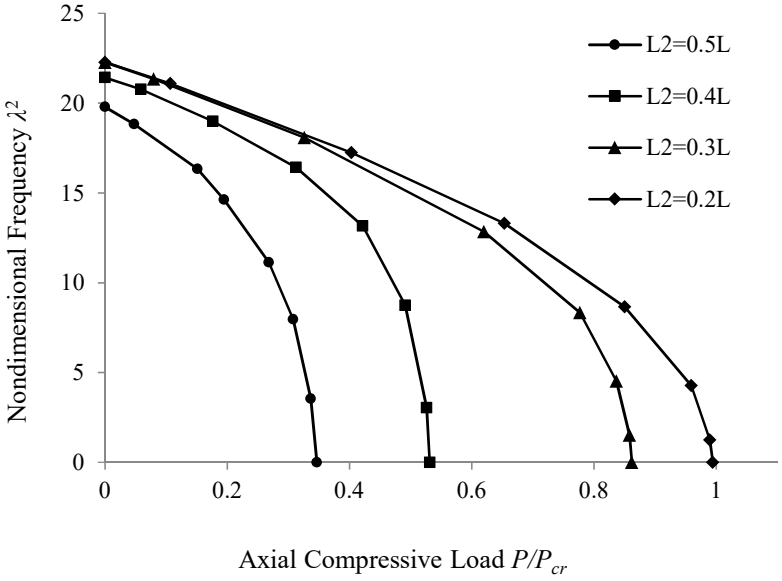

Figure 53: Fundamental natural frequency λ^2 of an isotropic homogeneous beam with clamped-clamped boundary condition, M_{zz}/M_b=0.4 and central delamination located in mid-plane H_2/H=0.5, versus normalized axial force in 'free mode' model for different values of L_2/L.

Figure 54 demonstrates the change in the first and second natural frequencies with respect to normalized buckling load P/P_{cr} for H_2/H=0.3. Results are shown for different delamination lengths of L_2/L=0.2, 0.3, 0.4 and 0.5. This figure reveals similar trends to those observed in Figure 53. Fundamental frequency results of 'constrained mode' are compared to 'free mode' data in Figure 55. As can be observed, the difference between predicted frequencies from these two modes increases as the applied axial load increases. This is related to the difference in nature of constrained and free mode models. The 'constrained mode' model is more similar to an intact beam model while 'free mode' model considers no constraints between beam segments II and III. This makes 'free mode' a better method for modeling delamination. Knowing that delamination causes stiffness reduction and that a larger pre-load makes this stiffness reduction bolder, increase in axial pre-load makes the difference between the predicted natural frequency results larger. Also inferred from Figure 54, for both natural modes, the larger the compressive axial load is the smaller the natural

frequency will be. It can be observed that as P increases, the natural frequency λ^2 first decreases slowly, but by getting close to buckling load it decreases drastically and eventually goes to zero. As can also be seen from Figure 55, the 'constrained mode' comparing to 'free mode', over predicts the natural frequencies especially for compressive load values close to buckling load. Additionally, from the same trends observed in Figure 53 to Figure 55, it can be inferred that compressive axial load causes a reduction in the structural stiffness leading, in turn, to lower natural frequencies. Similarly, increasing the delamination length results in lower stiffness and natural frequencies.

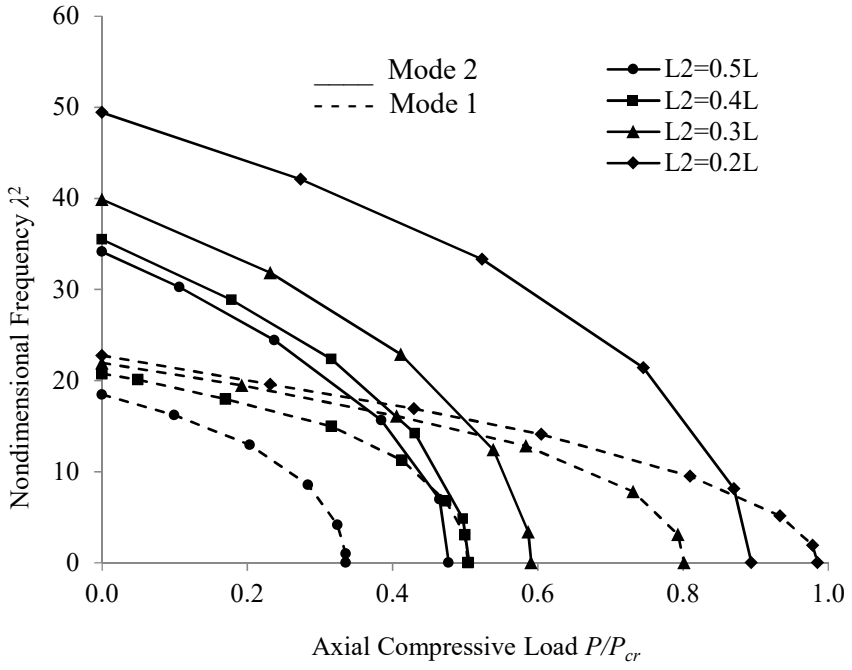

Figure 54: Variation of the first and second natural frequencies (λ^2) with respect to normalized buckling load P/P_{cr} for H_2/H=0.3, M_{zz}/M_b=0.4 and different values of L_2/L.

Figure 56 presents the normalized natural frequency, λ^2, versus the normalized end moment, M_{zz}/M_b. Referring to Figure 56, the same trends as in the previous graphs (for axial force) is observed for

variation of natural frequency versus buckling moment. Once again, it can also be observed that as the end moment increases, the stiffness decreases, leading to lower natural frequencies.

Figure 57 shows the first opening mode shape for a delaminated beam with a central delamination on the mid-plane using 'free mode'. As also reported in the literature ([89], [90] and [93]), not all the mode shapes obtained from 'free mode' model are admissible since unlike 'constrained mode' no constraints are imposed between the two delaminated layers, which results in some physically impossible mode shapes. It is also worth noting that the experimentally observed delamination openings have been reported to be significantly less than those calculated by the free model, which would rather justify the use of the constrained model for further analysis [93].

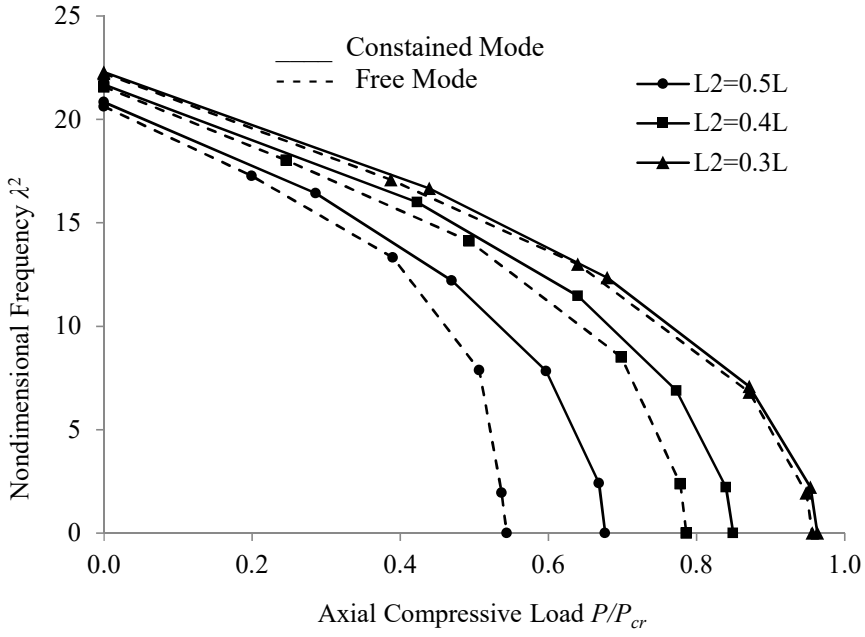

Figure 55: Trend of change in fundamental natural frequencies (λ^2) with respect to normalized buckling load P/P_{cr} for both constrained and free modes with H_2/H=0.5, M_{zz}/M_b=0.4 and different values of L_2/L.

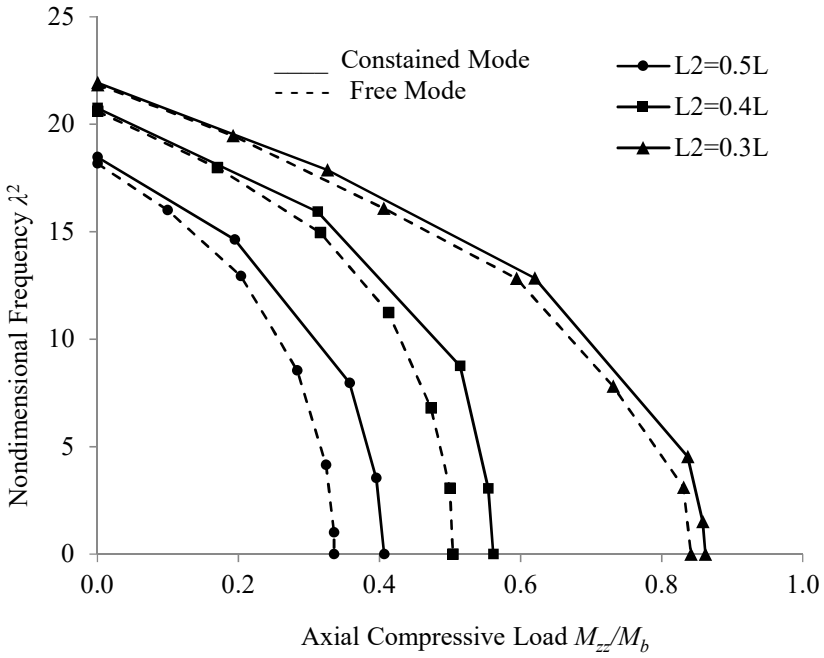

Figure 56: Fundamental natural frequencies (λ^2) with respect to normalized applied end moment M_{zz}/M_b for both constrained and free modes with H_2/H=0.5, P/P_{cr}=0.4 and different values of L_2/L.

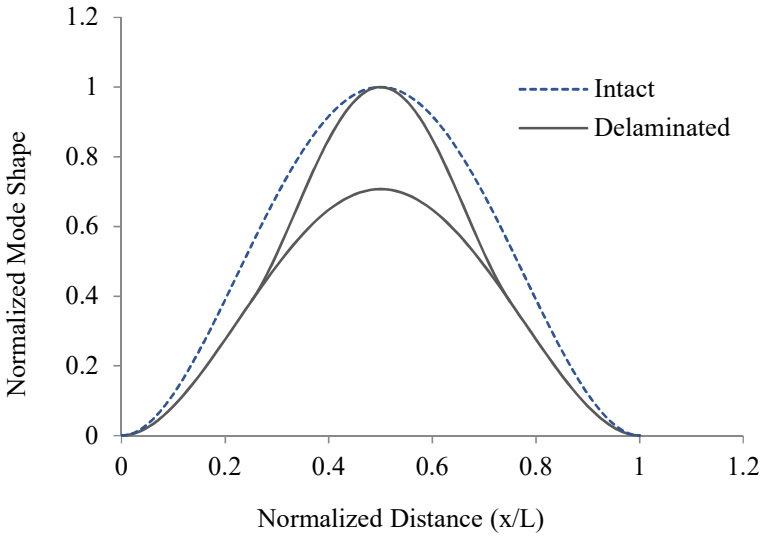

Figure 57: The first opening mode shape for a delaminated beam with a central delamination on the mid-plane using 'free mode' model.

In Table 30, the first two non-dimensional natural frequencies, λ^2, of a clamped–clamped beam with a through-the-width delamination occurring symmetrically about the mid-section (L_1=L_4) on the mid-plane (H_2=H_3) for various delamination lengths using DFE formulation as well as the analytical results reported by Wang *et al.* [77], the DSM [89] and FEM data [90] by Erdelyi and Hashemi are reported and in Figure 58 the first and second natural frequencies variation with respect to normalized buckling load is presented.

Table 30: Non-dimensional first natural frequency (λ_1^2) of a clamped–clamped isotropic beam with a mid-plane delamination using DFE formulation.

Delamination Length (L_2/L)	1st Natural Freq.					
	DFE 5 Elements	Wang *et al.* [77]	FEM [90]	DSM [89]	Della & Shu [88]	Layerwise FEM [79]
0.00	22.39	22.39	22.39	--	22.37	22.36
0.10	22.37	22.37	22.37	22.37	22.37	22.36
0.20	22.36	22.35	22.36	22.36	22.36	22.35
0.30	22.24	22.23	22.24	22.24	22.24	22.23
0.40	21.83	21.83	21.84	21.83	21.83	21.82
0.50	20.89	20.88	20.89	20.89	20.89	20.88
0.60	19.30	19.29	19.29	19.30	19.30	19.28

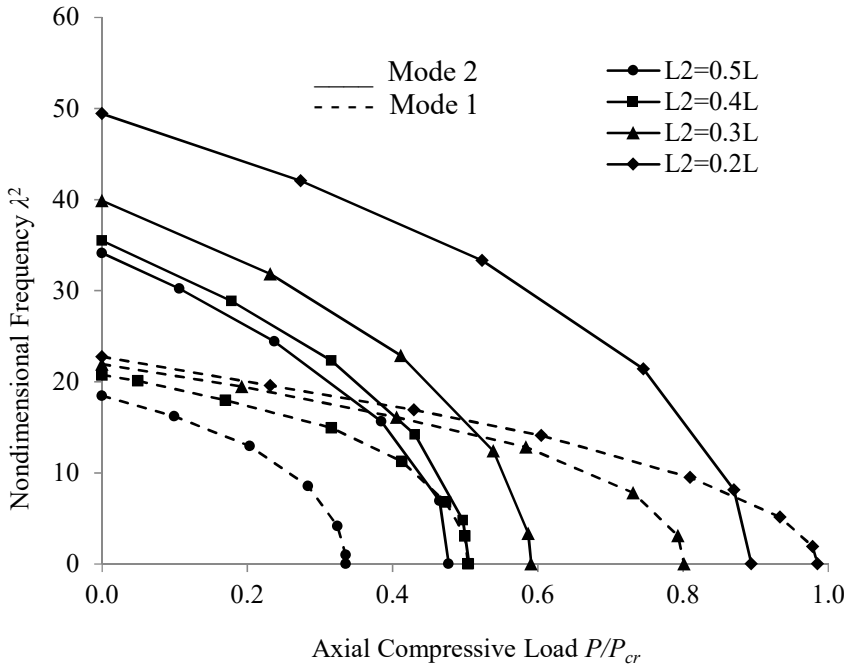

Figure 58: First and second natural frequencies (λ^2) versus normalized buckling load P/P_{cr} for H_2/H=0.3, M_{zz}/M_b=0.4 and different values of L_2/L using DFE method.

Finally, it has been recently shown and experimentally verified [73] that the opening is amplitude dependent. In other words, the delamination opening takes place only at certain critical amplitudes. The mode shapes are asymmetric and can be approximated by the superposition of the global shape of the entire beam and the local buckling shape of the delaminated part based on a dynamic stability analysis [93]. Further investigation on this topic, however, is beyond the scope of this Chapter.

5.8 Discussion and Concluding Remarks

A systematic FEM-based formulation and a dynamic finite element solutions for the free vibration modelling and analysis of delaminated beams under axial compressive load and end moment were presented. The defective beam, containing a central through-the-width delamination was modeled and analyzed as an assembly of four Euler–Bernoulli beams connected at the delamination

boundaries. Both the ‘free mode’ and ‘constrained mode’ delamination assumptions in buckling and vibration analysis were used and the solutions were verified and validated against the analytical and other numerical results presented in the literature. A parametric study is performed to analyze the effect of the axial load and end moment on the natural frequencies and mode shapes of the delaminated beam. The results showed a monotonic relation between the natural frequency and both axial compressive load and end moment. Both compressive axial load and end moment reduce the structural stiffness and results in lower natural frequencies. Similarly, increasing the length of delamination results in lower stiffness and natural frequencies. The present ‘free mode’ solution was also used to investigate the first and second mode buckling loads of the delaminated beams. It was shown that, when compared to ‘free mode’, the ‘constrained mode’ over predicts the natural frequencies specifically when compressive load approached to values close to buckling load. Finally, the difference between predicted frequencies from ‘free mode’ and ‘constrained mode’ increases as the applied axial load or end moment increases.

6 Discussion on the presented methods

In this section a brief discussion on the methods developed in this study as well as comparisons between the convergence rate and accuracy of these methods are presented.

In Figure 59, percentage of fundamental natural frequency errors for DFE and FEM, with M_{zz}=6.14MN.m and P=1.23MN using 5 elements and including all the four different cases with fixed-free boundary condition, are presented. As it can be observed from this figure, for all the four cases, DFE error is much less, i.e., minimum 50% of those of conventional FEM, which means DFE has at least twice as higher rate of convergence. The defective models have slightly larger error which can be linked to more complex nature of defective beam model and the fact that for single delamination in this model four segments are assembled and solved simultaneously. Figure 60, compares the percentage of error for the first five natural frequencies of a cantilever isotropic homogeneous beam subjected to P=1.23MN and M_{zz}=0 using 5 elements. As expected, the error is larger for higher natural frequencies for both conventional FEM and DFE with an exception of the fourth natural frequency where the error is even less than the error for the second natural frequency. The reason is that fourth natural frequency in bending-torsion coupled vibration is the first torsion dominant mode (as it can be also seen in Figure 12, Chapter 2, Section 3) and is equivalent to the first torsion mode shape of uncoupled system. So this fourth mode or fist torsion dominant mode shape needs less number of elements comparing to second and third bending dominant modes to acquire same accuracy. Similar convergence behaviors for coupled vibrations have also been previously observed and reported in literature (see, e.g., [41]).

In Table 24 (Chapter 3, Section 9) the Layer-wise Beam Finite Element Method (LBFEM) results and Layer-wise Beam Dynamic Finite Element (LBDFE) method results for a cantilever sandwich beam were compared with homogenization method, DSM and experimental results [101]. Figure 61

shows the difference of method of homogenization, LBDFE and LBFEM methods, using 5 elements, in comparison with experimental results for fundamental natural frequency of steel-rubber-steel sandwich beam. Based on this figure, the LBDFE is more accurate than LBFEM and LBFEM is more accurate than method of homogenization. Although, there is a constant difference between the numerical and experimental results which could be related to the properties of the rubber material used in modelling. These properties are reported by Banerjee *et al.* [101], where it is mentioned that they might not exactly match the properties of the rubber specimen they used in their experiments. In summary, in all cases studied in this thesis, the convergence rates obtained from frequency-dependent Dynamic Finite Element (DFE) formulation are found to surpass those found from the conventional FEM, which in turn surpass the method of homogenization. Further detailed discussions can be found in the concluding remarks sections in each of the previous Chapters.

The higher convergence rate of DFE is mainly attributed to the application of the solutions to the uncoupled part of equations as the basis functions. These solutions are much better approximations for non-nodal displacements between two nodes in comparison with conventional FEM which uses simple polynomials to describe non-nodal displacements.

It is also worth mentioning that the developed FEM here has advantages over FEM based software, ANSYS in modeling prestressed beams, since here the axial force and end moment are included in the equations of motion and the developed FEM gives the natural frequency and mode shapes of vibration directly while modal mode in ANSYS only solves the unstressed equations and in order to include the prestress effects the model needs to be solved statically first and then the results of static analysis is used to find the new stiffness of prestressed beam which will be used later in modal mode to find natural frequencies.

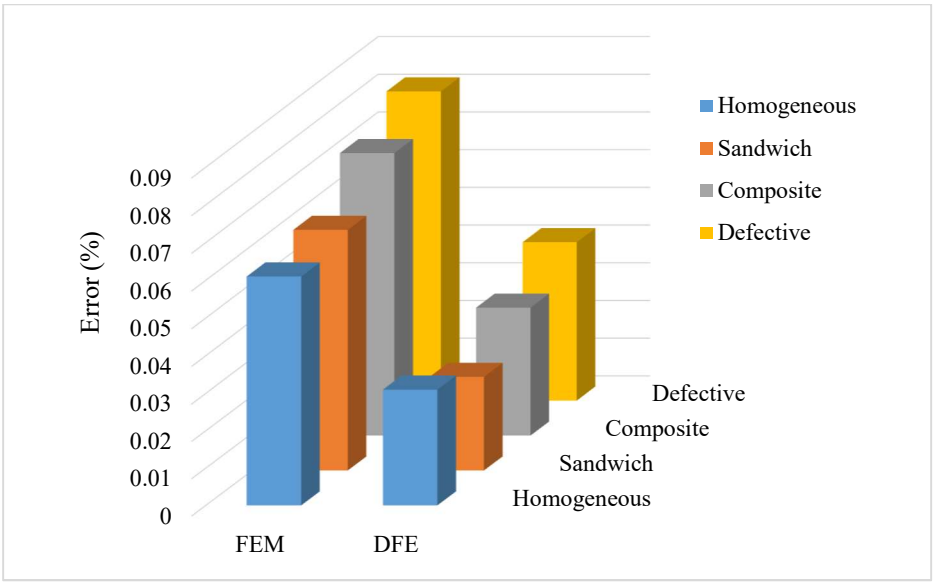

Figure 59: Percentage of fundamental natural frequency error for DFE and FEM with M_{zz}=6.14MN.m and P=1.23MN using 5 elements including the four different cases with cantilever boundary condition.

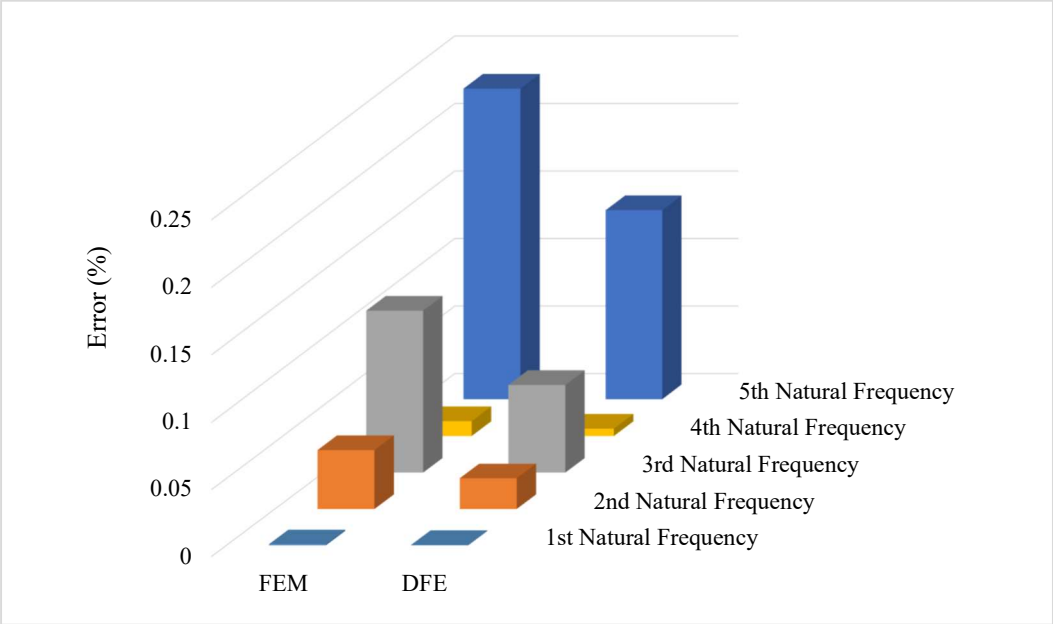

Figure 60: Percentage of error for cantilever steel beam with P=1.23MN and M_{zz}=0 using 5 elements.

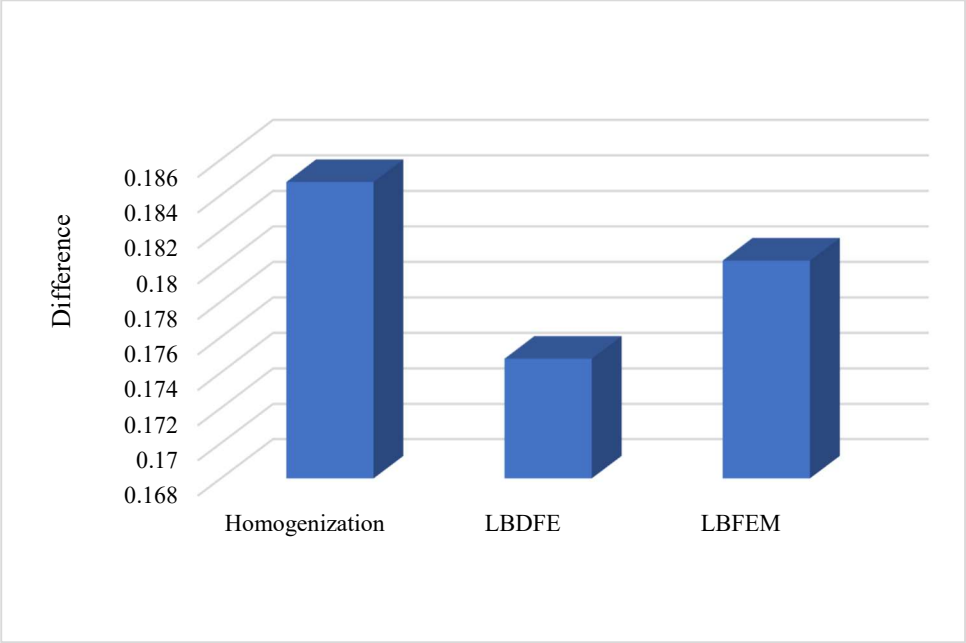

Figure 61: Difference of LBDFE and LBFEM methods, using 5 elements, with experimental results for fundamental natural frequency of steel-rubber-steel sandwich beam [101].

7 Conclusion

7.1 Contributions

In what follows, the author's contributions in terms of new concepts and strategies for free vibration analysis of pre-stressed uniform, sandwich, composite and delaminated beams are summarized:

1) Revisiting the dynamic analysis of flexible pre-stressed structural elements, and exploiting Hamilton principle, the differential equations governing coupled bending-torsion vibrations of beams caused by the end moment, are first developed. Cases considered in this development include,

   a) single-layer pre-stressed beams,

   b) multi-layer pre-stressed beams,

   c) pre-stressed composite beams, exhibiting both coupling caused by the end moment, as well as the Material coupling associated with the fiber angle, and finally

d) defective pre-stressed multi-layer beams including delaminations.

2) Development of conventional Finite Element (FEM) formulations for the free vibration analysis of all the above-mentioned pre-stressed beam configurations, by exploiting the equivalent single-layer theory, tested and validated against limited existing analytical data, where applicable, method of homogenization and numerical tests.
3) Exploiting the equivalent single-layer theory, new frequency-dependent Dynamic Finite Element (DFE) formulations for the free vibration analysis of all the above-mentioned pre-stressed beam configurations, were devised, tested and validated against limited data available in the literature, where applicable, method of homogenization, and numerical (FEM) tests.
4) Development of a novel layer-wise finite element formulation for bending-torsion coupling vibration analysis of pre-stressed layered and sandwich beams subjected to axial force and end moment.
5) Deriving frequency dependent dynamic finite element model for pre-stressed layered and sandwich beams subjected to axial force and end moment using layer-wise formulation as well as performing numerical test on model.
6) Modeling a pre-stressed composite beam with bending-torsion coupling rigidity with axial force and end moment using finite element method.
7) Developing dynamic finite element model for a composite pre-stressed beam with double bending-torsion couplings, and finally
8) Frequency dependent dynamic finite element modeling of a pre-stressed defective beam exhibiting bending-torsion coupling.

The motivation behind this study was the lack of established methods and formulation for free vibration modeling of pre-stressed defective beam-like structures subjected to combined axial force and end moment. This type of pre-stress effect arises in many structures and machines, for instance, imperfect joints in beam-columns which are mainly used for framing or truss structures. For this purpose, the equations of motion were first derived from Hamilton principles and in the absence of any analytical solution for the governing differential equations, the conventional finite element and a frequency dependent dynamic finite element formulations were developed. For different configuration, including the uniform isotropic, layered, composite and defective beams were modeled and for each case a number of numerical tests were conducted. Based on the results and for all the four cases studied, the DFE exhibits higher convergence rates than conventional FEM. This could potentially lead to considerable reduction in the modeling and analysis time, when it comes to large scale designs. Presently, the DFE technique is especially advantageous at the preliminary design/analysis stage. For the detailed design and analysis stage, however, an elaborated FEM model would be a better option.

Concerning the pre-stress effect of axial force and end moment on the beam vibrational behavior, the results for all the cases show that, as expected, the tensile force increases the natural frequencies of the beam while they are reduced by compressive forces and end moments. The reason can be justified by taking a look at the developed stiffness matrices. In all the four cases, and for both methods, an increase in tensile axial force results in larger entry values in stiffness matrix while higher compressive axial force or higher end moment leads to smaller ones, where lower stiffness, in turn, means lower natural frequencies. For each case, four classical boundary conditions are considered and the results have been compared and validated against, where available, analytical, experimental data from literature.

7.2 Future work

Future work includes but is not limited to:

- Enhancing the defective model formulation to a more generalize form for a beam with *n* number of delamination.
- Enhancing the beam models used, to incorporate the shear and rotary inertia effects; i.e., Timoshenko instead of Euler-Bernoulli beam bending theory.
- To extend the models to thin-walled, symmetric, open cross-section beams, where the warping should be also included in the torsion equation.
- To extend the latter to non-symmetric open cross-section beams with triple Bending-Bending-Torsion couplings.
- Experimentally testing all the investigated cases.
- Expanding all the 1D (beam) formulations into 2D (plane) models.
- Developing vibrational mode-based structural health monitoring approaches to predict the location, size, and number of delamination defects by comparing the experimental results with the numerical results of FEM or DFE.

Appendices

Appendix A; Modeling in ANSYS:

The vibrational mode of each beam configuration is solved using the commercially available software ANSYS. ANSYS is a powerful multipurpose analytical software package that is trusted in the industry. This software employs the conventional Finite Element Method (FEM). To account for axial loading and end moments the model is pre-stressed using ANSYS's static structural tool. SOLID-186 elements are used in the meshes of all the models generated for this report. SOLID-186 is a higher order 3D, 20 node solid elements capable of 3 degrees of freedom (x, y, and z directions) per node.

Models are developed for both homogenous and non-homogenous cross section as well as single delamination. Figure B-1 illustrates ANSYS model geometry and applied axial force and end moment.

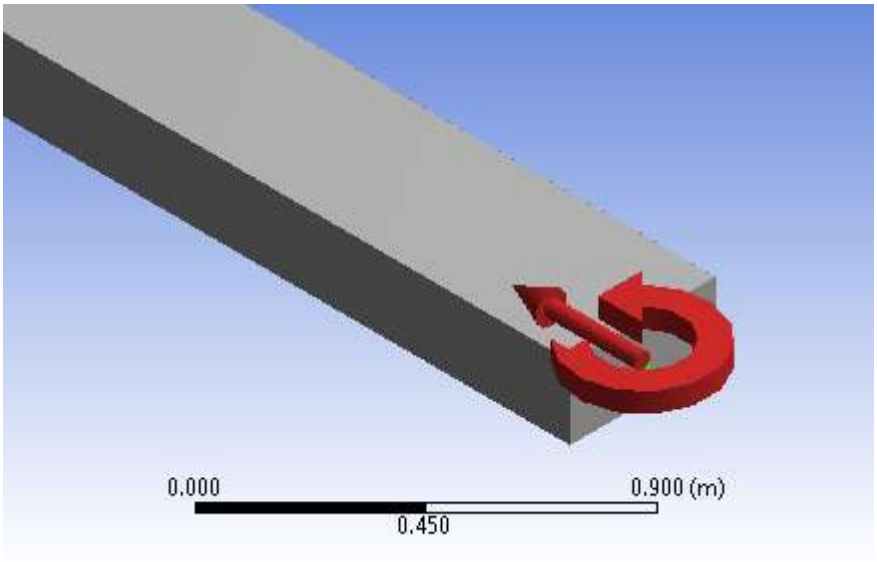

Figure A-1: ANSYS model geometry and applied axial force and end moment.

ANSYS 15 Workbench is capable of performing many analyses simultaneously. For example for modal analysis a pre-stressed beam requires ANSYS to first solve for the stiffness matrix in a static structural analysis. The results from the static structural analysis are directly linked to the modal analysis model. In what follows, the overall steps to perform pre-stressed modal analysis will be discussed.

The first step involves, (1) setting up the analysis system; for the purposes of this report this involved linking a static structural analysis with a modal analysis. This is followed by (2) defining material properties; ANSYS 15 Workbench contains and Engineering Database where general material properties can be found for analysis. It also supports editing of existing materials as well as the capability to add new materials. The third step is to (3) Define the Geometry; ANSYS 15 Workbench contains a design model tool which provides the capabilities to create 2D sketches and 3D models. If the geometry is too complex ANSYS 15 has the option of importing CAD models created from other software. The next step is to (4) Define Part Behavior; this step involves adding the boundary conditions, contact constraints, and loading. The final step before an analysis can be performed is the (5) Meshing of the System.

The element type used in this analysis is SOLID186. This element type is a high order 3D, 20 node solid element. This element exhibits quadratic displacement behavior. Each node in the element has three degrees of freedom, translation in the nodal x, y, and z directions. SOLID186 has the capability to support plasticity, hyper elasticity, creep, stress stiffening, large deflection and strain capabilities. SOLID 186 is subject to some restrictions and assumptions:

- The element must not have a zero volume.
- The element cannot be twisted such that the element contains two separate volumes.
- The edge displacement varies linearly rather than parabolically if a midside node is removed.

- At least two elements should be used in each direction.

In Figures A-2 through A-19 the selective modes of free vibration for isotropic, layered and defective beams with cantilevered boundary condition are presented

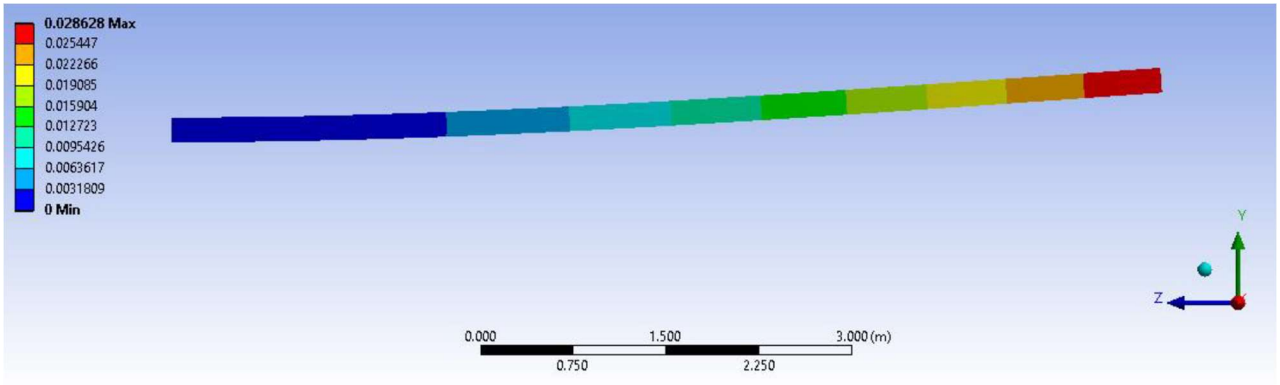

Figure A-2: First mode for a steel beam under compressive load.

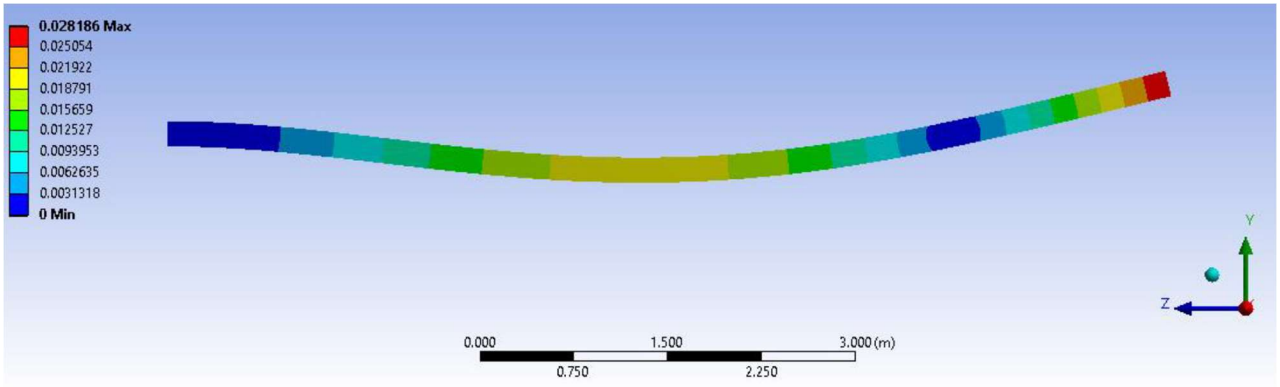

Figure A-3: Second mode for a steel beam under compressive load.

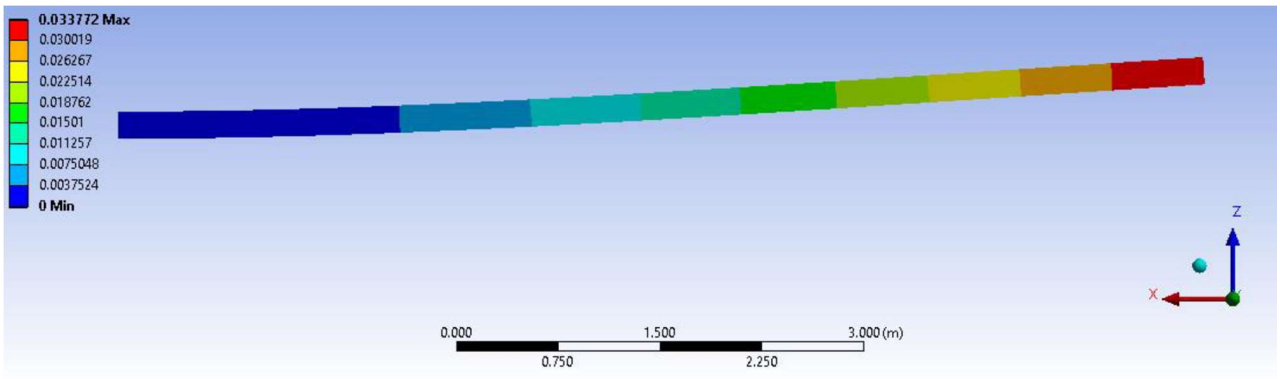

Figure A-4: First mode for a steel - aluminum beam under tensile load.

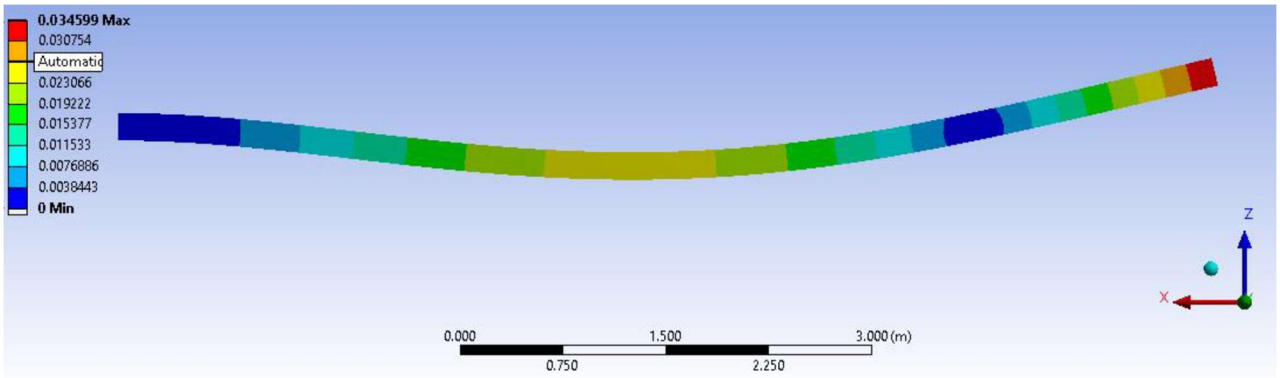

Figure A-5: Second mode for a steel - aluminum beam under tensile load.

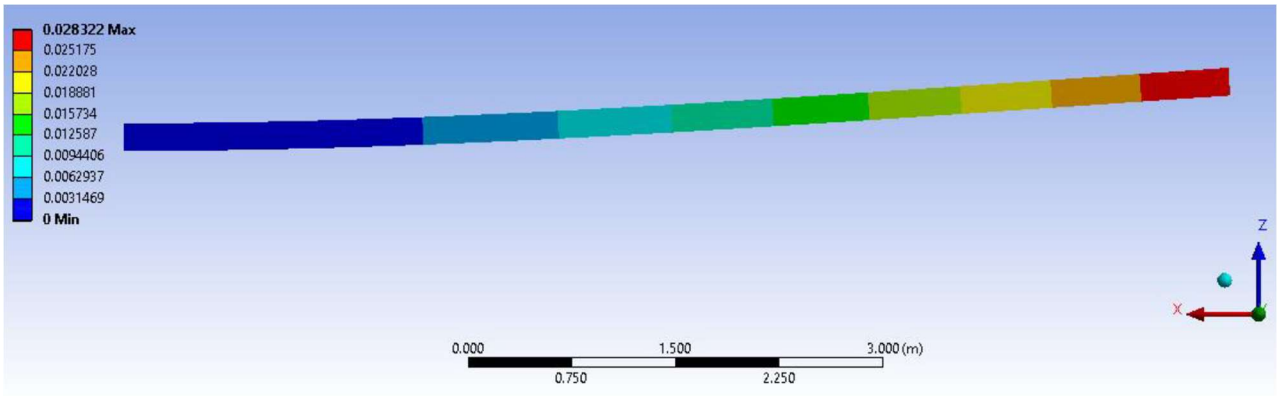

Figure A-6: First mode for a double layered steel beam under no load.

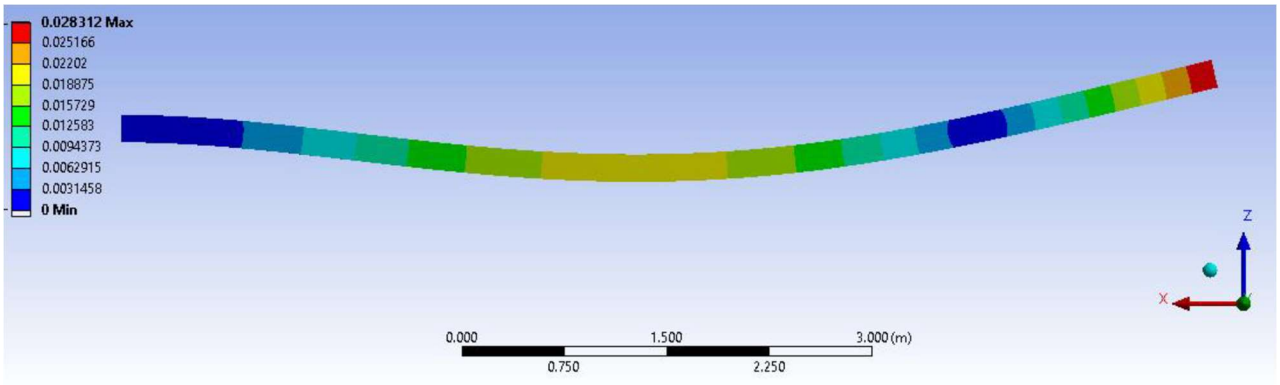

Figure A-7: Second mode for a double layered steel beam under no load.

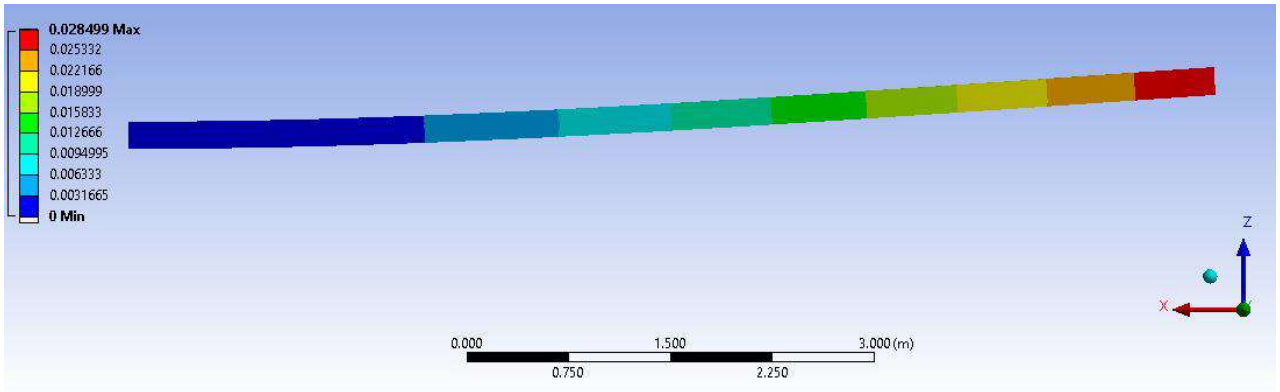

Figure A-8: First mode for a triple layered steel beam under end moment loading.

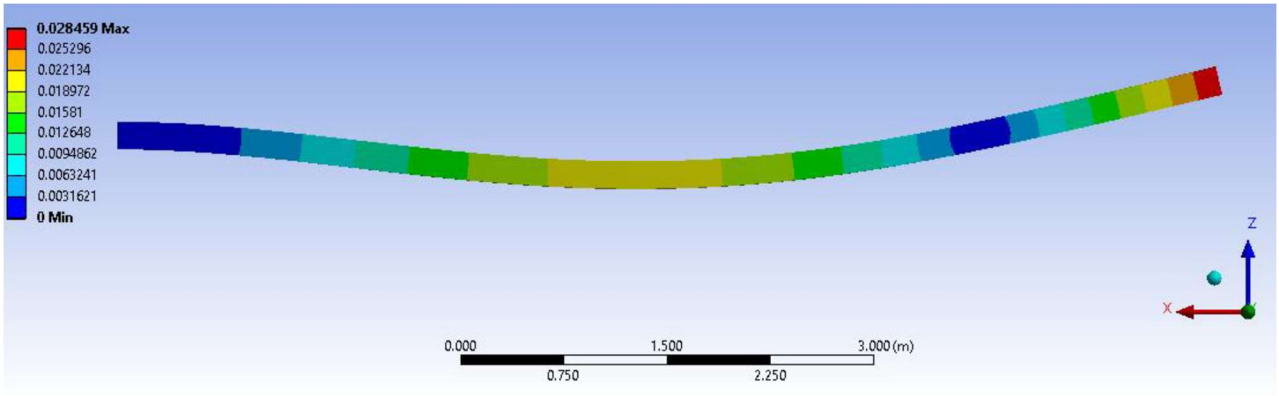

Figure A-9: Second mode for a triple layered steel beam under end moment loading.

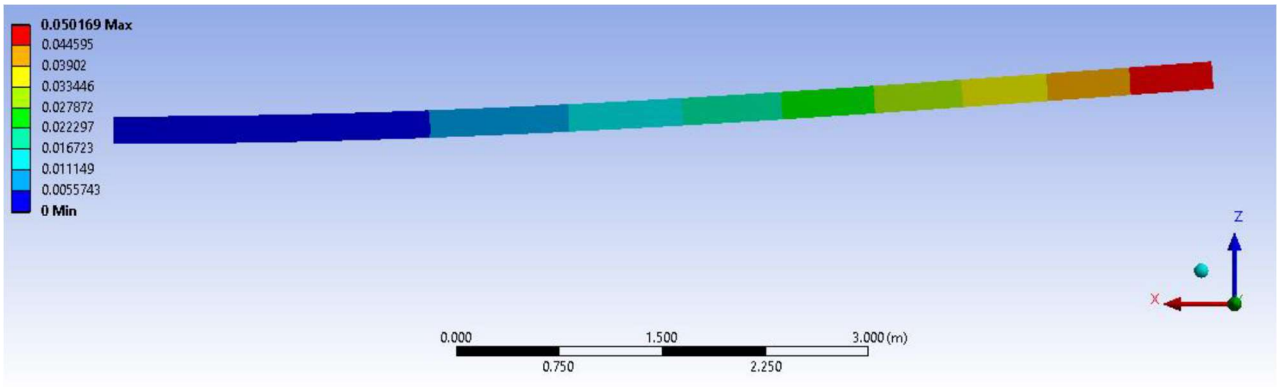

Figure A-10: First mode for the GLARE beam under compressive loading.

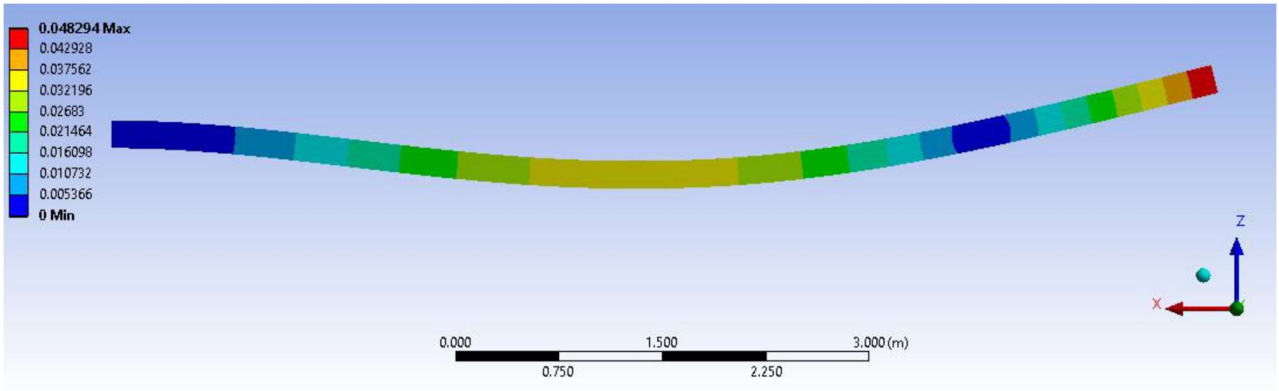

Figure A-11: Second mode for the GLARE beam under compressive loading.

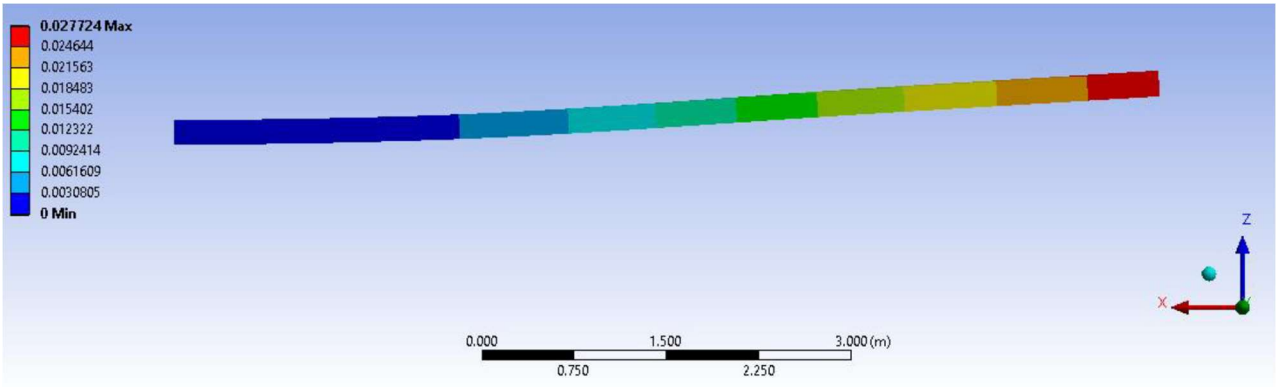

Figure A-12: First mode for the single delaminated steel beam with end moment loading at 50% delamination.

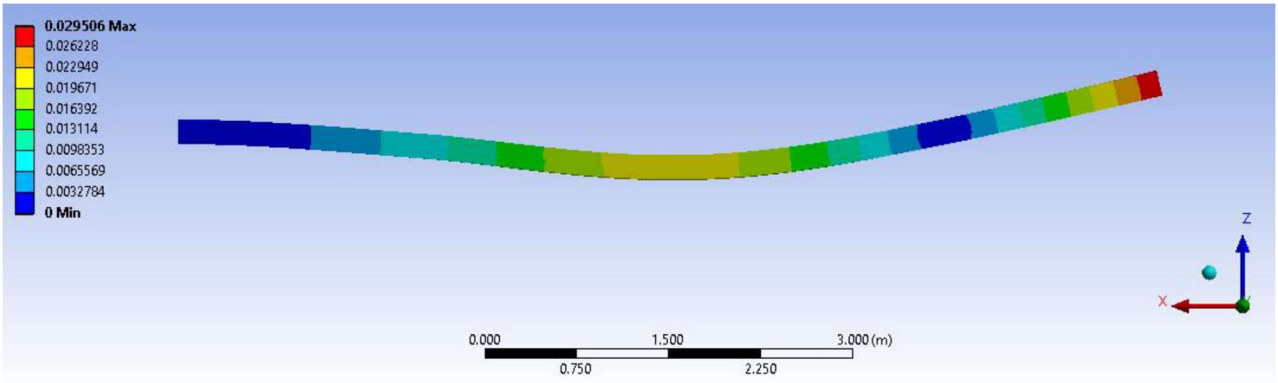

Figure A-13: Second mode for the single delaminated steel beam with end moment loading at 50% delamination.

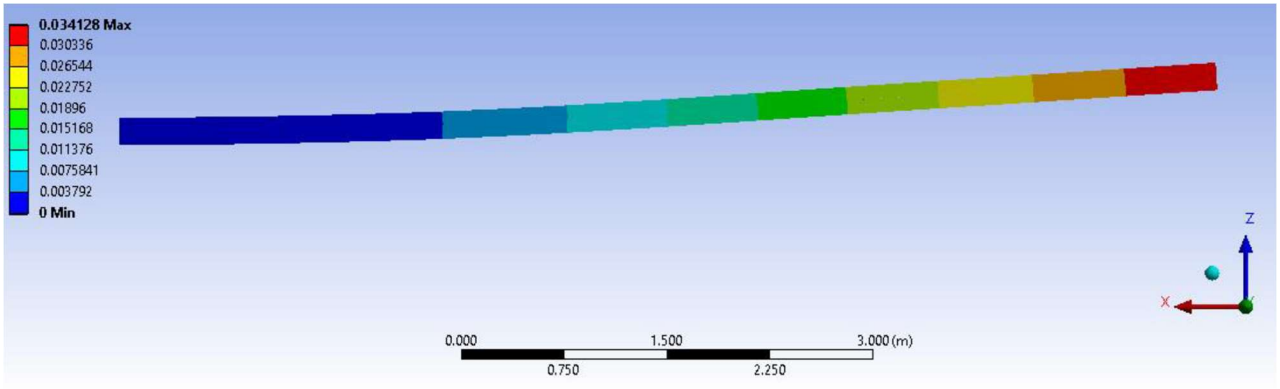

Figure A-14: First mode for the delaminated steel - aluminum beam with compressive loading and 50% delamination.

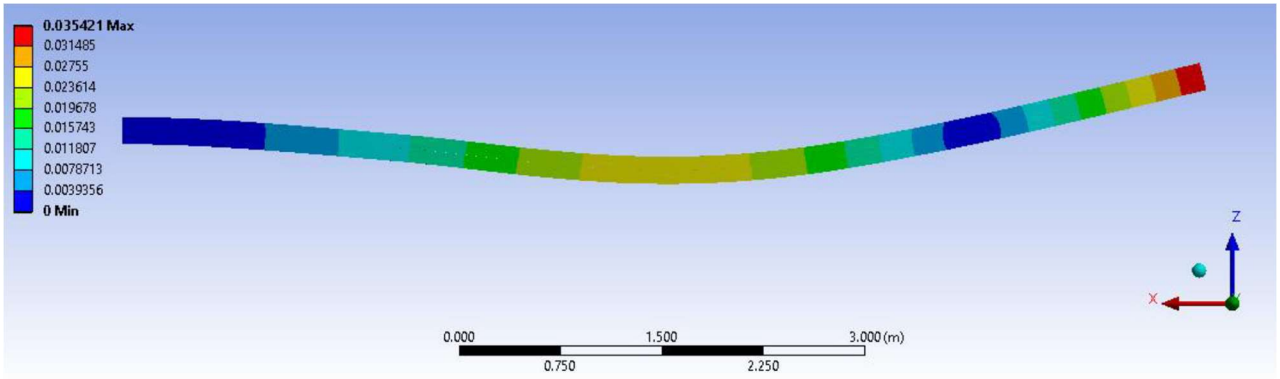

Figure A-15: Second mode for the delaminated steel - aluminum beam with compressive loading and 50% delamination.

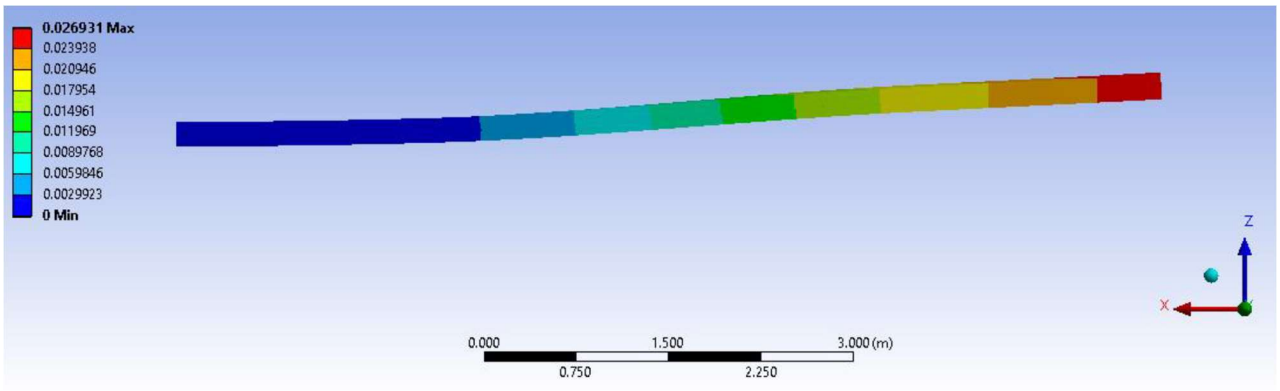

Figure A-16: First mode for triple layered steel beam at 50% delamination and compressive loading.

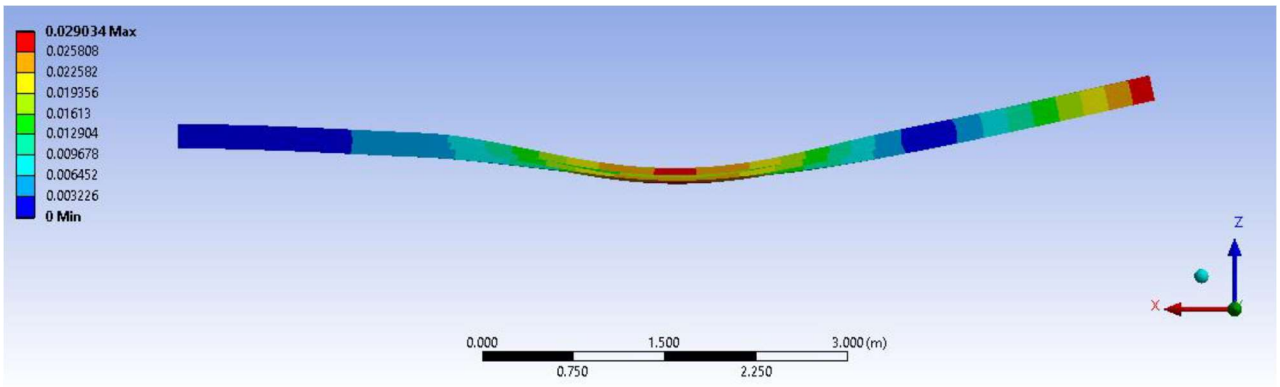

Figure A-17: Penetrated second mode for triple layered steel beam at 50% delamination and compressive loading.

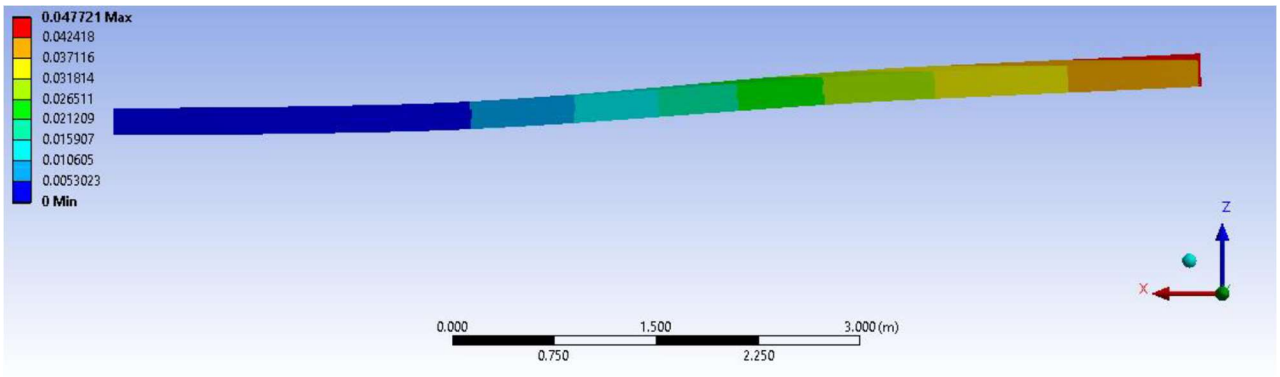

Figure A-18: First mode for a GLARE beam at 50% delamination and end moment loading.

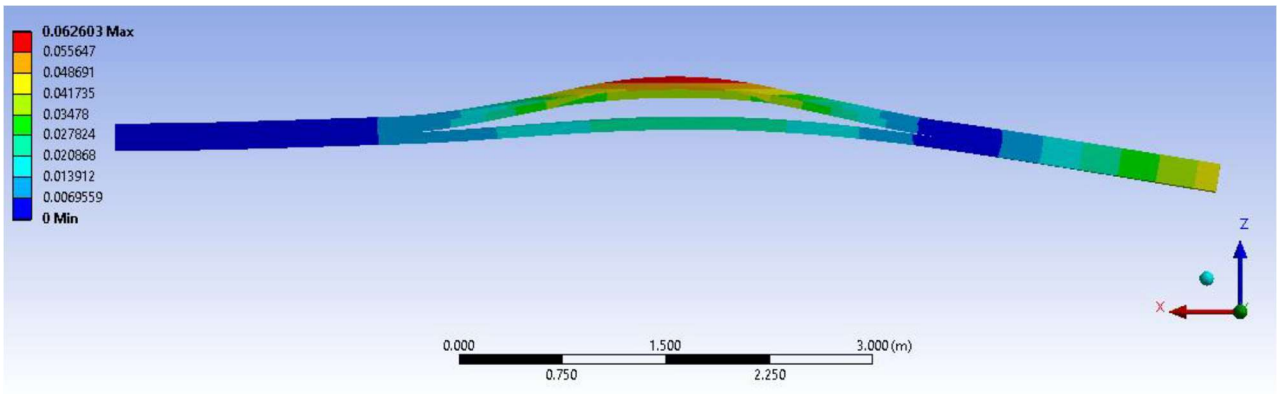

Figure A-19: Second penetrated mode for a GLARE beam at 50% delamination and end moment loading.

Appendix B; Effective rigidities for a solid cross-section:

The reduced stiffness constants in the material principle directions are:

$$Q_{12} = \frac{\upsilon_{LT} E_T}{1 - \upsilon_{LT}\upsilon_{TL}} = \upsilon_{LT} Q_{22} \tag{B.1}$$

$$Q_{22} = \frac{E_T}{1 - \upsilon_{LT}\upsilon_{TL}} = \frac{E_T}{1 - \frac{E_T}{E_L}\upsilon_{LT}^2} = \frac{E_T}{E_L} Q_{11} \tag{B.2}$$

$$Q_{66} = G_{LT} \tag{B.3}$$

where, E_L, is the elastic modulus is the longitudinal direction. E_T, is the elastic modulus in the transverse direction. Poisson's ratio is denoted by υ_{LT} and the principal shear modulus is denoted by G_{LT}. For a plane stress state these reduced stiffness constants are sufficient to describe the stress-strain relationship as follows:

$$\begin{bmatrix} \sigma_1 \\ \sigma_2 \\ \tau_{12} \end{bmatrix} = \begin{bmatrix} Q_{11} & Q_{12} & Q_{16} \\ Q_{12} & Q_{22} & Q_{26} \\ Q_{16} & Q_{26} & Q_{66} \end{bmatrix} \begin{bmatrix} \varepsilon_1 \\ \varepsilon_2 \\ \varepsilon_{12} \end{bmatrix} \tag{B.4}$$

In order to find the stresses and strains in the (*x, y, z*) coordinate system a simple rotational transformation is needed as:

$$\left[\overline{Q_{ij}}\right] = [T]^{-1}\left[Q_{ij}\right][T] \tag{B.5}$$

Then, the resulting transformed reduced stiffness constants for a unidirectional or orthotropic composite from its principal directions is:

$$
\begin{aligned}
\overline{Q_{11}} &= Q_{11}\cos^4\phi + Q_{22}\sin^4\phi + 2(Q_{12}+2Q_{66})\sin^2\phi\cos^2\phi \\
\overline{Q_{12}} &= \left(Q_{11}+Q_{22}-4Q_{66}\right)\sin^2\phi\cos^2\phi + Q_{12}(\cos^4\phi+\sin^4\phi) \\
\overline{Q_{16}} &= (Q_{11}-Q_{12}-2Q_{66})\sin\phi\cos^3\phi + (Q_{12}-Q_{22}+2Q_{66})\sin^3\phi\cos\phi \\
\overline{Q_{22}} &= (Q_{11}\sin^4\phi + 2(Q_{12}+Q_{66})\sin^2\phi\cos^2\phi + Q_{22}\cos^4\phi \\
\overline{Q_{26}} &= (Q_{11}-Q_{12}-2Q_{66})\sin^3\phi\cos\phi + (Q_{12}-Q_{22}+2Q_{66})\sin\phi\cos^3\phi \\
\overline{Q_{66}} &= \left(Q_{11}+Q_{22}-2(Q_{12}+Q_{66})\right)\sin^2\phi\cos^2\phi + Q_{66}(\sin^4\phi+\cos^4\phi)
\end{aligned}
\tag{B.6}
$$

Banerjee [65], the in-plane resultant matrix N(x, y) is:

$$
N(x,y) = \int_{-t/2}^{t/2}[\sigma]dz \tag{B.7}
$$

and the resultant moment is:

$$
M(x,y) = \int_{-t/2}^{t/2} z[\sigma]dz \tag{B.8}
$$

Both equations (above) can be merged into a single equation commonly known as the “Constitutive Equation”. The constitutive equation describes the stiffness matrix of a laminate plate. The resultant forces and moments are functions of the in-plane strains and curvatures.

$$
\begin{bmatrix} N_x \\ N_y \\ N_{xy} \\ M_x \\ M_y \\ M_{xy} \end{bmatrix} =
\left[\begin{array}{ccc|ccc}
A_{11} & A_{12} & A_{16} & B_{11} & B_{12} & B_{16} \\
A_{12} & A_{22} & A_{26} & B_{12} & B_{22} & B_{26} \\
A_{16} & A_{26} & A_{66} & B_{16} & B_{26} & B_{66} \\
\hline
B_{11} & B_{12} & B_{16} & D_{11} & D_{12} & D_{16} \\
B_{12} & B_{22} & B_{26} & D_{12} & D_{22} & D_{26} \\
B_{16} & B_{26} & B_{66} & D_{16} & D_{26} & D_{66}
\end{array}\right]
\begin{bmatrix} \varepsilon_{xx} \\ \varepsilon_{yy} \\ \varepsilon_{xy} \\ \kappa_x \\ \kappa_y \\ \kappa_{xy} \end{bmatrix}
\tag{B.9}
$$

The sub-matrix A is called the extensional stiffness matrix, sub-matrix B is called the coupling stiffness matrix and sub-matrix D is called the bending stiffness matrix. When the laminate is symmetric, by ply orientation and thickness, with respect to the mid-plane layer, the coupling matrix B is eliminated ($B_{ij} = 0$). The coefficients corresponding to a bending-twist coupling are D_{12} *and* D_{26}.

The stiffness coefficients are defined by the following expressions:

$$A_{ij} = \sum_{k=1}^{NL} (\overline{\mathrm{Q_{ij}}})_k \ (h_k - h_{k-1})$$
$$B_{ij} = \frac{1}{2} \sum_{k=1}^{NL} (\overline{\mathrm{Q_{ij}}})_k \ (h_k^2 - h_{k-1}^2) \qquad \text{(B.10)}$$
$$D_{ij} = \frac{1}{3} \sum_{k=1}^{NL} (\overline{\mathrm{Q_{ij}}})_k \ (h_k^3 - h_{k-1}^3)$$

where h_k is the distance from the mid-plane of the laminate (Figure B-1). Then,

$$\begin{bmatrix} M_x \\ M_y \\ M_{xy} \end{bmatrix} = \left[\begin{array}{c|cc} D_{11} & D_{12} & D_{16} \\ \hline D_{12} & D_{22} & D_{26} \\ D_{16} & D_{26} & D_{66} \end{array}\right] \begin{bmatrix} \kappa_x \\ \kappa_y \\ \kappa_{xy} \end{bmatrix} \qquad \text{(B.11)}$$

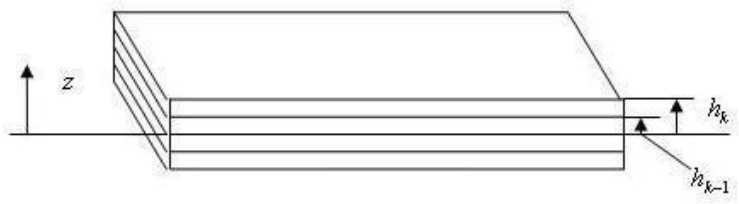

Figure A-1: Composite Laminate beam consisting of multiple plies, where h_k is the distance from the mid-plane of the composite.

For a bending-torsion coupling behavior the chord wise moment M_x is assumed to be zero so that the κ_x curvature can be eliminated from (above) and then the matrix (B.11) reduces to the following form:

$$\begin{bmatrix} M_y \\ M_{xy} \end{bmatrix} = \begin{bmatrix} D_{22} & D_{26} \\ D_{26} & D_{66} \end{bmatrix} - \begin{bmatrix} D_{12} \\ D_{16} \end{bmatrix} \left[D_{11}\right]^{-1} \begin{bmatrix} D_{12} & D_{16} \end{bmatrix} \qquad \text{(B.12)}$$

The resulting matrix is then:

$$\begin{bmatrix} M_y \\ M_{xy} \end{bmatrix} = \begin{bmatrix} D_{22} - \dfrac{D_{12}^2}{D_{11}} & D_{26} - \dfrac{D_{12}D_{16}}{D_{11}} \\ D_{26} - \dfrac{D_{12}D_{16}}{D_{11}} & D_{66} - \dfrac{D_{16}^2}{D_{11}} \end{bmatrix} \begin{bmatrix} \kappa_y \\ \kappa_{xy} \end{bmatrix} \tag{B.13}$$

The bending and torque intensities are related to the resultant moment and torque by Banerjee [65]:

$$\begin{aligned} M &= -bM_y \\ T &= 2bM_{xy} \end{aligned} \tag{B.14}$$

which results in:

$$\begin{aligned} EI &= b\left(D_{22} - \frac{D_{12}^2}{D_{11}} \right) \\ GJ &= 4b\left(D_{66} - \frac{D_{16}^2}{D_{11}} \right) \\ K &= 2b\left(D_{26} - \frac{D_{12}D_{16}}{D_{11}} \right) \end{aligned} \tag{B.17}$$

The *EI, GJ* and *K* represent the rigidities of the beam in the global coordinate system. *EI, GJ,* and *K* represent, the bending rigidity, torsion rigidity and bending-torsion coupled rigidity, respectively.

Appendix C

The governing differential equations of motion for a pre-stressed laminated composite beam can be derived using Hamilton's principle as follows:

The total potential energy (U) of the beam is given by (coupling rigidity terms are from [103] energy term for end moment is from [104] and rest of the terms are from [65]):

$$U = \frac{1}{2}\int_0^L \left[b\left(D_{22} - \frac{D_{12}^2}{D_{11}} \right)\left(\frac{\partial^2 w}{\partial x^2} \right)^2 + 2b\left(D_{26} - \frac{D_{12}D_{16}}{D_{11}} \right)\left(\frac{\partial^2 w}{\partial x^2} \right)\left(\frac{\partial \theta}{\partial x} \right) + 4b\left(D_{66} - \frac{D_{16}^2}{D_{11}} \right)\left(\frac{\partial \theta}{\partial x} \right)^2 + P\left\{ \left(\frac{\partial w}{\partial x} \right)^2 + \left(\frac{I_P}{m} \right)\left(\frac{\partial \theta}{\partial x} \right)^2 \right\} + M_{zz}\left(\frac{\partial w}{\partial x} \right)\left(\frac{\partial \theta}{\partial x} \right) \right] dx \tag{C.1}$$

using the rigidities definitions from B.17, equation C.1 can be re-written as:

$$U = \frac{1}{2}\int_0^L \left[EI\left(\frac{\partial^2 w}{\partial x^2} \right)^2 + K\left(\frac{\partial^2 w}{\partial x^2} \right)\left(\frac{\partial \theta}{\partial x} \right) + GJ\left(\frac{\partial \theta}{\partial x} \right)^2 + P\left\{ \left(\frac{\partial w}{\partial x} \right)^2 + \left(\frac{I_P}{m} \right)\left(\frac{\partial \theta}{\partial x} \right)^2 \right\} + M_{zz}\left(\frac{\partial w}{\partial x} \right)\left(\frac{\partial \theta}{\partial x} \right) \right] dx \tag{C.2}$$

The total kinetic energy (T) is given by [105]:

$$T = \frac{1}{2}\int_0^L \left[m\left(\frac{\partial w}{\partial t} \right)^2 + I_P\left(\frac{\partial \theta}{\partial t} \right)^2 \right] dx \tag{C.3}$$

Based on Hamilton's principle, for Lagrangian (L=T-U), $\int_{t_1}^{t_2} L\, dt$ is stationary between any arbitrary intervals of time (t_1, t_2) which means:

$$\delta \int_{t_2}^{t_2} (T - U) dt = 0 \tag{C.4}$$

where δ is the variational operator. By substituting C.2 and C.3 into C.4, integrating each term by parts, using δ operator, knowing that δh and $\delta\theta$ are arbitrary and finally collecting all the terms, the governing differential equations 142 and 143 are obtained.

References

[1] W. Chen and E. Lui , Handbook of Structural Engineering, Florida USA: CRC Press, 2005.

[2] O. Blodgett, Design of Welded Structures, Cleveland, USA: Lincoln Arc Welding Foundation, 2002.

[3] R. Mobley, Vibration Fundamentals, Elsevier, 1999.

[4] J. Neogy and M. K. S. Murthy, "Determination of fundamental natural frequencies of axially loaded columns and rames," *Journal of the Institution of Engineers (India),* vol. 49, pp. 203-212, 1969.

[5] K. S. R. K. Prasad, A. Krishnamurthy and A. V. Mahabaliraja, "Iterative type Rayleigh-Ritz method for natural vibration," *American institude of Aeronutics and Aeronutics Journal,* vol. 8, pp. 1884-1886, 1970.

[6] M. Gellert and J. Gluck, "The influence of axial load on eigenfrequencies of a vibrating lateral restraint cantilever," *International Journal of Mechanical Sciences,* vol. 14, pp. 723-728, 1972.

[7] D. Pilkington and J. Carr, "Vibration of beams subjected to end and axially distributed loading," *Journal of Mechanical Engineering Science,* vol. 12, no. 1, p. 70–72, 1970..

[8] J. T. S. Wang, D. Shaw and O. Mahrenholz, "Vibration of rotating rectangular plates," *Journal of Sound and Vibration,* vol. 112, pp. 455-468, 1987.

[9] T. Tarnai, "Variational methods for analysis of lateral buckling of beams hung at both ends," *International Journal of Mechanical Sciences,* vol. 21, no. 6, pp. 329-335, 1979.

[10] D. W. Jensen and E. F. Crawley, "Frequency determination techniques for cantilevered plates with bending-torsion coupling," *American Institute of Aeronautics and Astronautics Journal,* vol. 22, no. 3, pp. 415-420, 1984.

[11] A. Joshi and S. Suryanarayan, "Coupled Flexural-torsional Vibration Of Beams In The Presence Of Static Axial Loads And End Moments," *Journal of Sound and Vibration,* vol. 92, no. 4, pp. 583-589, 1984.

[12] A. Joshi and S. Suryanarayan, "Unified Analytical Solution For Various Boundary Conditions For The Coupled Flexural-torsional Vibration Of Beams Subjected To Axial Loads And End Moments," *Journal ofSound and Vibration,* vol. 129, no. 2, pp. 313-326, 1989.

[13] A. Joshi and S. Suryanarayan, "Iterative Method For Coupled Flexural-torsional Vibration Of Initially Stressed Beams," *Journal of Sound and Vibration,* vol. 146, no. 1, pp. 81-92, 1991.

[14] M. E. Mohsin and E. A. Sadek, "The distributed mass-stiffness technique for the dynamical analysis of complex frameworks," *The Structural Engineer,* vol. 46, no. 345-351, 1968.

[15] J. R. Banerjee and S. A. Fisher, "Coupled bending-torsional dynamic stiffness matrix for axially loaded beam elements," *International journal for numerical methods in engineering,* vol. 33, no. 4, pp. 739-751, 1992.

[16] V. Kolousek, "Anwendung des Gesetzes der virtuellen Verschiebungen und des Reziprozitatssatzes in der Stabwerksdynamic," *Ingenieur Archiv,* vol. 12, pp. 363-370, 1941.

[17] V. Kolousek, "Berechnung der schwingenden Stockwcrkrahmen nach der Deformationsmethode," *Der Stahlbau,* vol. 16, pp. 5-6, 11-13, 1943.

[18] V. Kalousek, Dynamics in Engineering Structures, Butterworths, London, 1973.

[19] W. L. Hallauer and Y. L. Liu , "Beam bending-torsion dynamic stifness method for calculation of exact vibration modes," *Journal of sound and vibration,* vol. 85, pp. 105-113, 1982.

[20] F. Y. Cheng, "Vibration of Timoshenko beams and frameworks," *Journal of the Structural Division,* vol. 96, pp. 551-571, 1970.

[21] F. Y. Cheng and . W. H. Tseng, "Dynamic matrix of Timoshenko beam columns," *Journal of the Structural Division,* vol. 99, pp. 527-549, 1973.

[22] T. M. Wang and T. A. Kinsman, "Vibration of frame structures according to the Timoshenko theory," *Journal of Sound and Vibration,* vol. 14, pp. 215-227, 1971.

[23] B. A. Akesson, "A computer program for plane frame vibration analysis by an exact method," *International Journal for Numerical Methods in Engineering ,* vol. 10, pp. 1221-1231, 1976.

[24] T. H. Richards and A. Y. T. Leung, "An accurate method in structural vibration analysis," *Journal of Sound and Vibration,* vol. 55, pp. 363-376, 1977.

[25] R. Lunden and B. A. Akesson, "Damped second-order Rayleigh-Timoshenko beam vibration in space—an exact complex dynamic member stiffness matrix," *International Journal for Numerical Methods in Engineering,* vol. 19, pp. 43 l-449, 1983.

[26] J. R. Banerjee and F. W. Williams, "Exact Dynamic Stiffness Matrix for Composite Timoshenko Beams With Applications," *Journal of Sound and Vibration,* vol. 194, no. 4, pp. 573-585, 1996.

[27] F. W. Williams and D. Kennedy, "Exact dynamic member stiffnesses for a beam on an elastic foundation," *Earthquake Engineering & Structural Dynamics,* vol. 15, pp. 133-136, 1987.

[28] M. S. Issa, "Natural frequencies of continuous curved beams on Winkler-type foundation," *Journal of Sound and Vibration,* vol. 127, pp. 291-301, 1988.

[29] J. T. Oden, "A general theory of finite elements. II. Applications," *International Journal for Numerical Methods in Engineering,* vol. 1, no. 3, pp. 247-259, 1969.

[30] E. Cohen and H. Mccallion, "Improved deformation functions for the finite element anlysis of beam systems," *International Journal for Numerical Methods in Engineering,* vol. 1, no. 2, pp. 163-167, 1969.

[31] W. Woodward and J. Morris, "Improving productivity in finite element analysis through interactive processing," *Finite Elements in Analysis and Design,* vol. 1, no. 1, pp. 35-48, 1985.

[32] C. Norwood, N. Cubitt and B. Downs, "A note on the equations of motion for the transverse vibration of a Timoshenko beam subjected to an axial force," *Journal of Sound and Vibration,* vol. 70, no. 4, pp. 475-479, 1980.

[33] C. V. Girijavallabhan and L. C. Reese, "Finite element method applied to some problems in soil mechanics," *Journal of Terramechanics,* vol. 5, no. 2, pp. 73-74, 1968.

[34] W. Howson and F. Williams, "Natural frequencies of frames with axially loaded Timoshenko Members," *Journal of Sound and Vibration,* vol. 26, no. 4, pp. 503-515, 1973.

[35] S. M. Hashemi, Free-vibrational analysis of rotating beam-like structures: A dynamic finite element approach, Laval University: PhD thesis, 1998.

[36] S. M. Hashemi and M. J. Richard, "Free vibrational analysis of axially loaded bending-torsion coupled beams: a dynamic Fnite element," *Computers and Structures,* vol. 77 , pp. 711-724, 2000.

[37] P. O. Friberg, "Beam element matrices derived from Vlasov's theory of open thin-walled elastic beams," *International Journal for Numerical Methods in Engineering,* vol. 21, pp. 1205-1228, 1985.

[38] S. M. Hashemi, M. J. Richard and G. Dhatt, "A New Dynamic Finite Elements (DFE) Formulation For Lateral Free Vibrations of Euler-Bernoulli Spinning Beams Using Trigonometric Shape Functions," *Journal of Sound and Vibrations,* vol. 220, no. 4, pp. 601-624, 1999.

[39] S. M. Hashemi and M. J. Richard, "A Dynamic Finite Element (DFE) For Free Vibrations of Bending-Torsion Coupled Beams," *Aerospace Science and Technology,* vol. 4, pp. 41-55, 2000.

[40] S. M. Hashemi and M. J. Richard, "Natural Frequency of Uniform Rotating Cantilever Beams with Coriolis Effects," *ASME Journal of Vibration and Acoustics,* vol. 123, no. 4, pp. 444-455, 2001.

[41] S. M. Hashemi, "The use of trigonometric interpolation functions for vibration analysis of beam structures - Bridging gap between FEM and exact formulations," *Advances in Fluid Mechanics,* vol. 36, pp. 197-206, 2003.

[42] S. M. Hashemi and A. Roach, "Application of A Reduced Mesh Dynamic Finite Element Method in Coupled Vibration Analysis of Structural Elements," *Advances in Boundary Elements,* vol. 19, pp. 163-172, 2004.

[43] M. Shavezipur and S. M. Hashemi, "Free vibration of triply coupled centrifugally stiffened nonuniform beams using a refined dynamic finite element method," *Aerospace Science and Technology,* vol. 13, p. 59–70, 2009.

[44] F. Plantema, Sandwich construction: the bending and buckling of sandwich beams, plates, and shells, New York: Wiley, 1966.

[45] R. Di Taranto, "Theory of vibratory bending for elastic and viscoelastic layered finite length beams," *Journal of Applied Mechanics,* vol. 87, p. 881–886, 1965.

[46] D. J. Mead and S. Markus, "The forced vibration of a three-layer, damped sandwich beam with arbitrary boundary conditions," *Journal of Sound and Vibration ,* vol. 10, no. 2, pp. 163-175, 1968.

[47] K. M. Ahmed, "Free vibration of curved sandwich beams by the method of finite elements.," *Journal of Sound and Vibration ,* vol. 18, no. 1, pp. 61-74, 1971 .

[48] T. T. Baber, R. A. Maddox and C. E. Orozco, "A finite element model for harmonically excited viscoelastic sandwich beams," *Computers and Science,* vol. 66, no. 1, pp. 105-113, 1998.

[49] A. Fasana and S. Marchesiello, "Rayleigh-Ritz analysis of sandwich beams," *Journal of Sound and Vibration ,* vol. 241, no. 4, pp. 643-652, 2001.

[50] M. G. Sainsbury and Q. J. Zhang, "The Galerkin element method applied to the vibration of damped sandwich beams," *Computers and Science ,* vol. 71, pp. 239-256, 1999.

[51] J. R. Banerjee and A. J. Sobey, "Dynamic stiffness formulation and free vibration analysis of a three-layered sandwich beam," *International Journal of Sounds and Structures,* vol. 42, pp. 2181-2197, 2005.

[52] W. P. Howson and A. and Zare, "Exact dynamic stiffness matrix for flexural vibration of three layered sandwich beams," *Journal of Sound and Vibration ,* vol. 282, pp. 753-767, 2005.

[53] S. M. Hashemi and E. J. Adique, "Free Vibration Analysis of Sandwich Beams: A Dynamic Finite Element," *International Journal of Vehicle Structures & Systems,* vol. 1, no. 4, 2009.

[54] S. M. Hashemi and E. J. Adique, "Quasi-Exact Dynamic Finite Element for Free Vibration Analysis of Sandwich Beams," *Applied Composite Materials,* vol. 17, no. 2, pp. 259-269, 2010.

[55] S. M. Hashemi and E. J. Adique , "Free Vibration Analysis of Curved Sandwich Beams: A Dynamic Finite Element," in *Advances in Vibration Analysis Research*, InTech, 2011, pp. 37-42.

[56] R. M. Jones, Mechanics of Composite Materials Second Edition, Taylor and Francis Inc., 1998.

[57] J. M. Berthelot, Composite Materials Mechanical Behaviour and Structural Analysis, New York: Springer-Verlag Inc., 1999.

[58] S. M. Hashemi and S. Borneman, "Application of Frequency Dependent Trigonometric Shape Functions in the Vibration Analysis of Laminated Composite Beams," in *The Fourth Canadian-International Composites Conference (cancom), proceedings*, 2003.

[59] S. M. Hashemi and S. Borneman, "Doubly-Coupled Vibrations of Nonuniform Composite Wings: A Dynamic Finite Element," *Mathematical Problems in Engineering, Aerospace and Sciences,* vol. 5, pp. 141-152, 2011.

[60] H. Abramovich and A. Livshits, "Free Vibration of Non-Symmetric Cross-Ply Laminated Composite Beams," *Journal of Sound and Vibration,* vol. 176, no. 5, pp. 597-612, 1994.

[61] L. Jaehong and S. Kim, "Flexural-Torsional Coupled Composite Beams with Channel Sections," *Computer and Structures,* vol. 80, pp. 133-144, 2002.

[62] X. L. Chen, G. R. Liu and S. P. Lim, "An Element Free Galerkin Method for the Free Vibration Analysis of Composite Laminates of Complicated Shape," *Composite Structures,* vol. 59, pp. 279-289, 2003.

[63] S. N. Jung, V. T. Nagaraj and I. Chopra, "Refined Structural Dynamics Model for Composite Rotor Blades," *AIAA Journal,* vol. 39, no. 2, pp. 339-348, 2001.

[64] J. R. Banerjee and F. W. Williams, "Free Vibration of Composite Beams- An Exact Method Using Symbolic Computation," *Journal of Aircraft,* vol. 32, no. 3, pp. 636-642, 1995.

[65] J. R. Banerjee, "Free Vibration of Axially Loaded Composite Timoshenko Beams Using the Dynamic Stiffness Matrix Method," *Computer and Structures,* vol. 69, pp. 197-208, 1998.

[66] J. R. Banerjee and F. W. Williams, "Free Vibration of Composite Beams- An Exact Method Using Symbolic Computation," *Journal of Aircraft,* vol. 32, no. 3, pp. 636-642, 1995.

[67] S. M. Hashemi and A. Roach, "Dynamic Finite Element Analysis of Extensional-Torsional Coupled Vibration in Nonuniform Composite Beams," *Applied Composite Materials,* vol. 18, no. 6, p. 521–538, 2011.

[68] S. M. Hashemi and S. Borneman, "Vibration Analysis of Composite Wings Undergoing Material and Geometrical Couplings: A Dynamic Finite Element Formulation," in *ASME International Mechanical Engineering Congress (ICMECE2004)*, 2004.

[69] J. Starnes, M. Rhodes and J. Williams, "Effect of impact damage and holes on the compressive strength of a graphite/epoxy laminate.," in *Nondestructive Evaluation and Flaw Criticality forComposite Materials, STP 696.*, philadelphia, 1979.

[70] S. Benmedakhene, M. Kenane and M. Benzeggagh, "Initiation and growth of delamination in glass/epoxy composites subjected to static and dynamic loading by acoustic emission monitoring," *Composites Science and Technology,* vol. 2, no. 59, pp. 201-208, 1999.

[71] X. Zhuang and X. Yan, "Investigation of damage mechanisms in self-reinforced polyethylene composites by acoustic emission," *Composites Science and Technology,* Vols. 3-4, no. 66, pp. 444-449, 2006.

[72] D. Crivelli, M. Guagliano, M. Eaton, M. Pearson, S. Al-Jumali, K. Holford and R. Pullin, "Localisation and identification of fatigue matrix cracking and delamination in a carbon fibre panel by acoustic emission," *Composites Part B: Engineering,* no. 74, pp. 1-12, 2015.

[73] A. Szekrényes, "A special case of parametrically excited systems: Free vibration of delaminated composite beams," *European Journal of Mechanics – A/Solids,* vol. 49, pp. 82-105, 2015.

[74] A. Szekrényes and Z. Juhasz, "Estimation of Local Delamination Buckling in Orthotropic Composite Plates Using Kirchhoff Plate Finite Elements," *Mathematical Problems in Engineering,* vol. 2015, p. 14, 2015.

[75] S. Kulkarni and D. Fredericks, "Frequency as a parameter in delamination problem—a preliminary investigation," *Journal of Composite Material,* vol. 5, pp. 112-19, 1971.

[76] R. Ramkumar, S. Kulkarni and R. Pipes, "Free vibration frequencies of a delaminated beam," in *34th Annual Technical Conference, Reinforced Plastics/Composites Institute*, New York, 1979.

[77] J. Wang, Y. Liu and J. Gibby, "Vibrations of split beams," *Journal of sound and vibration,* vol. 4, no. 84, p. 491–502, 1982.

[78] P. Mujumdar and S. Suryanarayan, "Flexural Vibrations of Beams with Delaminations.," *Journal of Sound and Vibration,* vol. 125, pp. 441-461., 1988.

[79] W. Lestari and S. Hanagud, "Health Monitoring of Structures: Multiple Delamination Dynamics in Composite Beams.," *Report for American Institute of Aeronautics and Astronautics,* vol. 99, pp. 1509-1519, 1999.

[80] M. Shen and J. Grady, "Free Vibrations of Delaminated Beams.," *AIAA Journal,* vol. 5, no. 30, pp. 253-277., 1992.

[81] J. J. Tracy and G. C. Pardoen, "Effect of Delamination on the Natural Frequencies of Composite Laminates.," *Journal of Composite Materials,* vol. 23, no. 12, pp. 289-301., 1989.

[82] G. Nagesh Babu and S. Hanagud, "Delamination in smart structures—a parametric study on vibrations.," in *31st SDM Conference*, Long Beach, 1990.

[83] M. Shen and J. Grady, "Free vibrations of delaminated beams.," *AIAA Journal,* vol. 30, no. 5, p. 1361–70., 1992.

[84] B. Stamos, V. Kostopoulos and S. Paipetis, "Identification of delamination by eigenfrequency degradation—an inverse problem," in *AGARD Conference Proceedings 530, Debonding/Delamination of Composites*, Patras, 1992.

[85] H. Chen, "Free vibration of prebuckled and postbuckled plate with delamination.," *Composites Science and Technology,* vol. 51, no. 3, p. 457–62, 1994.

[86] H. Chen, J. Tracy and R. Nonato, "Vibration analysis of delaminated composite laminates in prebuckled states based on a new constrained model.," *Journal of Composite Materials,* vol. 29, no. 2, p. 229–56, 1995.

[87] C. Della and D. Shu, "Free vibration analysis of composite beams with overlapping delaminations," *European Journal of Mechanics A/Solids,* vol. 24, p. 491–503, 2005.

[88] C. Della, "Free Vibration Analysis of Multiple Delaminated Beams Under Axial Compressive Load," *Journal of Reinforced Plastics and Composites,* vol. 28, pp. 1365-1381, 2009.

[89] N. Erdelyi and S.M. Hashemi, "A Dynamic Stiffness Element for Free Vibration Analysis of Delaminated Layered Beams," Modelling and Simulation in Engineering, Volume 2012 (2012). Article ID 492415, 8 pages, doi:10.1155/2012/492415.

[90] N.H. Erdelyi and S.M. Hashemi "On the Finite Element Free Vibration Analysis of Delaminated Layered Beams - A New Assembly Technique," Shock & Vibration, vol. 2016, Article ID 3707658, 14 pages, 2016. doi:10.1155/2016/3707658.

[91] J. Lee, "Free vibration analysis of delaminated composite beams," *Computers and Structures,* vol. 74, pp. 121-129, 2000.

[92] Y. Liu and D. W. Shu, "Coupled bending-torsion vibration of a homogeneous beam with a single delamination subjected to axial loads and static end moments," *Acta Mechanica Sinica,* vol. 30, no. 4, pp. 607-614, 2014.

[93] A. Szekrényes, "Coupled flexural–longitudinal vibration of delaminated composite beams with local stability analysis," *Journal of Sound and Vibration,* vol. 333, no. 20, pp. 5141-5164, 2014.

[94] H. Luo and S. Hanagud, "Dynamics of Delaminated Beams," *International Journal of Solids and Structures,* vol. 37, pp. 1501-1519, 2000.

[95] N. H. Erdelyi and S. M. Hashemi, "Dynamic finite element (DFE) modeling of multiple delaminated beams," presented at the *Mechanics of Nano, Micro and Macro Composite Structures conference*, Torino, 18-20 June 2012.

[96] D. V. Hutton, Fundamentals of Finite Element Analysis, New york: McGraw-Hill, 2003.

[97] J. R. Banerjee and F. W. Williams, "Exact Bernoulli-Euler dynamic stiffness matrix for a range of tapered beams," *International Journal for Numerical Methods in Engineering,* vol. 21, pp. 2289-2302, 1985.

[98] W. Wittrick and F. W. Williams, "A General Algorithm for Computing Natural Frequencies of Elastic Structures," *Quarterly Journal of Mechanics and Applied Mathematics,* vol. 24, pp. 263-284, 1971.

[99] S. Laux, "Estimation of Axial Load in Timber Beams Using Resonance Frequency Analysis," in *Master of Science thesis, Chalmers University of Technology*, Göteborg, Sweden, 2012.

[100] K. L. Lawrence, ANSYS Tutorial Release 13, SDC Publications, 2011.

[101] J. R. Banerjee, C. Cheung, R. Morishima, . M. Perera and J. Njuguna, "Free vibration of a three-layered sandwich beam using the dynamic stiffness method and experiment," *International Journal of Solids and Structures,* vol. 44, p. 7543–7563, 2007.

[102] M.T. T. Kashani, S. Jayasinghe, and S.M. Hashemi "On the Flexural–Torsional Vibration and Stability of Beams Subjected to Axial Load and End Moment," Journal of Shock and Vibration, Vol. 2014 (2014), Article ID 153532, 11 pages. http://dx.doi.org/10.1155/2014/153532.

[103] I. Lottati, "Flutter and Divergence Aeroelastic Characteristics for Composite Forward Swept Cantilevered Wing," *Journal of Aircraft,* vol. 22, no. 11, pp. 1001-1007, 1985.

[104] A. Joshi, "Vibration of thin-walled tubular structures in the presence of static axial stress fields, Bombay," India: Ph.D. Thesis Department of Aeronautical Engineering, Indian institute of Technology, 1983.

[105] J. R. Banerjee, H. Su and C. Jayatunga, "A dynamic stiffness element for free vibration analysis of composite beams and its application to aircraft wings," *Computers and Structures ,* vol. 86 , p. 573–579, 2008.

[106] C. D. Mote Jr., "Divergence buckling of an edge-loaded axially moving band," *International Journal of Mechanical Sciences,* vol. 10, no. 4, pp. 281-295, 1968.

[107] M.T. Kashani, S. Jayasinghe, and S.M. Hashemi " Dynamic Finite Element Analysis of Bending-Torsion Coupled Beams Subjected to Axial Load and End Moment," Shock & Vibration, vol. 2015, Article ID 471270, 12 pages, 2015. doi:10.1155/2015/471270.